

Towards the investigation of microbe-mineral interaction by means of Raman spectroscopy



seit 1558

Dissertation

Zur Erlangung des akademischen Grades
doctor rerum naturalium (Dr. rer. nat.)

vorgelegt dem Rat der Chemisch-Geowissenschaftlichen Fakultät der
Friedrich-Schiller-Universität Jena von

M. Sc. Valerian Ciobotă

geb. am 20. November 1981 in Toplița, Rumänien

Gutachter:

1.

.....

.....

2.

.....

.....

Tag der öffentlichen Verteidigung:

Contents

Zusammenfassung	2
1 Summary	4
1.1 Motivation	4
1.2 State of the Art	6
1.2.1 PHB-producing bacteria and Raman spectroscopy.....	6
1.2.2 Biologically mediated iron oxides and hydroxides formation /transformation in sediments and their precursors.....	9
1.3 Own research results	13
1.3.1 Towards the identification of microorganisms potentially involved in the biomineralization processes by means of Raman spectroscopy.....	13
1.3.2 Qualitative analysis of the pelagic particulate matter from Lake 77.....	15
1.3.3 Quantification of the inorganic phase of the pelagic aggregates formed in the acidic lignite mine lake.....	18
1.3.4 Investigation of Middle Eocene ironstones – confirmation of the microorganisms’ involvement in the ooidal ironstone formation process...	20
1.4 Conclusions and further work	22
Bibliography	24
2 Publications	36
2.1 The influence of intracellular storage material on bacterial identification by means of Raman spectroscopy [VC1]	36
2.2 Pelagic boundary conditions affect the biological formation of iron-rich Particles (iron snow) and their microbial communities [VC2].....	46
2.3 Identification of minerals and organic materials of the Middle Eocene ironstones, the Bahariya Depression, Western Desert, Egypt by means of micro-Raman spectroscopy [VC3]	60
2.4 Quantification of the Inorganic Phase of the Pelagic Aggregates of an Iron Contaminated Lake by means of Raman Spectroscopy [VC4]	67
3 Conference Contributions	88
4 Publications List	90
Acknowledgments	93
Curriculum Vitae	95
Selbstständigkeitserklärung	96

Zusammenfassung

Im Laufe der Erdgeschichte waren Mikroben sowohl direkt als auch indirekt für teils dramatische Veränderungen der Erdoberfläche verantwortlich. Dennoch sind bisher sowohl Ausmaß als auch Art und Weise ungeklärt, in welchen Mikroorganismen an der Bildung und Auflösung von Mineralien teilhaben oder mit der wässrigen Umgebung interagieren. Weiterhin stellt die eindeutige Unterscheidung zwischen Biomineralien und Mineralien aus rein anorganischem Ursprung eine der größten Herausforderungen in der Geobiologie dar. Ferner mangelt es an Informationen über jene Faktoren, die die Wechselwirkung zwischen Mikroorganismen und Mineralien beeinflussen sowie über die Folgen dieser Interaktionen innerhalb definierter Umgebungen.

Die Erforschung der wechselseitigen Beeinflussung von Mikroorganismen und abiotischen Faktoren erlaubt eine wesentlich bessere Vorhersage zahlreicher Stoffkreisläufe. Das Wissen darüber kann sich in vielen Feldern als vorteilhaft erweisen, etwa zur Verbesserung der Schwermetallextraktion bei der Biolaugung oder während der Biosanierung belasteter Ökosysteme.

Zielstellung dieser Dissertation ist die Gewinnung von Informationen über die Wechselwirkungsprozesse zwischen biotischen und abiotischen Bestandteilen in der Natur. Um solche Prozesse zwischen Mikroorganismen und Mineralien zu untersuchen, bietet sich die Raman-Spektroskopie als geeignete Methode an. Größter Vorteil der Raman-Spektroskopie gegenüber anderen Techniken ist die Möglichkeit, sowohl organisches als auch anorganisches Material sehr schnell und nach lediglich minimaler Probenpräparation analysieren zu können. Deshalb kann die Raman-Spektroskopie zur Identifizierung nicht nur von Bakterien, sondern auch von Mineralien angewandt werden.

Im Zuge dieser Arbeit wurden Bedingungen erforscht, die eine sichere Raman-spektroskopische Identifizierung von PHB-produzierenden Bakterien erlauben. Weiterhin wurde der Effekt mikrobieller Gemeinschaften auf die mineralogische Zusammensetzung neu gebildeten *lake snow* in einem sauren Restsee eines Braunkohletagebaus untersucht. Eine Quantifizierung der mineralischen Phasen in pelagischen Aggregaten sowie Informationen über Biozönosen und geochemische Parameter der aquatischen Umwelt führen zu einem besseren Verständnis der

Faktoren, welche Art und Umfang mineralogischer Zusammensetzung regulieren. Zusätzlich konnte die direkte Beteiligung von Mikroorganismen am Prozess der Eisenoolithbildung durch Raman-Spektroskopie nachgewiesen werden.

1 Summary

1.1 Motivation

During Earth history, the microbes were directly or indirectly responsible for dramatic changes of the Earth surface. For example, around 2.4 billion years ago, as a result of oxygenic photosynthesis by cyanobacteria, the Great Oxygenation Event occurred. The emergence of molecular oxygen as one of the main constituents of the Earth's atmosphere is a milestone in the history of life [1]. The abiotic oxidation of many chemical elements led to a tremendous growth in the diversity of minerals [2]. The Great Oxygenation Event attests the tremendous potential of the microbes to affect the environment. However the degree to which the microorganisms participate in mineral dissolution reactions, formation of new minerals or chemical exchange with aqueous solutions is not clear [3]. To definitively differentiate between a biomineral and an inorganically formed mineral represents one of the biggest challenges in the geobiology field. Furthermore, there is a lack of information concerning the factors which influence the interactions between the microorganisms and minerals as well as the outcome of these interactions occurring in a defined environment.

By determining how the microorganisms affect the abiotic factors, and how the abiotic factors influence the microbial consortium, various element cycles in nature could be predicted better. The implications are enormous, from improving metal extraction rate of bioleaching processes to bioremediation of polluted environments [4].

The aim of this doctoral thesis is to gain more information about the interaction processes which take place in nature between the biotic and abiotic components. The ultimate goal is to be able to increase the bioremediation rate by modifying accordingly the factors which influence the bioremediation. To be able to reach this goal, detailed studies focused on biomineralization, biotransformation and biodissolution are required. The influences of various geochemical factors on the microbial communities of an environment, and the response of microorganisms to those factors have to be studied.

Furthermore, information regarding the identity of the microorganisms forming the microbial consortium and their role played in the investigated environment is imperatively necessary [5].

Since more than 99% of the microbes are currently not cultivable in laboratory [6-8], an identification method which does not require cultivation is needed. Identification of the relevant population of a biological system mostly relies on phylogenetic based molecular techniques such as PCR-based methods or fluorescence *in situ* hybridization (FISH) [9]. Application of these genetic-based molecular techniques, however, is limited to species, for which, part of the genetic information is already available [10]. As an alternative to these molecular techniques, we propose Raman spectroscopy as a method for the identification of microorganisms. Previous investigations have shown that bulk and single cell bacterial identification is doable by means of Raman spectroscopy [11-20]. In addition, Raman spectroscopy can be used for identification of minerals [21-26], organic matter[27], liquids [28, 29] or gases [28-30] presented in the rocks. The high sensitivity, the minimal sample preparation required for Raman measurements and the possibility to investigate minerals instable at atmospheric conditions make Raman spectroscopy a valuable tool for the investigation of the minerals.

Hence, this spectroscopic technique might offer precious information regarding the bioremediation since it has the ability to investigate the biotic and abiotic elements involved in the interaction.

1.2 State of the art

1.2.1 PHB-producing bacteria and Raman spectroscopy

The microbial diversity of aquatic environments was initially studied through microscopy and cultivation. However, big discrepancies between the initial bacterial diversity and the outcome of the cultivation processes were noticed (“Great plate count anomaly”), and the scientific community realized that only a small number of microorganisms can be cultivated on solid or liquid media [31]. Later, analysis of the fatty acid methyl ester were performed for the analysis of microbial diversity [32]. However, the sensitivity of the method is low, identification at species level being impossible. The use of ribosomal DNA enabled investigation of bacterial communities by fingerprinting methods which separates fragments of rDNA based on length and/or nucleotide composition [33]. These methods includes: automated rRNA intergenic spacer analysis (ARISA), terminal restriction fragment length polymorphism (T-RFLP), temperature gradient gel electrophoresis (TGGE) or denaturing gradient gel electrophoresis (DGGE). The disadvantage of the fingerprinting approaches represents the poor sensitivity of the methods [33]. In addition, the abundance of various species can not be calculated using fingerprinting methods [34]. Other molecular methods for the study of microbial diversity include fluorescence *in situ* hybridization (FISH) and cloning/sequencing approaches [33]. The polymerase chain reaction (PCR) step used by the molecular methods for the amplification of targeted genes introduce discrepancies in microbial diversity since the DNA fragments are unequally amplified, depending on the DNA polymerase used and number of PCR cycles performed [33]. As alternative, PCR free approaches, for example whole-genome amplification (WGA) or whole-genome sequencing (WGS) could be used [35, 36]. However, the costs and complexity of the above mentioned methods represent important impediments for the large scale use [33, 36]. In addition, the DNA extraction step required by some of the molecular approaches can bias the outcome [37].

As an alternative to molecular methods for microbial identification, Raman spectroscopy is a technique relatively often applied for the identification of clinically relevant microorganisms [12, 16-20, 38-42]. The limited number of pathogens, the high sensitivity and specificity of Raman spectroscopy, minimal sample preparation

and the short time required for the spectroscopic measurements made Raman spectroscopy an attractive tool for the identification of clinically relevant microorganisms. Identification of microorganisms by means of Raman spectroscopy can be performed on bulk samples [11, 17-19] or on single cells [12, 43]. In case of bulk measurements, the acquired Raman spectrum represents the average Raman signal over thousands or millions of cells in a sample. Therefore, the phenotypic heterogeneity of a genetically homogeneous microbial culture is usually masked for bulk measurements [44]. For single cell measurements the phenotypic heterogeneity of a culture has much higher influence on the Raman outcome. This is particularly true when the microorganisms can accumulate storage materials within the cells, produce various dyes or sporulate [44, 45]. However, by performing single cell identification, the microorganisms' cultivation step can be omitted. This allows a fast identification process (very important in clinical investigations) and also identification of microorganisms which can not be cultivated in laboratory. Since only a minute number of bacteria can be currently cultivated in laboratory, a bacterial identification method independent of cultivation is essential in microbial ecology field.

Seldom Raman spectroscopy was used for the microbial identification from environmental samples. One of the reasons represent the high diversity of microorganism species present in natural environments [46]. A high diversity of microorganisms will impede the use of Raman spectroscopy for the study of bacterial community, since for the identification of microorganisms a Raman database is required. It is believed that the bacterial diversity and abundance in aquatic environments is usually orders of magnitude smaller than in soils and sediments [47]. In addition, geochemical factors like pH, salinity or heavy metals' concentrations have capital influence on the microorganisms' diversity. Torsvik *et al.* used a genomic approach for the study of bacterial consortium from various natural environments and found more than 11000 different genomes in sediments and soils with high organic content while in a salt-crystallizing pond (22% salinity) only 7 different genomes were detected [47]. Analysis of the microbial consortium of an ecosystem affected by the acid mine drainage reveal that few organism types dominate the analyzed communities [48]. Therefore, Raman spectroscopy could be used for the microbial identification from extreme environments.

Microorganisms which are able to live in extreme environments use various protection strategies for survival. One common strategy of microorganisms growing

in aquatic environments is the production of exopolysaccharides (EPS) which help them to adhere on hard surfaces, grow, and resist adverse conditions [49-52]. Carotenoids are used by various microbes as protective agents against UV radiation or as reactive oxygen species scavengers [53-57]. Endospores can be formed by various Gram-positive bacteria (mainly belonging to Firmicute phylum) in response to environmental stresses as a means to ensure the preservation and propagation of the genetic material of the cell [58, 59]. Numerous bacteria can synthesize and accumulate within the cells various substances as energy materials [60, 61]. Polyhydroxyalkanoates (PHAs) are polyesters of hydroxyalkanoates (HAs) produced by some bacteria under limiting nutrient conditions and in the presence of excess carbon source [62, 63]. These polymers are stored in the form of granules within the cells. Polyhydroxyalkanoates are considered interesting polymers because of their biodegradation potential. Therefore many investigations were performed towards increasing the rate of polymers accumulation in microbial cells [64-70], detection [71, 72] and quantification [10, 73-76] of the amounts of polymers stored by microorganisms or abiotic synthesis [77], and degradation of the biopolymers [78, 79]. Studies performed on various PHA-producing bacteria have shown that the polymers' species produced by these microorganisms are dependent on the carbon source used in the cultivation process [60]. More than 92 different storage polymers were identified until now in the bacterial cells, however, by far the most common is polyhydroxybutyrate (PHB) [80]. In addition, also the biosynthesis of copolymers is a relatively widespread phenomenon among PHA-producing bacteria [81]. However, very often polyhydroxybutyrate is the main phase of the carbon storage granules, other polymers being present only in small amounts [60]. The amounts of carbon storage granules varies from species to species, concentrations of PHB up to 80% of the total dry weight being measured for *Cupriavidus necator* (formerly *Ralstonia eutropha*, *Alcaligenes eutrophus*) cells [82]. PHB is considered to be a highly crystalline polymer, with a crystallinity between 50 and 80% [83]. However, X-ray diffractometry measurements performed by Kawaguchi *et al.* on native PHB granules of *Cupriavidus necator* revealed that the PHB granules in the intact cells were completely amorphous, but after treatment with sodium hypochlorite the PHB became crystalline. The authors speculated that a lipid is responsible for the stability of PHB granules in amorphous form, and only after the removal of the lipid the crystallization reaction can take place [84].

Since Raman spectroscopy is a technique which is not strongly affected by the amorphous state of a substance (in contrast to X-ray diffraction (XRD), for example), Raman measurements can and were performed for the investigation of the PHB and other polymers produced by bacteria. The crystallinity of PHB/poly(L-lactic acid) (PLLA) blends, a promising material in the biomedical applications, was investigated by means of Raman spectroscopy. In accordance with previous reports, the investigators found that PHB presented a high crystallinity even when it was mixed with the other polymer [85].

A semiquantification of the amount of polyhydroxyvalerate (PHV) in the copolymer PHB-co-PHV was performed by Izumi *et al.*. Although the Raman spectra of the copolymers were very similar, the authors showed that using FT Raman spectroscopy, the amount of PHV in the copolymer could be predicated [85]. Combining Raman spectroscopy with high-performance liquid chromatography (HPLC), De Gelder *et al.* showed that the amount of PHB intracellularly stored by *Cupriavidus necator* DSM 428 can be monitored using Raman spectroscopy [75]. While De Gelder *et al.* carried out Raman measurements on bulk samples, Hermelink *et al.* opted for single cell Raman measurements for the study of PHB production as a function of time in a bacterial culture of *Legionella bozemanii* [45].

Structural differences between the synthetic PHB, microbial PHB and PHB produced by genetically modified plants were also investigated using the Raman approach [86]. Based on the Raman signal of various storage molecules synthesized by distinct bacteria groups, discrimination between functionally relevant populations in enhanced biological phosphorus removal processes can be achieved [9]. However, to the best of our knowledge, we were the first research group which investigated the effect of the carbon storage molecules on the Raman identification results and defined the conditions required for a successful identification at species level of PHB-producing bacteria by means of this spectroscopic approach.

1.2.2 Biologically mediated iron oxides and hydroxides formation/transformation in sediments and their precursors

Iron is the most common element on Earth [87]. It can form a multitude of minerals, among these iron oxides and hydroxides being probably the most investigated forms of iron-containing minerals. The iron oxides are ubiquitous in almost all the

compartments of the global system: pedosphere, lithosphere, hydrosphere, atmosphere or biosphere [88], playing a tremendous role in soil science, geology, corrosion science, biology and industry [89]. Iron oxides have a multitude of commercial applications, being hard to imagine the world without them. However, there is also a negative side regarding them. Iron oxides and hydroxides appear all around the world as pollutants in acid mine drainage (AMD). A famous case of pollution by AMD is the Rio Tinto river from Spain, well known for the intense orange color of its water. AMD refers to acidic water rich in iron which appears as a result of biotic and abiotic oxidation of iron sulfides (mainly pyrite and marcasite) from metal and coal mines [26, 90, 91]. The products of iron sulfide oxidation are sulfuric acid which lowers the pH of the water and ferrous iron (Fe^{2+}) [90]. In addition, other heavy metals which were adsorbed or coprecipitated with the pyrite or marcasite can be mobilized. Ferrous iron is soluble in slightly acidic waters, in contrast to the oxidized form of iron, ferric iron (Fe^{3+}) which has a high solubility only at pH lower than ~ 2.5 [92, 93]. The orange color of the water affected by AMD is given by the precipitation of ferric hydroxides in the aquatic environment, formed as a result of the oxidation of ferrous iron [26]. The composition of the ferric precipitates is thought to be mainly determined by the pH and the concentration of sulfate in the aquatic system [94]. Analyses of various mine drainage ochres using XRD, scanning electron microscopy (SEM), transmission electron microscopy (TEM) and Fourier transform infrared spectroscopy (FTIR) have identified poorly crystalline ferrihydrite, lepidocrocite ($\gamma\text{-FeOOH}$), goethite ($\alpha\text{-FeOOH}$), jarosite ($\text{KFe}_3(\text{OH})_6(\text{SO}_4)_2$) and schwertmannite (ideal formula $\text{Fe}_8\text{O}_8(\text{OH})_6\text{SO}_4$) as the main iron phases precipitated from acid mine drainage [92, 95, 96]. To the best of our knowledge, no investigations of the inorganic phase of newly formed suspended particulate matter in iron rich aquatic environments were performed.

The study on the stability of different phases of iron oxides and hydroxides have revealed that, concentration, temperature, pH, size of the crystals or organic additives are factors which can decide the stable iron oxide/hydroxide phase in a particular environment [90, 97, 98]. The phase of the iron oxide/hydroxide present in a particular environment can influence the mobility of other elements since sorption processes can occur at the surface of the iron mineral [99, 100]. Not only the abiotic components are affected by the iron mineral phase, but also the biotic components. Dissolved organic compounds adsorbed by the iron minerals can serve as potential

electron donor for the activity of heterotrophic microorganisms. In addition, many bacteria use iron as electron donor or electron acceptor [101]. Investigations of the bacteria interaction with iron minerals have shown that the microorganisms usually prefer minerals with high surface area, for example ferrihydrite or schwertmannite [92, 102, 103]. It is well known that a high diversity of iron-reducing microorganisms can use ferrihydrite or schwertmannite as electron acceptor substrate [87, 104].

The iron minerals can influence the bacterial community structure, but also vice versa. In acidic aquatic environments, the abiotic oxidation of ferrous iron is a very slow process, bacteria being able to readily compete with the chemical oxidation [87]. As a result, microorganisms are responsible for the initiation of iron mineral formation. Not only in acidic aquatic environments bacteria play an important role in mineral formation; bacteria can oxidize ferrous iron also at circumneutral pH, however, in aerobic conditions the chemical oxidation of Fe^{2+} by oxygen is a fast process. Therefore many iron-oxidizing bacteria prefer microoxic or anoxic conditions, where the concurrence for ferrous iron is lower [87].

The initial iron colloids produced as a result of the biotic oxidation of ferrous iron have a poor crystallinity and can undergo transformations into more crystalline iron species. The transformations of the initial precipitates are dependent on the geochemistry of the environment and can involve a dissolution/reprecipitation step to form goethite, or a solid-state conversion to form hematite or magnetite [88, 105]. The precipitated iron minerals accumulate on the bottom of the aquatic environment where the iron-reducing microorganisms can use the precipitates as electron donor. In this way an iron cycle is created at water/sediment interface between the iron-oxidizing and iron-reducing microorganisms [92].

Redeposition of the freshly deposited iron minerals and their diagenesis in the sediments are common phenomena in the nature. As a result, in nature, the iron oxides and hydroxides tend to transform in time into their most thermodynamic stable forms under atmospheric surface conditions, goethite and hematite, respectively [89]. A common sedimentary rock type rich in ferrous minerals, often goethite and/or hematite is ironstone. Ironstones are defined as fine-grained sedimentary rocks having more than 15 wt.% iron [106, 107]. If the ironstones contain more than 5 vol.% ooids (spherical or ellipsoidal coated grains smaller than 2 mm), the rocks are called ooidal ironstones [107]. The origin of the ooids and the environmental conditions where the formation of those coated grains took place is still controversial, although the ooidal

ironstones are the most studied ironstone species [106, 108-110]. However, it is believed that at least in the case of some ooidal ironstones, bacteria, algae and/or fungi were directly involved in the formation of the laminar structure in ooids [109, 111-113].

Common techniques used for the study of ooidal ironstones include XRD [110-113], electron/proton microprobe [110, 113, 114], SEM [109, 111, 112] or energy-dispersive X-ray spectroscopy (EDX) [108, 114]. The structures similar with the bacterial, algal or fungal cells observed in some SEM images of oncoids made a number of researchers to conclude that microorganisms were intimately involved in the process of formation of the laminar structures. However, for a direct confirmation of the biotic origin of those structures, samples very well conserved (which contain organic matter) are required. To the best of our knowledge, our investigation was the first Raman spectroscopy study on ooidal ironstones.

For the analysis of various rocks, XRD is probably the most common technique employed [90, 96]. The main mineral phases of investigated samples can be detected by means of XRD, however problems appear for the identification of poorly crystalline or amorphous materials [115]. Other methods like SEM and TEM have a very good spatial resolution and provide information regarding the minerals' structures of the probe. Usually imaging techniques are combined with EDX or X-ray fluorescence (XRF), approaches which provide information regarding the elemental composition of the sample, for an unambiguously identification of the minerals [116, 117].

Raman spectroscopy became in the last decade a fast and reliable tool in the field of mineral identification. The minimal sample preparation required for analysis of minerals, the high sensitivity and specificity of the method and the possibility to analyze matter in solid, liquid or gaseous state made this spectroscopic technique attractive for mineralogists and geologists. However, the biggest advantage of Raman spectroscopy in comparison with other techniques represents the possibility to investigate both organic and inorganic materials very fast and with minor sample preparation. Therefore, for the study of interactions between the microbes and minerals, the potential of Raman spectroscopy is enormous.

1.3 Own research results

In the following sections, results obtained within the framework of the thesis are presented. Our aim was to investigate the interaction between the biotic and the abiotic components of an iron contaminated aquatic environment. The investigation of the bacterial-mineral interactions implies two studies: the influence of the microbial communities on the mineral phases of the pelagic aggregates, and the effect of the geochemical conditions of the aquatic environment on the microbial consortia. To be able to study differences in the bacterial communities by means of Raman spectroscopy, the identification of the microbes is required.

The starting point of the research was the Raman investigation of microorganisms which could play an important role in bioremediation of freshwater habitats affected by acid mine drainage.

1.3.1 Towards the identification of microorganisms potentially involved in the biomineralization processes by means of Raman spectroscopy

Preliminary investigations of our collaborators have shown that *Acidiphilium cryptum* JF-5 was present in different samples collected from various locations of the lignite mine lake and this strain might be important for the ferric iron reduction process in the lake (Lake 77, located in the Lusatian mining area in east-central Germany). Therefore, the first bacterium investigated by means of Raman spectroscopic technique was *Acidiphilium cryptum* JF-5. *A. cryptum* JF-5 is an acidophilic facultative anaerobe bacterium which can reduce both Fe(III) and Cr(VI) to Fe(II) and Cr(IV), respectively. Bacteria using different electron acceptors (oxygen and ferric iron), and in various physiological status (lag phase, exponential phase and stationary phase), were investigated using micro-Raman spectroscopy. Surprisingly, the obtained Raman spectra showed important differences in comparison with the Raman spectra of various microorganisms reported in literature (Fig. 1 in [VC1]) [11, 12]. In addition, important differences in the Raman spectra of the cells both in exponential phase and stationary phase were detected (Fig. 4 in [VC1]). In the Raman spectra of the microbial cells in stationary phase, the signals from an unknown substance completely covered the Raman signals from the other cell components. In case of the bacteria in exponential phase, the signals from the unidentified compound were weaker, the Raman bands of the nucleic acids and proteins, for example, being still

visible. For the identification of the unknown compound we combined Raman spectroscopy with fluorescence imaging. *A. cryptum* JF-5 cells were stained with Nile red, a fluorescent dye used for the detection of polyhydroxybutyrate (PHB) in microorganisms [118]. Both types of cells, fluorescent and non-fluorescent, were afterwards measured by means of Raman spectroscopy. The Raman spectra of the fluorescent cells were similar with the Raman spectra of the cells containing the unknown compound, while the Raman spectra of the non-fluorescent cells resembled the bacterial Raman spectra reported by various researchers in literature (Fig. 2 in [VC1]). Based on this outcome, we were able to conclude that the unknown compound stored in the cells was PHB. Polyhydroxybutyrate is a polymer produced by a large number of microorganisms as carbon and energy storage [119, 120]. The compound is usually produced by bacteria growing under stress conditions, and can be accumulated intracellularly by microbes in high amounts [69]. Therefore, it is expected that a high number of microorganisms living in contaminated habitats have the ability to produce storage materials. Since our ultimate aim is to investigate microorganisms from polluted environments, an investigation focused on identification of PHB-producing bacteria was imperative. Furthermore, the conditions required for a successful identification by means of Raman spectroscopy should be determined.

Bacillus megaterium DSM 90 (Firmicutes; Gram positive), three strains of *Bacillus thuringiensis* (DSM 530, DSM 5725 and ATCC10782) (Firmicutes; Gram positive), *Azohydromonas lata* DSM 1122 (Betaproteobacteria; Gram negative), *Cupriavidus necator* DSM 428 (Betaproteobacteria; Gram negative) and *Acidiphilium cryptum* JF-5 (Alphaproteobacteria; Gram negative) were used in this study. Single bacterial cell Raman measurements were performed on the above mentioned bacterial culture in exponential phase.

By combining Raman spectroscopy with chemometrical methods, circa 90% of the measured microorganisms have been correctly identified using a Support Vector Machine (SVM) (Table 2 in [VC1]). Since the production of storage materials depends on the physiological status of the microorganisms, the identification rate is influenced by the age of the investigated culture. In case of a culture of bacteria producing high amounts of PHB in stationary phase, the identification by means of Raman spectroscopy is not doable due to the fact that the Raman spectra of the

microorganisms will contain only signals from the storage material, the signals from the other components of the cell will be completely overlapped.

The present contribution demonstrates that the presence of PHB in microbial cells does not hamper Raman spectroscopic identification as long as the microorganisms are in the exponential growth phase.

The outcome of the study defines the conditions required for a successful identification of PHB producing bacteria. Since a high number of bacteria can produce carbon storage molecules, the implications of the above presented study are enormous. As we already mentioned in the second chapter, production of carbon storage molecules is a strategy used by some bacteria to survive in harsh conditions [121]. Ayub *et al.* have suggested a connection between PHB accumulation and high stress resistance developed by the bacteria adopted to extreme environments [122]. Therefore, it is expected (and our preliminary results have shown) that many microorganisms living in an extreme environment to be able to produce and accumulate PHB. Consequently, for a successful identification of microorganisms grown in a harsh environment using Raman spectroscopy, the outcome of the present study should be considered.

1.3.2 Qualitative analysis of the pelagic particulate matter from Lake 77

To investigate the effect of bacterial community on the formation process of pelagic aggregates, data regarding the mineralogy of the freshly formed colloids are required. In addition, identification of the microbes forming the bacterial community is needed. Microbial consortium of a natural aquatic environment is dependent on a multitude of geochemical factors. Therefore, the information regarding the bacterial identity and the mineralogy of the freshly formed pelagic aggregates has to be correlated with the data concerning the geochemical parameters for a correct understanding of the interaction processes which occur in the aquatic environment.

Our aim was to perform a qualitative analysis on the mineralogy of the pelagic aggregates formed in Lake 77 and to correlate the Raman outcome with the information concerning other biogeochemical parameters.

Lake 77 is an acidic lignite mine lake having a surface area of $\sim 0.24 \text{ km}^2$, a volume of $\sim 1 \text{ km}^3$ and a maximum depth of about 9 m. The Northern basin of the lake is separated from the rest by a sill in the bottom of the lake that rise to about 4 m depth

(Fig. 1 in [VC2]). Central basin shows a dimictic stratification scenario with spring and fall mixes, while the stratification remains stable in the Northern basin with an oxic surface water layer and a deeper anoxic water layer separated by a sharp redoxcline. The oxic water layer showed similar characteristics in both basins with pH values of about 3, sulfate concentrations of circa 8 mM and Fe(III) concentrations of about 8 mM and 2 mM respectively. No Fe(II) was detected in the two basins in the oxic region (Fig. 2 in [VC2]). In the anoxic layer of the Central and Northern basin, the pH has a value of 3 and 6, sulfate concentrations reach 10.3 and 15.4 mM, whereas Fe(II) concentrations increased to 1.1 and 1.7 mM, respectively (Table 1 in [VC3]).

The analysis of the microbes habiting the anoxic layer from Northern and Central basin of the lake reveal important differences in the bacterial consortia (Fig. 7 in [VC2]).

Due to the considerable variations in the bacterial communities and water chemistry of the Central basin and Northern basins, different mineral phases of iron minerals were expected to be present in the two anoxic regions.

Pelagic aggregates called Iron Snow (IS), formed in the Lake 77 were collected from the anoxic regions of the Northern and Central basins. These aggregates are formed in the redoxcline region of the aquatic environment and contain a relatively low amount of organic matter. Since the pH values of the redoxcline basins are around 3, the oxidation of the Fe(II) to Fe(III) is mainly biologically mediated. Therefore, the iron oxidizing bacteria are directly involved in the initiation of the mineral formation process.

Preliminary Raman measurements of the IS samples performed under anoxic conditions (the samples were measured in a glass cell in the absence of oxygen) and oxic conditions (the samples were dried on the substrate and measured in atmospheric conditions) revealed no difference in the mineral phases of the samples. Since a higher signal noise ratio was obtained for the spectra measured under oxic conditions, therefore, all further measurements of IS samples were performed in atmospheric conditions.

A detailed Raman analysis of the inorganic phase of the IS from the two locations has revealed the presence of schwertmannite in many of the investigated spots. Schwertmannite is a mineral which is usually formed in acidic fresh waters rich in dissolved iron and sulfate, and is stable at a pH falling in the range of 3 to 5.

However, in anoxic conditions at higher pH values and in the presence of ferrous iron, the stability of the schwertmannite decrease drastically [123]. The interactions between Fe(III) and $(\text{SO}_4)^{2-}$ in schwertmannite and in acidic liquid solution are similar, being probably the reason why schwertmannite is a common mineral of the acid main drainage [124]. The transformation rate of schwertmannite into goethite is enhanced a few order of magnitude by the sorption of Fe(II) cations on the surface of the mineral.

Goethite was identified in samples from the Central basin. Goethite might appear in the samples as a result of the dissolution/recrystallization process of the schwertmannite colloids. Alternatively, goethite could be a direct product of the biotic oxidation of ferrous iron.

Using Raman spectroscopy, ferrihydrite was detected in a small amount in the lake aggregates from the anoxic layer of the Central basin. Due to the poor crystallinity of schwertmannite and ferrihydrite, discrimination between the two minerals is difficult by means of conventional X-ray diffraction approach [125]. However, the Raman spectra of the two iron minerals are quite different, a fast and reliable identification of the two minerals by means of Raman spectroscopy being doable.

Ferrihydrite is a common iron mineral, utilized by various bacteria as a sink for electrons or produced by other iron oxidizing microorganisms, especially at circum-neutral pH conditions. The presence of ferrihydrite in a region where the pH of the water is 3 could be due to a number of acidophilic or acid tolerant microorganisms which preferentially dictate the formation of this mineral in the anoxic layer of the Central basin.

Jarosite was also detected by means of Raman spectroscopy in the samples from the Central basin. Jarosite is a mineral which can be formed only in acid environments, being stable at pH lower than 3 [90, 94, 126].

In addition to the above mentioned iron minerals, disordered carbon, quartz and gypsum were detected in samples from the Central basin.

The probes originating from the Northern basin mainly consists of schwertmannite, ferrihydrite, disordered carbon and gypsum as revealed by the Raman investigation.

The presence of ferrihydrite in the samples collected from Central basin (pH 3), and of schwertmannite in the probes from Northern basin (pH 6) could be explained by the biotic influence on the inorganic phase of the pelagic aggregates. The formation of

schwertmannite appeared to be a microbial mediated process, which is independent of the pH and the microbial community structures.

Our investigation attests that the microbes affect the inorganic phases of the aggregates formed in an iron-contaminated environment.

However, the magnitude of the biotic effect on the mineralogy of the aggregates is not clear from the qualitative results presented here. In addition, it is difficult to correlate the Raman results with the microbial identification results obtained by our collaborators.

Therefore, for a better understanding of the influence of microbes on the geochemical parameters of the environment, a semi-quantitative investigation of the mineralogy of the pelagic aggregates is required.

1.3.3 Quantification of the inorganic phase of the pelagic aggregates formed in the acidic lignite mine lake

The pelagic aggregates are thought to be formed in the redoxcline region of the aquatic environment. Therefore, investigation of the mineral phase of the aggregates collected from the redoxcline and the anoxic region of a basin would provide information about the transformations of the metastable minerals which could occur after the formation of the aggregates and till their deposition on the bottom of the lake. Therefore, we decided to investigate the organic and inorganic phases of the aggregates collected from the redoxcline and anoxic regions of the Central and Northern basin.

Analysis of the bacterial communities from the Central basin (redoxcline and anoxic layers) revealed similar communities. Surprisingly, also the microbial consortia from the Northern basins are extremely similar, although the differences in the pH value and the concentration of ferrous iron between the two layers are important. These similarities suggested the majority of the microorganisms are metabolically active over the broad pH and oxygen range detected from redoxcline to the deeper water layer. However, communities of IS particles sampled in the Central and in the Northern basin were in accordance with our previous study - dissimilar (Fig. 4 in [VC3]).

For the quantification of the inorganic phase of the IS, we use the Raman imaging approach. The IS samples were spread in a thin layer on a glass substrate and dried at room temperature.

The Raman analysis of the lake aggregates revealed that the dominated mineral in all four locations was schwertmannite (Table 2, in [VC3]). The amount of schwertmannite in the IS varies from 88% in the samples from the anoxic layer of the Northern basin to 97% in the samples from the redoxcline of the Central basin. The high amounts of schwertmannite detected also in the samples from the anoxic monimolimnion of the north site could be explained by the presence of organic matter on the surface of the aggregates which hinders the sorption of Fe(II) on the IS [127].

The other mineral presented in all the investigated samples is disordered carbon, a typical compound of an acidic lignite mine lake.

Ferrihydrite was detected in small amounts in the anoxic waters of both basins and in the microcline region of the Northern basin. In the samples from the anoxic region of the Northern basin goethite was identified by means of Raman spectroscopy. Goethite represents probably the product of the abiotic transformation of schwertmannite at higher pH values. In the microoxic layer of the same basin, hematite was detected. The occurrence of the iron oxide only in the redoxcline of the Northern basin and not in the anoxic region might be due to the enhanced activity of Fe(III) reducing bacteria, the reduction of the mineral taking place before reaching the bottom layer of the lake. Other minerals detected by means of Raman spectroscopy in the IS samples were quartz, calcite, barite, anatase and rutile.

In our previous Raman investigation, small amount of jarosite and goethite were detected in the aggregates from Central basin. However, no jarosite was found in this study while goethite was detected only in anoxic layer of the Northern basin. This could be due to sampling variation or different sampling time, or the above mentioned minerals were formed only under some known specific conditions from schwertmannite, and/or might be present in the IS in very small amounts, below the Raman detection limit.

The Raman imaging results have shown that schwertmannite represent the dominated mineral phase in the Iron Snow, irrespective to the microbial communities from different spots of the lake. Although the microorganisms initiate the process of formation of iron minerals, the geochemical conditions of the aquatic environment dictate the main mineral phases of the aggregates. However, the microorganisms

influence the stability of the newly formed particulates by reducing the number of available sorption sites on the surface of the iron minerals.

1.3.4 Investigation of Middle Eocene ironstones – confirmation of the microorganisms' involvement in the ooidal ironstone formation process

Till now we saw that Raman spectroscopy can be reliably applied to study the newly formed precipitates. The next step was to apply the same technique for investigations of million of years old sediments, which were subjected to various diagenesis processes.

Micro-Raman spectroscopy was applied in the solution of a geological problem concerning the origin of the Egyptian Middle Eocene ironstones. These ironstone deposits are subdivided into two, lower and upper, sequences. The ironstone sequences investigated in this study consist of four shallow marine iron ore types: manganese mud-ironstone, fossiliferous ironstone, stromatolitic ironstone and nummulitic-ooidal-oncoidal ironstone. Due to the subaerial weathering of the upper surfaces of these sequences, a lateritic iron ore type was formed.

The aim of the investigation was to gain more information about the complex environmental conditions prevailed during and after the ironstone formation.

As the name of the rocks suggests, the main components of the stones are the iron minerals. Raman spectroscopic analysis of the mud and fossiliferous ironstones reveals that goethite and hematite are the main components of the rocks. A high diversity of manganese minerals was identified in these stones: aurorite ((Mn²⁺,Ag,Ca)Mn⁴⁺₃O₇•3(H₂O)), hollandite ((Ba(Mn²⁺,Mn⁴⁺)₈O₁₆) romanechite ((Ba,H₂O)₂(Mn⁴⁺,Mn³⁺)₅O₁₀), manjiroite ((Na,K)(Mn⁴⁺,Mn²⁺)₈O₁₆ •n(H₂O)), todorokite ((Na,Ca,K)₂(Mn⁴⁺,Mn³⁺)₆O₁₂•3–4.5(H₂O)) and pyrolusite (MnO₂) were detected. In addition to iron and manganese minerals, detrital minerals such as microcline, orthoclase, quartz, rutile and late-cementic minerals as anhydrite, calcite and barite were identified in the samples.

The stromatolitic laminae and the cortical laminae of the ooids and oncoids are primarily composed of goethite mixed with small amounts of jarosite, whereas hematite is mainly detected as cement surrounding the ooids and oncoids. As we already mentioned earlier, jarosite is a mineral that can only be formed in acidic environments via oxidation of iron sulfates. The identification of another mineral

formed in acidic conditions, romanechite, supports the conclusion that during the formation or diagenesis of the stromatolites, ooids and oncooids, the aquatic environment became acidic.

Other manganese minerals detected in the laminae using the Raman approach were pyrolusite and hollandite. Sulfates (gypsum ($\text{CaSO}_4 \cdot 2\text{H}_2\text{O}$), anhydrite (CaSO_4) and barite (BaSO_4)), carbonates (calcite (CaCO_3) and dolomite ($\text{CaMg}(\text{CO}_3)_2$)), silicates (quartz (SiO_2)) and phosphates (apatite ($\text{Ca}_5(\text{PO}_4, \text{CO}_3)_3(\text{F}, \text{Cl}, \text{OH}, \text{CO}_3)$)) were also detected in the stromatolitic and ooidal-oncooidal ironstones. The presence of apatite demonstrates the involvement of biotic components in the formation of these ironstones, since phosphorous is thought to originate from the decay of organic matter [128, 129].

In addition to minerals, organic matter was detected in the laminae of the stromatolitic and ooidal-oncooidal ironstones, as well (Figure 5, in [VC3]). Figure 5(a) displays the Raman spectrum of a carotenoid with its characteristic sharp Raman bands at 1000, 1150 and 1515 cm^{-1} . The position and the sharpness of the Raman bands suggest that the organic compounds were very well preserved in the rocks. A large variety of organisms can produce different types of carotenoids, therefore the carotenoids can represent biomarkers for bacteria, fungi and/or algae. Also cellulose was detected in the investigated laminae. However, no lignin was detected in the samples, therefore the cellulose probably originates from algae and/or cyanobacteria and not from more complex organisms.

In conclusion, detection of various preserved organic materials inside the stromatolitic laminae and the cortical laminae of the ferrous oncooids and ooids support the hypothesis that the formation of the laminae was a biological mediated process. Earlier studies of the stromatolitic and oncooidal-ooidal cortical laminae performed mostly by means of electron microscopy suggested that cyanobacteria or in some cases fungi were the main microorganisms involved in the formation process of these structures [109, 111, 130, 131]. Almost all cyanobacteria produce carotenoids, therefore the Raman outcome support the hypothesis regarding the involvement of cyanobacteria in the minerals' formation process. Furthermore, the Raman results suggest that also algae might be involved in the bio-mediated process of minerals' formation.

In addition, Raman spectroscopic investigations of the mineral phase of the iron stones reveal information regarding changes in the environmental conditions during

the ironstones formation/diagenesis. The detection of romanechite, jarosite and anglesite attests that during the rocks formation/diagenesis process, the aquatic environment became acidic. The presence of sulfate and carbonate minerals as cavity filling materials indicates mineralogical and chemical alterations typical for the young weathering crusts in the arid zone of NE Africa's desert.

To the best of our knowledge, this contribution is the first which directly confirms the active role of microorganisms in the formation of stromatolites, oncoids and ooids. Until now, the only data attesting the involvement of microorganisms in the formation of the laminae structures were provided by the SEM images showing structures similar with bacterial or algal cells. Using Raman spectroscopy we were able to undoubtedly identify organic compounds, typical for cyanobacteria and algae, in the stromatolitic and oncoidal-ooidal cortical laminae.

1.4. Conclusions and further work

The outcome of the investigations presented in the previous chapter demonstrates that spectroscopic techniques, especially Raman spectroscopy, can be successfully applied to gain valuable information regarding the interaction between microorganisms and minerals. By detecting organic material within the laminae of stromatolites, ooids and oncoids, we were able to demonstrate that the microorganisms were intimately involved in the formation of the Eocene ironstones from Bahariya Depression, West Desert, Egypt. Furthermore, the Raman results suggest that not only cyanobacteria could be involved in the minerals formation process but also algae.

This spectroscopic technique can be used not only for the analysis of millions years old stones but also for the investigation of recently formed minerals. Combining Raman spectroscopy with denaturing gradient gel electrophoresis (DGGE) and water chemistry measurements, we were able to investigate the role played by microorganisms in the process of minerals formation in an acidic iron-rich mine lake. Quantitative analysis of freshly formed minerals in an acidic lignite mine lake performed by means of Raman spectroscopy showed that, although the iron oxidation is mainly a microbial process, the iron mineral species forming the pelagic aggregates are dictated by the geochemical conditions of the aquatic environment. Only minor amounts of iron minerals species could be directly related to bacterial activity.

For a better understanding of the role played by bacteria in the biomineralization process, identification of the microorganisms' species which form the bacterial community of the aquatic environment is required. A possible approach of this problem is single cell bacterial identification by means of micro-Raman spectroscopy. A preliminary analysis of *Acidiphilium cryptum* JF-5, a microorganism isolated from the investigated lignite mine lake, showed that storage materials are produced in large amounts within the bacterial cells belonging to this strain. Therefore, investigation of the influence on storage materials on the identification ability of Raman spectroscopy in combination with chemometrical methods was performed. The outcome suggests that the bacterial identification by means of Raman spectroscopy is still doable as long as the bacterial cell do not present PHB in crystalline form.

Further work should be focused on the direct identification of bacteria from the studied aquatic environment. A bacterial extraction procedure based on the dissolution of iron minerals has been already established in our laboratory. A Raman database of the microbial isolates from the investigated lake should be constructed. Based on this database, an attempt to identify the elements of the microbial community of the lake should be made. The above proposed approach can be applied for the identification of the cultivable bacteria which were isolated from the studied aquatic environment. If the large majority of the microorganisms forming the bacterial community of the lake are cultivable species, then the Raman output will provide valuable information about the microbial consortium and the role played by various species in the aquatic environment. However, if only a minute part of the bacterial community is represented by the cultivable microorganisms, then a new approach is required. An alternative is to combine Raman spectroscopy with other bacterial identification technique which does not require microorganisms' cultivation, for the creation of the Raman database. For example, Raman spectroscopy can be elegantly combined with fluorescence *in situ* hybridization (FISH). However, in this case the accuracy of the Raman results will be directly related to the accuracy of the method used for the identification of the microbes which were measured for the Raman database.

Bibliography

- [1] A.L. Sessions, D.M. Doughty, P.V. Welander, R.E. Summons, D.K. Newman, *Current Biology*, The continuing puzzle of the Great Oxidation Event 19 (2009) R567-R574.
- [2] D.A. Sverjensky, N. Lee, *Elements*, The Great Oxidation Event and mineral diversification 6 (2010) 31-36.
- [3] A. Templeton, E. Knowles, *Annual Review of Earth and Planetary Sciences*, Microbial transformations of minerals and metals: Recent advances in geomicrobiology derived from synchrotron-based X-ray spectroscopy and X-ray microscopy 37 (2009) 367-391.
- [4] J.-c. Lee, B.D. Pandey, *Waste Management*, Bio-processing of solid wastes and secondary resources for metal extraction - A review 32 (2012) 3-18.
- [5] A. Konopka, *The ISME Journal*, What is microbial community ecology? 3 (2009) 1223-1230.
- [6] W.E. Huang, A.D. Ward, A.S. Whiteley, *Environmental Microbiology Reports*, Raman tweezers sorting of single microbial cells 1 (2009) 44-49.
- [7] W.E. Huang, M. Li, R.M. Jarvis, R. Goodacre, S.A. Banwart, I.L. Allen, S. Sima, M.G. Geoffrey, *Advances in applied microbiology*, Academic Press, 2010, pp. 153-186.
- [8] S.G. Tringe, E.M. Rubin, *Nature Reviews Genetics*, Metagenomics: DNA sequencing of environmental samples 6 (2005) 805-814.
- [9] N. Majed, T. Chernenko, M. Diem, A.Z. Gu, *Environmental Science & Technology*, Identification of functionally relevant populations in enhanced biological phosphorus removal processes based on intracellular polymers profiles and insights into the metabolic diversity and heterogeneity (2012) DOI: 10.1021/es300044h.
- [10] N. Majed, A.Z. Gu, *Environmental Science & Technology*, Application of Raman microscopy for simultaneous and quantitative evaluation of multiple intracellular polymers dynamics functionally relevant to enhanced biological phosphorus removal processes 44 (2010) 8601-8608.
- [11] K. Maquelin, L.-P.i. Choo-Smith, T. van Vreeswijk, H.P. Endtz, B. Smith, R. Bennett, H.A. Bruining, G.J. Puppels, *Analytical Chemistry*, Raman spectroscopic method for identification of clinically relevant microorganisms growing on solid culture medium 72 (2000) 12-19.

-
- [12] M. Harz, P. Rosch, K.D. Peschke, O. Ronneberger, H. Burkhardt, J. Popp, *Analyst*, Micro-Raman spectroscopic identification of bacterial cells of the genus *Staphylococcus* and dependence on their cultivation conditions 130 (2005) 1543-1550.
- [13] P. Rösch, M. Harz, M. Schmitt, K.-D. Peschke, O. Ronneberger, H. Burkhardt, H.-W. Motzkus, M. Lankers, S. Hofer, H. Thiele, J. Popp, *Applied and Environmental Microbiology*, Chemotaxonomic identification of single bacteria by micro-Raman spectroscopy: Application to clean-room-relevant biological contaminations 71 (2005) 1626–1637.
- [14] P. Rösch, M. Harz, K.-D. Peschke, O. Ronneberger, H. Burkhardt, A. Schüle, G. Schmauz, M. Lankers, S. Hofer, H. Thiele, H.-W. Motzkus, J. Popp, *Analytical Chemistry*, On-line monitoring and identification of bioaerosols 78 (2006) 2163-2170.
- [15] P. Rösch, M. Harz, K.D. Peschke, O. Ronneberger, H. Burkhardt, J. Popp, *Biopolymers*, Identification of single eukaryotic cells with micro-Raman spectroscopy 82 (2006) 312-316.
- [16] C. Kirschner, K. Maquelin, P. Pina, N.A. Ngo Thi, L.-P. Choo-Smith, G.D. Sockalingum, C. Sandt, D. Ami, F. Orsini, S.M. Doglia, P. Allouch, M. Mainfait, G.J. Puppels, D. Naumann, *Journal of Clinical Microbiology*, Classification and identification of enterococci: a comparative phenotypic, genotypic, and vibrational spectroscopic study 39 (2001) 1763–1770.
- [17] K. Maquelin, C. Kirschner, L.P. Choo-Smith, N. van den Braak, H.P. Endtz, D. Naumann, G.J. Puppels, *Journal of Microbiological Methods*, Identification of medically relevant microorganisms by vibrational spectroscopy 51 (2002) 255-271.
- [18] P.C.A.M. Buijtels, H.F.M. Willemsse-Erix, P.L.C. Petit, H.P. Endtz, G.J. Puppels, H.A. Verbrugh, A. van Belkum, D. van Soolingen, K. Maquelin, *Journal of Clinical Microbiology*, Rapid identification of mycobacteria by Raman spectroscopy 46 (2008) 961–965.
- [19] A.J. Berger, Q. Zhu, *Journal of Modern Optics*, Identification of oral bacteria by Raman microspectroscopy 50 (2003) 2375-2380.
- [20] K. Maquelin, L.-P. Choo-Smith, H.P. Endtz, H.A. Bruining, G.J. Puppels, *Journal of Clinical Microbiology*, Rapid identification of *Candida* species by confocal Raman microspectroscopy 40 (2002) 594–600.
- [21] S.K. Sharma, A.K. Misra, P.G. Lucey, R.C.F. Lentz, *Spectrochimica Acta Part A: Molecular and Biomolecular Spectroscopy*, A combined remote Raman and LIBS

instrument for characterizing minerals with 532 nm laser excitation 73 (2009) 468-476.

[22] P. Vargas Jentsch, B. Kampe, P. Rösch, J. Popp, *The Journal of Physical Chemistry A*, Raman spectroscopic study of crystallization from solutions containing MgSO₄ and Na₂SO₄: Raman spectra of double salts 115 (2011) 5540-5546.

[23] R.L. Frost, R.-A. Wills, M.L. Weier, W. Martens, S. Mills, *Spectrochimica Acta Part A: Molecular and Biomolecular Spectroscopy*, A Raman spectroscopic study of selected natural jarosites 63 (2006) 1-8.

[24] J. Jehlička, P. Vitek, H.G.M. Edwards, M. Heagraves, T. Čapoun, *Spectrochimica Acta Part A: Molecular and Biomolecular Spectroscopy*, Application of portable Raman instruments for fast and non-destructive detection of minerals on outcrops 73 (2009) 410-419.

[25] Z.C. Ling, A. Wang, *Icarus*, A systematic spectroscopic study of eight hydrous ferric sulfates relevant to Mars 209 (2010) 422-433.

[26] P. Sobron, A. Sanz, T. Acosta, F. Rull, *Spectrochimica Acta Part A: Molecular and Biomolecular Spectroscopy*, A Raman spectral study of stream waters and efflorescent salts in Rio Tinto, Spain 71 (2009) 1678-1682.

[27] P. Vandenberghe, H.G.M. Edwards, L. Moens, *Chemical Reviews*, A decade of Raman spectroscopy in art and archaeology 107 (2007) 675-686.

[28] A. Wesełucha-Birczyńska, M. Słowakiewicz, L. Natkaniec-Nowak, L.M. Proniewicz, *Spectrochimica Acta Part A: Molecular and Biomolecular Spectroscopy*, Raman microspectroscopy of organic inclusions in spodumenes from Nilaw (Nuristan, Afghanistan) 79 (2011) 789-796.

[29] N. Zhang, Z. Tian, Y. Leng, H. Wang, F. Song, J. Meng, *Science in China Series D: Earth Sciences*, Raman characteristics of hydrocarbon and hydrocarbon inclusions 50 (2007) 1171-1178.

[30] N. Guilhaumou, D. Jouffre, B. Velde, C. Beny, *Bulletin de minéralogie*, Raman microprobe analysis on gaseous inclusions from the diagenetically altered Terres noires (S-E, France) 111 (1988) 577-585.

[31] J.T. Staley, A. Konopka, *Annual Review of Microbiology*, Measurement of *in situ* activities of nonphotosynthetic microorganisms in aquatic and terrestrial habitats 39 (1985) 321-346.

-
- [32] B.J. Brown, L.G. Leff, *Applied and Environmental Microbiology*, Comparison of fatty acid methyl ester analysis with the use of API 20E and NFT strips for identification of aquatic bacteria 62 (1996) 2183-2185.
- [33] L. Zinger, A. Gobet, T. Pommier, *Molecular Ecology*, Two decades of describing the unseen majority of aquatic microbial diversity 21 (2012) 1878-1896.
- [34] S.J. Bent, J.D. Pierson, L.J. Forney, *Applied and Environmental Microbiology*, Measuring species richness based on microbial community fingerprints: the emperor has no clothes 73 (2007) 2399-2401.
- [35] V. Lazarevic, K. Whiteson, N. Gaia, Y. Gizard, D. Hernandez, L. Farinelli, M. Osteras, P. Francois, J. Schrenzel, *Journal of Clinical Bioinformatics*, Analysis of the salivary microbiome using culture-independent techniques 2 (2012) 4.
- [36] A.C. Schürch, D. van Soolingen, *Infection, Genetics and Evolution*, DNA fingerprinting of *Mycobacterium tuberculosis*: From phage typing to whole-genome sequencing 12 (2012) 602-609.
- [37] F.V. Wintzingerode, U.B. Göbel, E. Stackebrandt, *FEMS Microbiology Reviews*, Determination of microbial diversity in environmental samples: pitfalls of PCR-based rRNA analysis 21 (1997) 213-229.
- [38] A. Tripathi, R.E. Jabbour, P.J. Treado, J.H. Neiss, M.P. Nelson, J.L. Jensen, A.P. Snyder, *Applied Spectroscopy*, Waterborne pathogen detection using Raman spectroscopy 62 (2008) 1-9.
- [39] B.S. Luo, M.I.N. Lin, *Journal of Rapid Methods & Automation in Microbiology*, A portable Raman system for the identification of foodborne pathogenic bacteria 16 (2008) 238-255.
- [40] K.S. Kalasinsky, T. Hadfield, A.A. Shea, V.F. Kalasinsky, M.P. Nelson, J. Neiss, A.J. Drauch, G.S. Vanni, P.J. Treado, *Analytical Chemistry*, Raman chemical imaging spectroscopy reagentless detection and identification of pathogens: signature development and evaluation 79 (2007) 2658-2673.
- [41] S. Stöckel, S. Meisel, M. Elschner, P. Rösch, J. Popp, *Angewandte Chemie International Edition*, Raman spectroscopic detection of anthrax endospores in powder samples (2012) DOI: 10.1002/anie.201201266.
- [42] H. Yang, J. Irudayaraj, *Journal of Molecular Structure*, Rapid detection of foodborne microorganisms on food surface using Fourier transform Raman spectroscopy 646 (2003) 35-43.

-
- [43] S. Meisel, S. Stöckel, M. Elschner, F. Melzer, P. Rösch, J. Popp, *Applied and Environmental Microbiology*, Raman spectroscopy as a potential tool for detection of *Brucella* spp. in milk (2012) DOI: 10.1128/AEM.00637-00612
- [44] A. Hermelink, A. Brauer, P. Lasch, D. Naumann, *Analyst*, Phenotypic heterogeneity within microbial populations at the single-cell level investigated by confocal Raman microspectroscopy 134 (2009) 1149-1153.
- [45] A. Hermelink, M. Stammer, D. Naumann, *Analyst*, Observation of content and heterogeneity of poly- β -hydroxybutyric acid (PHB) in *Legionella bozemanii* by vibrational spectroscopy 136 (2011) 1129-1133.
- [46] V. Torsvik, F.L. Daae, R.-A. Sandaa, L. Øvreås, *Journal of Biotechnology*, Novel techniques for analysing microbial diversity in natural and perturbed environments 64 (1998) 53-62.
- [47] V. Torsvik, L. Øvreås, T.F. Thingstad, *Science*, Prokaryotic diversity - magnitude, dynamics, and controlling factors 296 (2002) 1064-1066.
- [48] P.L. Bond, G.K. Druschel, J.F. Banfield, *Applied and Environmental Microbiology*, Comparison of acid mine drainage microbial communities in physically and geochemically distinct ecosystems 66 (2000) 4962-4971.
- [49] N.P. Ivleva, M. Wagner, A. Szkola, H. Horn, R. Niessner, C. Haisch, *The Journal of Physical Chemistry B*, Label-free *in situ* SERS imaging of biofilms 114 (2010) 10184-10194.
- [50] A. Poli, G. Anzelmo, B. Nicolaus, *Marine Drugs*, Bacterial exopolysaccharides from extreme marine habitats: Production, characterization and biological activities 8 (2010) 1779-1802.
- [51] N. Pradhan, S.K. Pradhan, B.B. Nayak, P.S. Mukherjee, L.B. Sukla, B.K. Mishra, *Research in Microbiology*, Micro-Raman analysis and AFM imaging of *Acidithiobacillus ferrooxidans* biofilm grown on uranium ore 159 (2008) 557-561.
- [52] C. Sandt, T. Smith-Palmer, J. Pink, L. Brennan, D. Pink, *Journal of Applied Microbiology*, Confocal Raman microspectroscopy as a tool for studying the chemical heterogeneities of biofilms *in situ* 103 (2007) 1808-1820.
- [53] H.G.M. Edwards, M.A. Mohsin, F.N. Sadooni, N.F. Nik Hassan, T. Munshi, *Analytical and Bioanalytical Chemistry*, Life in the sabkha: Raman spectroscopy of halotrophic extremophiles of relevance to planetary exploration 385 (2006) 46-56.
- [54] H.G.M. Edwards, S.E. Jorge Villar, D. Pullan, M.D. Hargreaves, B.A. Hofmann, F. Westall, *Journal of Raman Spectroscopy*, Morphological biosignatures

from relict fossilised sedimentary geological specimens: a Raman spectroscopic study 38 (2007) 1352-1361.

[55] S.E. Jorge-Villar, H.G.M. Edwards, L.G. Benning, *Analytical and Bioanalytical Chemistry*, Raman spectroscopic analysis of arctic nodules: relevance to the astrobiological exploration of Mars 401 (2011) 2927-2933.

[56] B. Tian, Z. Xu, Z. Sun, J. Lin, Y. Hua, *Biochimica et Biophysica Acta (BBA) - General Subjects*, Evaluation of the antioxidant effects of carotenoids from *Deinococcus radiodurans* through targeted mutagenesis, chemiluminescence, and DNA damage analyses 1770 (2007) 902-911.

[57] B. Tian, Y. Hua, *Trends in Microbiology*, Carotenoid biosynthesis in extremophilic *Deinococcus thermus* bacteria 18 (2010) 512-520.

[58] S. Stöckel, S. Meisel, R. Böhme, M. Elschner, P. Rösch, J. Popp, *Journal of Raman Spectroscopy*, Effect of supplementary manganese on the sporulation of *Bacillus* endospores analysed by Raman spectroscopy 40 (2009) 1469-1477.

[59] P.A. Fulmer, J.H. Wynne, *ACS Applied Materials & Interfaces*, Coatings capable of germinating and neutralizing *Bacillus anthracis* endospores 4 (2012) 738-743.

[60] A.J. Anderson, E.A. Dawes, *Microbial Reviews*, Occurrence, metabolism, metabolic role, and industrial uses of bacterial polyhydroxyalkanoates 54 (1990) 450-472.

[61] N. Majed, C. Matthäus, M. Diem, A.Z. Gu, *Environmental Science & Technology*, Evaluation of intracellular polyphosphate dynamics in enhanced biological phosphorus removal process using Raman microscopy 43 (2009) 5436-5442.

[62] K. Grage, A.C. Jahns, N. Parlane, R. Palanisamy, I.A. Rasiah, J.A. Atwood, B.H.A. Rehm, *Biomacromolecules*, Bacterial polyhydroxyalkanoate granules: Biogenesis, structure, and potential use as nano-/micro-beads in biotechnological and biomedical applications 10 (2009) 660-669.

[63] A. Lopez-Cortes, A. Lanz-Landazuri, J.Q. Garcia-Maldonado, *Microbial Ecology*, Screening and isolation of PHB-producing bacteria in a polluted marine microbial mat 56 (2008) 112-120.

[64] D. Bourque, Y. Pomerleau, D. Groleau, *Applied Microbiology and Biotechnology* High cell density production of poly- β -hydroxybutyrate (PHB) from

methanol by *Methylobacterium extorquens*: Production of high-molecular-mass PHB 44 (1995) 367-376.

[65] T. Suzuki, T. Yamane, S. Shimizu, Applied Microbiology and Biotechnology, Mass production of poly- β -hydroxybutyric acid by fully automatic fed-batch culture of methylotroph 23 (1986) 322-329.

[66] P.J. Senior, G.A. Beech, G.A. Ritchie, E.A. Dawes, Biochemical Journal, The role of oxygen limitation in the formation of poly- β -hydroxybutyrate during batch and continuous culture of *Azotobacter beijerinckii* 128 (1972) 1193-1201.

[67] W.J. Page, O. Knosp, Applied and Environmental Microbiology, Hyperproduction of poly- β -hydroxybutyrate during exponential growth of *Azotobacter vinelandii* UWD 55 (1989) 1334-1339.

[68] T. Yamane, Biotechnology and Bioengineering, Yield of poly-D(-)-3-hydroxybutyrate from various carbon sources: A theoretical study 41 (1993) 165-170.

[69] E.J. Bormann, M. Roth, Biotechnology Letters, The production of polyhydroxybutyrate by *Methylobacterium rhodesianum* and *Ralstonia eutropha* in media containing glycerol and casein hydrolysates 21 (1999) 1059-1063.

[70] J. Sun, X. Peng, J. Van Impe, J. Vanderleyden, Applied and Environmental Microbiology, The *nrB* and *nrC* genes are involved in the regulation of poly-3-hydroxybutyrate biosynthesis by ammonia in *Azospirillum brasilense* sp7 66 (2000) 113-117.

[71] D.B. Karr, J.K. Waters, D.W. Emerich, Applied and Environmental Microbiology, Analysis of poly- β -hydroxybutyrate in *Rhizobium japonicum* bacteroids by ion-exclusion high-pressure liquid chromatography and UV detection 46 (1983) 1339-1344.

[72] K. Hong, S. Sun, W. Tian, G.Q. Chen, W. Huang, Applied Microbiology and Biotechnology, A rapid method for detecting bacterial polyhydroxyalkanoates in intact cells by Fourier transform infrared spectroscopy 51 (1999) 523-526.

[73] K.E. Tyo, H. Zhou, G.N. Stephanopoulos, Applied and Environmental Microbiology, High-throughput screen for poly-3-hydroxybutyrate in *Escherichia coli* and *Synechocystis* sp. Strain PCC6803 72 (2006) 3412-3417.

[74] A. Degelau, T. Scheper, J.E. Bailey, C. Guske, Applied Microbiology and Biotechnology, Fluorometric measurement of poly- β -hydroxybutyrate in *Alcaligenes eutrophus* by flow cytometry and spectrofluorometry 42 (1995) 653-657.

-
- [75] J. De Gelder, D. Willemse-Erix, M.J. Scholtes, J.I. Sanchez, K. Maquelin, P. Vandenaabeele, P. De Boever, G.J. Puppels, L. Moens, P. De Vos, *Analytical Chemistry*, Monitoring poly(3-hydroxybutyrate) production in *Cupriavidus necator* DSM 428 (H16) with Raman spectroscopy 80 (2008) 2155-2160.
- [76] W. Page, C. Tenove, *Biotechnology Techniques*, Quantitation of poly- β -hydroxybutyrate by fluorescence of bacteria and granules stained with Nile blue A 10 (1996) 215-220.
- [77] C. Chen, C.H. Yu, Y.C. Cheng, P.H.F. Yu, M.K. Cheung, *European Polymer Journal*, Preparation and characterization of biodegradable nanoparticles based on amphiphilic poly(3-hydroxybutyrate)-poly(ethylene glycol)-poly(3-hydroxybutyrate) triblock copolymer 42 (2006) 2211-2220.
- [78] T. Freier, C. Kunze, C. Nischan, S. Kramer, K. Sternberg, M. Saß, U.T. Hopt, K.-P. Schmitz, *Biomaterials*, In vitro and in vivo degradation studies for development of a biodegradable patch based on poly(3-hydroxybutyrate) 23 (2002) 2649-2657.
- [79] D. Jendrossek, I. Knoke, R. Habibian, A. Steinbüchel, H. Schlegel, *Journal of Environmental Polymer Degradation*, Degradation of poly(3-hydroxybutyrate), PHB, by bacteria and purification of a novel PHB depolymerase from *Comamonas* sp 1 (1993) 53-63.
- [80] B. Kessler, N.J. Palleroni, *International Journal of Systematic and Evolutionary Microbiology*, Taxonomic implications of synthesis of poly- β -hydroxybutyrate and other poly- β -hydroxyalkanoates by aerobic pseudomonads 50 (2000) 711-713.
- [81] H. Abe, Y. Doi, T. Fukushima, H. Eya, *International Journal of Biological Macromolecules*, Biosynthesis from gluconate of a random copolyester consisting of 3-hydroxybutyrate and medium-chain-length 3-hydroxyalkanoates by *Pseudomonas* sp. 61-3 16 (1994) 115-119.
- [82] E.J. Bormann, M. Leißner, M. Roth, B. Beer, K. Metzner, *Applied Microbiology and Biotechnology*, Production of polyhydroxybutyrate by *Ralstonia eutropha* from protein hydrolysates 50 (1998) 604-607.
- [83] S.Y. Lee, *Biotechnology and Bioengineering*, Bacterial polyhydroxyalkanoates 49 (1996) 1-14.
- [84] Y. Kawaguchi, Y. Doi, *FEMS Microbiology Letters*, Structure of native poly(3-hydroxybutyrate) granules characterized by X-ray diffraction 70 (1990) 151-155.

-
- [85] T. Furukawa, H. Sato, R. Murakami, J. Zhang, I. Noda, S. Ochiai, Y. Ozaki, *Polymer*, Raman microspectroscopy study of structure, dispersibility, and crystallinity of poly(hydroxybutyrate)/poly(L-lactic acid) blends 47 (2006) 3132-3140.
- [86] M. Wróbel-Kwiatkowska, M. Zuk, J. Szopa, L. Dyminska, M. Maczka, J. Hanuza, *Spectrochimica Acta Part A: Molecular and Biomolecular Spectroscopy*, Poly-3-hydroxy butyric acid interaction with the transgenic flax fibers: FT-IR and Raman spectra of the composite extracted from a GM flax 73 (2009) 286-294.
- [87] A. Kappler, K.L. Straub, *Reviews in Mineralogy and Geochemistry*, Geomicrobiological cycling of iron 59 (2005) 85-108.
- [88] R.M. Cornell, U. Schwertmann, *The iron oxides: structure, properties, reactions, occurrences and uses*, 2nd ed., Wiley-VCH Verlag GmbH, Weinheim, 2003.
- [89] U. Schwertmann, R.M. Cornell, *Iron oxides in the laboratory: Preparation and characterization*, 2nd ed., Wiley-VCH Verlag GmbH, Weinheim, 2000.
- [90] E. Murad, P. Rojik, *Clay Minerals*, Iron mineralogy of mine-drainage precipitates as environmental indicators: review of current concepts and a case study from the Sokolov Basin, Czech Republic 40 (2005) 427-440.
- [91] P.C. Singer, W. Stumm, *Science*, Acidic mine drainage: The rate-determining step 167 (1970) 1121-1123.
- [92] K. Küsel, *Water, Air and Soil Pollution: Focus*, Microbial cycling of iron and sulfur in acidic coal mining lake sediments 3 (2003) 67-90.
- [93] K.H. Gayer, L. Woontner, *The Journal of Physical Chemistry*, The solubility of ferrous hydroxide and ferric hydroxide in acidic and basic media at 25° 60 (1956) 1569-1571.
- [94] J.M. Bigham, U. Schwertmann, G. Pfab, *Applied Geochemistry*, Influence of pH on mineral speciation in a bioreactor simulating acid mine drainage 11 (1996) 845-849.
- [95] S.M. Equeenuddin, S. Tripathy, P.K. Sahoo, M.K. Panigrahi, *Environmental Earth Sciences*, Geochemistry of ochreous precipitates from coal mine drainage in India 61 (2010) 723-731.
- [96] J.M. Bigham, U. Schwertmann, L. Carlson, in: H.C.W. Skinner, R.W. Fitzpatrick (Eds), *Biomining processes of iron and manganese: Modern and ancient environments*, Catena Verlag, Reiskirchen, 1992, pp. 219-232.

-
- [97] A. Navrotsky, L. Mazeina, J. Majzlan, *Science*, Size-driven structural and thermodynamic complexity in iron oxides 319 (2008) 1635-1638.
- [98] R.G. Robins, *Journal of Inorganic and Nuclear Chemistry*, Hydrothermal precipitation in solutions of thorium nitrate, ferric nitrate and aluminium nitrate 29 (1967) 431-435.
- [99] W. Um, R.J. Serne, C.F. Brown, K.A. Rod, *Applied Geochemistry*, Uranium(VI) sorption on iron oxides in Hanford Site sediment: Application of a surface complexation model 23 (2008) 2649-2657.
- [100] U.G. Nielsen, Y. Paik, K. Julmis, M.A.A. Schoonen, R.J. Reeder, C.P. Grey, *The Journal of Physical Chemistry B*, Investigating sorption on iron-oxyhydroxide soil minerals by solid-state NMR spectroscopy: A ^6Li MAS NMR study of adsorption and absorption on goethite 109 (2005) 18310-18315.
- [101] L.J. Bird, V. Bonnefoy, D.K. Newman, *Trends in Microbiology*, Bioenergetic challenges of microbial iron metabolisms 19 (2011) 330-340.
- [102] J.M. Zachara, J.K. Fredrickson, S.W. Li, D.W. Kennedy, S.C. Smith, P.L. Gassman, *American Mineralogist*, Bacterial reduction of crystalline Fe^{3+} oxides in single phase suspensions and subsurface materials 83 (1998) 1426-1443.
- [103] E.E. Roden, *Environmental Science & Technology*, Fe(III) oxide reactivity toward biological versus chemical reduction 37 (2003) 1319-1324.
- [104] S. Lu, S. Gischkat, M. Reiche, D.M. Akob, K.B. Hallberg, K. Küsel, *Applied and Environmental Microbiology*, Ecophysiology of Fe-cycling bacteria in acidic sediments 76 (2010) 8174-8183.
- [105] C.M. Hansel, S.G. Benner, J. Neiss, A. Dohnalkova, R.K. Kukkadapu, S. Fendorf, *Geochimica et Cosmochimica Acta*, Secondary mineralization pathways induced by dissimilatory iron reduction of ferrihydrite under advective flow 67 (2003) 2977-2992.
- [106] T.P. Young, *Geological Society, London, Special Publications*, Phanerozoic ironstones: an introduction and review 46 (1989) ix-xxv.
- [107] A. Mücke, F. Farshad, *Ore Geology Reviews*, Whole-rock and mineralogical composition of Phanerozoic ooidal ironstones: Comparison and differentiation of types and subtypes 26 (2005) 227-262.
- [108] W. Salama, M. El Aref, R. Gaupp, *Gondwana Research*, Mineralogical and geochemical investigations of the Middle Eocene ironstones, El Bahariya Depression, Western Desert, Egypt 22 (2012) 717-736.

-
- [109] K. Dahanayake, W.E. Krumbein, *Mineralium Deposita*, Microbial structures in oolitic iron formations 21 (1986) 85-94.
- [110] J.B. Maynard, *Economic Geology*, Geochemistry of oolitic iron ores, an electron microprobe study 81 (1986) 1473-1483.
- [111] A. Preat, B. Mamet, C. De Ridder, F. Boulvain, D. Gillan, *Sedimentary Geology*, Iron bacterial and fungal mats, Bajocian stratotype (Mid-Jurassic, northern Normandy, France) 137 (2000) 107-126.
- [112] W. Salama, M.M. El Aref, R. Gaupp, *Geobiology*, Mineral evolution and processes of ferruginous microbialite accretion – an example from the Middle Eocene stromatolitic and ooidal ironstones of the Bahariya Depression, Western Desert, Egypt (2012) DOI: 10.1111/gbi.12011.
- [113] R.M. Burkhalter, *Sedimentology*, Ooidal ironstones and ferruginous microbialites: origin and relation to sequence stratigraphy (Aalenian and Bajocian, Swiss Jura mountains) 42 (1995) 57-74.
- [114] J.M. Heikoop, C.J. Tsujita, M.J. Risk, T. Tomascik, A.J. Mah, *Geology*, Modern iron ooids from a shallow-marine volcanic setting: Mahengetang, Indonesia 24 (1996) 759-762.
- [115] M.C. Rowe, B.S. Ellis, A. Lindeberg, *American Mineralogist*, Quantifying crystallization and devitrification of rhyolites by means of X-ray diffraction and electron microprobe analysis 97 (2012) 1685-1699.
- [116] E.A. Stefaniak, A. Alseacz, R. Frost, Z. Mathe, I.E. Sajo, S. Török, A. Worobiec, R. Van Grieken, *Journal of Hazardous Materials*, Combined SEM/EDX and micro-Raman spectroscopy analysis of uranium minerals from a former uranium mine 168 (2009) 416-423.
- [117] A.P. Ault, T.M. Peters, E.J. Sawvel, G.S. Casuccio, R.D. Willis, G.A. Norris, V.H. Grassian, *Environmental Science & Technology*, Single-Particle SEM-EDX analysis of iron-containing coarse particulate matter in an urban environment: Sources and distribution of iron within Cleveland, Ohio 46 (2012) 4331-4339.
- [118] V. Gorenflo, A. Steinbüchel, S. Marose, M. Rieseberg, T. Scheper, *Applied Microbiology and Biotechnology*, Quantification of bacterial polyhydroxyalkanoic acids by Nile red staining 51 (1999) 765-772.
- [119] N. Mercan, B. Aslim, Z.N. Yüsekdağ, Y. Beyatli, *Turkish Journal of Biology*, Production of poly- β -hydroxybutyrate (PHB) by some *Rhizobium* bacteria 26 (2002) 215-219.

-
- [120] B. Aslim, F. Çalışkan, Y. Beyatli, U. Gündüz, FEMS Microbiology Letters, Poly- β -hydroxybutyrate production by lactic acid bacteria 159 (1998) 293-297.
- [121] L. Cai, D.H. Zhao, J. Hou, J.H. Wu, S.F. Cai, P. Dassarma, H. Xiang, Science China Life Sciences, Cellular and organellar membrane-associated proteins in haloarchaea: Perspectives on the physiological significance and biotechnological applications 55 (2012) 404-414.
- [122] N.D. Ayub, M.J. Pettinari, J.A. Ruiz, N.I. Lopez, Current Microbiology, A Polyhydroxybutyrate-Producing *Pseudomonas* sp. Isolated from Antarctic Environments with High Stress Resistance 49 (2004) 170-174.
- [123] E.D. Burton, R.T. Bush, L.A. Sullivan, D.R.G. Mitchell, Geochimica et Cosmochimica Acta, Schwertmannite transformation to goethite via the Fe(II) pathway: Reaction rates and implications for iron-sulfide formation 72 (2008) 4551-4564.
- [124] J. Majzlan, S.C.B. Myneni, Environ. Sci. Technol., Speciation of Iron and Sulfate in Acid Waters: Aqueous Clusters to Mineral Precipitates 39 (2004) 188-194.
- [125] B. Dold, Applied Geochemistry, Dissolution kinetics of schwertmannite and ferrihydrite in oxidized mine samples and their detection by differential X-ray diffraction (DXRD) 18 (2003) 1531-1540.
- [126] V.c. Ettler, Z. Johan, D. Hradil, Comptes Rendus Geoscience, Natural alteration products of sulphide mattes from primary lead smelting 335 (2003) 1013-1020.
- [127] R.N. Collins, A.M. Jones, T.D. Waite, Geochimica et Cosmochimica Acta, Schwertmannite stability in acidified coastal environments 74 (2010) 482-496.
- [128] E.-S. El-Tarabili, Economic Geology, Paleogeography, paleoecology and genesis of the phosphatic sediments in the Quseir-Safaga area, U. A. R 64 (1969) 172-182.
- [129] N. Rittman, W. Machu, Bulletin of the Faculty of Engineering, Cairo University, On the origin of Egyptian phosphate deposits 3 (1955) 300-318.
- [130] M. Kretzschmar, Facies, Fossile Pilze in Eisen-Stromatolithen von Warstein (Rheinisches Schiefergebirge) 7 (1982) 237-259.
- [131] B. Mamet, A. Preat, Sedimentary Geology, Iron-bacterial mediation in Phanerozoic red limestones: State of the art 185 (2006) 147-157.

2 Publications

[VC1] The influence of intracellular storage material on bacterial identification by means of Raman spectroscopy

Authorship of publication

<u>V. Ciobota:</u>	concept development Raman measurements data analysis writing of manuscript
E.-M. Burkhardt:	sample preparation discussion of results writing of manuscript
W. Schumacher:	data analysis discussion of statistical concept
P. Rösch:	discussion of experimental concept and results proofreading of manuscript
K. Küsel:	discussion of experimental concept and results proofreading of manuscript
J. Popp:	project management discussion of concepts and results discussion and proofreading of manuscript

Analytical and Bioanalytical Chemistry 397 (2010) 2929-2937

Reprinted with kind permission from *Springer Science + Business Media*.

The influence of intracellular storage material on bacterial identification by means of Raman spectroscopy

Valerian Ciobotă · Eva-Maria Burkhardt ·
Wilm Schumacher · Petra Rösch · Kirsten Küsel ·
Jürgen Popp

Received: 12 March 2010 / Revised: 5 May 2010 / Accepted: 30 May 2010
© Springer-Verlag 2010

Abstract Previous studies dealing with bacterial identification by means of Raman spectroscopy have demonstrated that micro-Raman is a suitable technique for single-cell microbial identification. Raman spectra yield fingerprint-like information about all chemical components within one cell, and combined with multivariate methods, differentiation down to species or even strain level is possible. Many microorganisms may accumulate high amounts of polyhydroxyalkanoates (PHA) as carbon and energy storage materials within the cell and the Raman bands of PHA might impede the identification and differentiation of cells. To date, the identification by means of Raman spectroscopy have never been tested on bacteria which had accumulated PHA. Therefore, the aim of this study is to investigate the effect of intracellular polymer accumulation on the bacterial identification rate. Combining fluorescence imaging and Raman spectroscopy, we identified polyhydroxybutyrate (PHB) as a storage polymer accumulating in the investigated cells. The amount of energy storage material present within the cells was dependent on the physiological status of the microorganisms and strongly influenced the identification

results. Bacteria in the stationary phase formed granules of crystalline PHB, which obstructed the Raman spectroscopic identification of bacterial species. The Raman spectra of bacteria in the exponential phase were dominated by signals from the storage material. However, the bands from proteins, lipids, and nucleic acids were not completely obscured by signals from PHB. Cells growing under either oxic or anoxic conditions could also be differentiated, suggesting that changes in Raman spectra can be interpreted as an indicator of different metabolic pathways. Although the presence of PHB induced severe changes in the Raman spectra, our results suggest that Raman spectroscopy can be successfully used for identification as long as the bacteria are not in the stationary phase.

Keywords Raman spectroscopy · Polyhydroxybutyrate · Bacterial identification · Fluorescence staining

Introduction

An important concern in microbiology is to find a rapid method for reliable microbial identification. Ultimately, the goal in microbial identification is to link microbial cell identification with metabolic potentials *in situ*, i.e., on a single-cell level [1]. Microbial ecology studies the interactions of microorganisms with their biotic and abiotic environment. Since these interactions determine the occurrence, distribution, and activities of microbial species, to be able to describe an interaction, information about microbial species present in the environment and their activity are required [2].

Culture-dependent approaches are limited because only a minority of microorganisms can be cultivated with standard techniques in the laboratory that do not mimic *in situ* conditions [3]. The high cost and complexity of the molecular methods developed over the last two decades,

V. Ciobotă · W. Schumacher · P. Rösch · J. Popp
Institute of Physical Chemistry, Friedrich Schiller University Jena,
Helmholtzweg 4,
07743 Jena, Germany

E.-M. Burkhardt · K. Küsel
Institute of Ecology, Friedrich Schiller University Jena,
Dornburger Straße 159,
07743 Jena, Germany

J. Popp (✉)
Institute of Photonic Technology,
Albert-Einstein-Straße 9,
00745 Jena, Germany
e-mail: juergen.popp@ipht-jena.de

Published online: 27 June 2010

 Springer

currently used for identification, make them unsuitable for routine analyses [4].

Alternatively, spectroscopic methods can be used for single-cell identification. Recently, spectroscopic methods based on the physicochemical property of whole cells have been used to identify microorganisms [5–11]. Compared with other spectroscopic techniques, the advantages of this micro-Raman spectroscopic technique are its non-invasive character, minimal or no sample preparation, and the fact that only one bacterial cell is required to record the fingerprint Raman spectrum, which is used for microbial identification [12–14]. Variations in the biochemical composition between different microbial species communities enable their identification by means of Raman spectroscopy [5, 12, 15]. Raman spectroscopy is used not only for bacteria analyses but also for studies focused on plants and human cells [16–21]. In general, Raman spectroscopy has the potential for broad applicability, as it is successfully used in chemistry, material sciences, mineralogy, art, and archeology [22–24].

Raman spectra yield fingerprint-like information about all chemical components within the cell. Information about the functions of microorganisms in complex bacteria communities can also be collected using Raman spectroscopy alone [25] or in combination with other methods, e.g., FISH [10]. Identification to the strain level is also possible with Raman spectroscopy [26–32]. To perform Raman spectroscopic identification, an algorithm to differentiate between different microorganisms' taxa is required, and various statistical methods are applied to analyze the Raman signals. For a large Raman database, a dimensionality reduction of the data can be performed using principal component analysis (PCA), prior to any spectra classification. Classification or identification in previous studies was accomplished by either an unsupervised method (hierarchical cluster analysis) or a supervised one (K-nearest neighbor classifier, nearest mean classifier, linear discriminant analysis, or support vector machines (SVM)) [8, 26, 30, 31, 33]. Support vector machines have a wide variety of biological applications, including the classification of proteins and DNA sequences, microarray gene expression profiles [34, 35], or microorganisms [8, 11].

In order to make the transition from proof-of-principle studies to studies under field conditions, the influence of various parameters has to be investigated. For example, many microorganisms produce polyhydroxyalkanoates (PHA) not only as carbon and energy storage materials but also as an electron sink, usually under conditions of limited nutrients [36, 37]. Polyhydroxybutyrate (PHB) is the simplest and the most common PHA and has strong potential as a biodegradable polymer [38–40]. Consequently, numerous studies have been dedicated to increasing the rate of polymer accumulation in cells [36, 41–43], detection [44], and quantification [45, 46] of the quantity of PHB

stored by microorganisms. High amounts of these polymers have been detected in some bacteria, with concentrations of PHB up to 80% of the total dry weight reported [47]. Thus, the Raman bands generated by polyhydroxybutyrate might impede the identification and differentiation of some bacterial cells. However, none of the microorganisms identified by means of Raman spectroscopy up to this point have contained storage materials.

An identification method based on single-cell analysis is valuable in, e.g., microbial ecology since traditional cultivation-based methods are slow and, due to their inevitable selectivity, usually fail to achieve a complete picture of the true composition of complex communities [3]. A relatively large number of microorganisms are able to produce and accumulate within the cells' various energy storage polymers [37]; therefore, a study focused on the effects of PHB on microbial identification using Raman spectroscopy is required. Furthermore, identification of new strains which accumulate high amount of storage materials could positively influence the field of biodegradable materials since these microbes could be used for the production of polymers.

In this paper, we evaluate the robustness of the Raman spectroscopic approach in combination with statistical methods, for the identification of microorganisms. We investigate the effect of PHB accumulation in bacterial cells belonging to different classes on the identification results obtained by combining Raman spectroscopy with SVM.

Experimental procedures

Sample preparation

The microorganisms *Bacillus megaterium* DSM 90 (Firmicutes; Gram positive), three strains of *Bacillus thuringiensis* (DSM 530, DSM 5725, and ATCC10782) (Firmicutes; Gram positive), *Azohydromonas lata* DSM 1122 (Betaproteobacteria; Gram negative), and *Cupriavidus necator* DSM 428 (Betaproteobacteria; Gram negative) were cultivated on NA (nutrient agar) medium at 30 °C. *Acidiphilium cryptum* JF-5 (Alphaproteobacteria; Gram negative) was cultivated either in liquid tryptone soya broth medium enriched with 2 mM glucose at 32 °C under oxic conditions or under anoxic conditions with amended soluble $\text{Fe}_2(\text{SO}_4)_3$ (30 mM) as electron acceptor. From each liquid sample, an amount of 1.5 ml of culture was centrifuged three times at 12,000×g for 2 min and washed in each case with distilled water. In case of bacteria cultivated on agar plates, a part of the colony was scraped from plates using an inoculating loop, suspended in 1.5 ml of water, and washed as mentioned above. Thereupon, a droplet of suspension

was dried on air at room temperature on a fused silica surface. For all analyzed bacterial strains, the Raman spectra from at least two independent cultures obtained from different sets of media were recorded.

Fluorescence staining and observation

A solution with the concentration of 1 g/l was prepared by dissolving Nile red with dimethyl sulfoxide. A 1-ml aliquot of the culture was mixed with 0.3 μ l of Nile red solution and incubated for 30 min. After incubation, the culture was centrifuged three times at 12,000 \times g for 5 min and washed in each case with distilled water. Afterwards, a droplet of suspension was dried on air at room temperature on a fused silica surface. Subsequently, fluorescence imaging observations were performed. The fluorescence imaging observations were made by means of an inverse microscope (BX 41, Olympus) coupled to a CCD camera (CC12, Olympus). The fluorescence excitation is realized with a mercury lamp; different excitation and emissions wavelengths were obtained by exchanging the filters in the light path.

Spectroscopic instrumentation

The Raman spectra of the bacteria were recorded with a micro-Raman setup (HR LabRam inverse system, Jobin Yvon Horiba). Raman scattering was excited by a frequency doubled Nd:YAG laser at a wavelength of 532 nm with a laser power of about 2-mW incident on the sample. The laser beam was focused on individual cells by means of a Leica PLFluor \times 100/0.75 microscope objective down to a spot diameter of approximately 0.7 μ m, which is sufficient to resolve a single bacterium from the background. The dispersive spectrometer has an entrance slit of 100 μ m and a focal length of 800 mm and is equipped with a grating of 300 lines mm^{-1} . The Raman scattered light was detected by a CCD camera operating at 220 K. The acquisition time per spectrum was 60 s. The data were acquired over the course of several days. For the calibration procedure, titanium dioxide (anatase) was measured daily as a reference control.

Chemometric analysis

The analysis of Raman spectra was performed in two steps: (1) preprocessing of the spectra and (2) identification by using SVMs. A support vector machine is a computer algorithm that learns by example to assign labels to objects [35]. The SVM always solves two-class problems; therefore, a hyperplane is defined in order to discriminate the two classes. The hyperplane is characterized by the support vectors, which are data points belonging to one class and having the highest similarity to the other class [8].

The preprocessing was tested by different methods such as baseline correction, normalization, first, and second derivative. Baseline correction using the SNIP algorithm [52] plus vector normalization for single-bacterium analysis are the best obtained results and therefore were used for further preprocessing of the data. Baseline correction was applied to remove the background generated by the fluorescence emission. The SNIP baseline estimation was used because of the speed and the reliability of this method. To avoid the variation in the Raman intensity generated by the difference in the mass of the microbial cells, the vector normalized finger print region was used in all further computation. Thereafter, a PCA [53] was performed, with the first 20 scores being used for further data analysis. The dimension reduction was done first to reduce the cost of the computation, second to remove white noise from the spectrum, and third to avoid overfitting. With this data set of scores, a one-against-one [54] system of support vector machines [55] with a radial basis kernel was trained and tested on a completely independent set. With a one-against-the-rest schema, it is possible to build up a multiclass classifier out of single binary classifiers. The training set was composed from 266 Raman spectra recorded from five species. For the identification, 102 independent Raman spectra were used.

Results and discussion

The Raman spectrum of a microorganism is the sum of Raman signals of the individual cell components. Therefore, contributions from proteins, nucleic acids, and lipids are expressed in the spectrum. A typical bacterial spectrum (Fig. 1—spectrum a) shows two bands correlated to the presence of proteins in the microorganism: two bands at approx. 1,660 and 1,242 cm^{-1} are assigned to amide I and amide III vibrations, respectively. Contributions from the amino acids are detected at 1,001 cm^{-1} , a sharp band characteristic of phenylalanine, and approx. 1,610 cm^{-1} , which is assigned to phenylalanine and tyrosine. The band at 1,575 cm^{-1} is specific to nucleic acid ring stretching vibration, especially of guanine and adenine, while the band at 1,314 cm^{-1} is assigned to CH_2/CH_3 deformation vibrations [12, 32]. Another signal belonging to CH_2 deformation is the band at 1,342 cm^{-1} ; the band at 1,450 cm^{-1} is given by the CH_2 scissoring deformation [12]. The most prominent feature within the Raman spectrum of bacteria is the broad band centered at 2,932 cm^{-1} , which is the superposition of the CH stretching vibrations of CH_2 and CH_3 groups in proteins, lipids, nucleic acids, and carbohydrates [12, 32]. The broad bands at 785 and 1,075 cm^{-1} labeled with asterisk in Fig. 1 are generated by the fused silica slides on which the investigated bacteria were located.

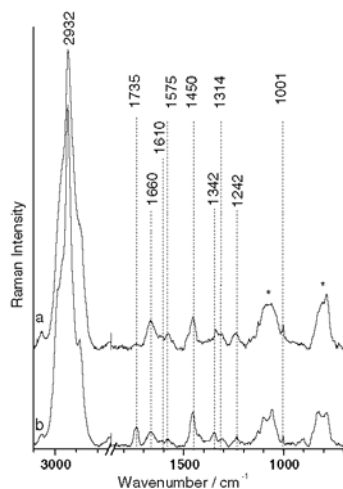


Fig. 1 Average Raman spectra of the *Bacillus megaterium* DSM 90 cells without (a) and with (b) PHB

The average spectra displayed in Fig. 1, each spectrum being the average of 20 single-cell spectra, were recorded from a culture of *B. megaterium* DSM 90. The main difference between the two spectra is the signal at $1,735\text{ cm}^{-1}$ in spectrum B, which can be assigned to stretching vibration from a carbonyl bond. The appearance of this C=O signal is accompanied by a decrease in the intensity of protein and nucleic acid bands, while the intensities of CH deformation bands increase. The outcome seems at first surprising since the Raman spectra of a single strain cultivated under various conditions are usually very similar, with chemometrical methods usually being required to differentiate between similar bacterial cells grown under different conditions [15]. However, the important differences between the two Raman spectra can be attributed to a new substance present in large quantities in the cells. The decrease in the Raman signals of the other cell components likely influences the Raman spectroscopy identification process, as the protein and nucleic acid bands are crucial for the discrimination between various bacteria. The same decrease in intensity of the protein and nucleic acid bands was also noticed in the Raman spectra of *A. cryptum* JF-5 (not shown here). Therefore, the starting point of this study was the identification of the substance responsible for the aforementioned changes in the Raman spectra. The analysis of the influence of this unknown substance on bacterial identification is vital for further applications of this spectroscopic method for classification and identification of microorganisms.

Many bacteria produce PHA as carbon and energy storage molecules and can accumulate high amounts of PHA in the cells [38]. To demonstrate that PHA was responsible for our observed changes in Raman spectra, a combination of fluorescence imaging and Raman spectroscopy technique was used. The bacteria were first stained with a fluorescent dye (Nile red) to illuminate the cells under fluorescence, which contained substrate storage materials. The cells containing PHA were then located on the slide surface by means of fluorescence imaging. By comparing the fluorescence images with bright field pictures, distinctions between cells with and without storage granules were possible. Further, Raman spectroscopy was applied to analyze the chemical composition of different cells. Figure 2 illustrates stained *A. cryptum* JF-5 cells, observed in brightfield image (a) and in fluorescence illumination (b), respectively. Based on the fluorescence images, two cells were selected for Raman measurements, one with and one without storage materials, and the spectra obtained are presented in Fig. 2c. The Raman spectrum of the fluorescent cell is dominated by bands assigned to CH stretching vibrations at $2,935\text{ cm}^{-1}$, CH deformation vibrations at $1,450\text{ cm}^{-1}$, and C=O stretching vibrations at $1,735\text{ cm}^{-1}$. The broad bands at 785 and $1,075\text{ cm}^{-1}$ are assigned to the fused silica substrate on which the investigated bacteria were placed. The intensity of the protein and nucleic acid bands is very low. The Raman spectrum of the cell without storage materials (b) is dominated by the signals assigned to amide I, amide III, and nucleic acids. In addition, the band assigned to C=O stretching vibration is completely absent. This indicates that a polyhydroxyalkanoate substance is likely responsible for the presence of the $1,735\text{ cm}^{-1}$ band.

Next, we identified the polymer produced by *A. cryptum* JF-5. Although a large variety of PHA storage granules may be synthesized by microorganisms, by far, the most common substance is polyhydroxybutyrate. The Raman spectrum of crystalline PHB is displayed in Fig. 3 c. The CH stretching band, centered at $2,932\text{ cm}^{-1}$, is the dominant signal in the spectrum, with five clearly separated bands being observed in this region. The signals are assigned to CH_2 and CH_3 symmetric and asymmetric stretching vibrations. In the region of $1,350$ – $1,450\text{ cm}^{-1}$, bands from various CH deformation vibrations are present. The Raman signals at $1,402$ and $1,364\text{ cm}^{-1}$ are assigned to CH_3 symmetric deformation and the band at $1,450\text{ cm}^{-1}$, to CH_3 as well as CH_2 deformation vibrations. The stretching vibration of the C=O double bond is located at $1,735\text{ cm}^{-1}$. The single bond CC stretching vibration is responsible for the Raman signal at 840 cm^{-1} and CO stretching vibration for the band at $1,048\text{ cm}^{-1}$ [15, 48]. An overview of the tentative assignment of the Raman signals obtained from bacterial cells is presented in Table 1.

Fig. 2 Microscope images of stained *A. cryptum* JF-5 cells with or without storage granules on a fused silica substrate. **a** displays brightfield illumination, and **b** is obtained from a fluorescence illumination at the same position like in **a**. Raman measurements were performed on the cells marked with circles (**c**)

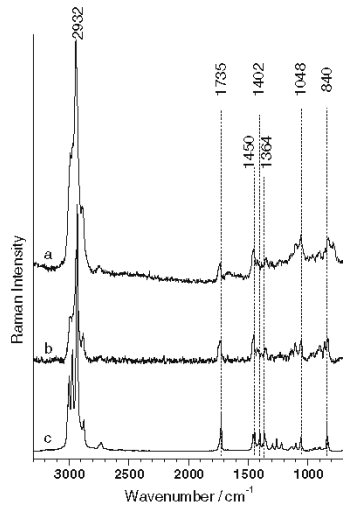
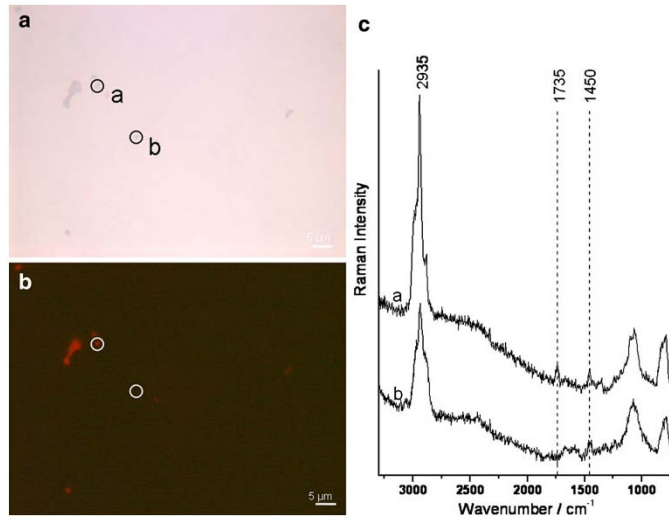


Fig. 3 Raman spectra of (a) spectrum single bacterium, (b) amorphous PHB, and (c) crystalline PHB

A comparison between the PHB crystalline spectrum (Fig. 3 c) and a spectrum recorded from a cell in exponential growth (Fig. 3 a) reveals important differences. The bands in the region 1,200–1,300 cm^{-1} are observed only in the crystalline PHB spectrum, the intensity of the CH_3 symmetric deformation vibrations (1,364 and 1,402 cm^{-1}) are very low in the bacterial spectrum, and

Table 1 Tentative wavenumber assignment of some of the Raman signals of bacterial cells

Wavenumber (cm^{-1})	Tentative assignment
840	Single-bond CC stretching vibration
1,001	Phenylalanine
1,048	CO stretching vibration
~1,242	Amide III
1,314	CH_2/CH_3 deformation vibrations
1,342	CH deformation
1,365	CH_3 symmetric deformation
1,402	CH_3 symmetric deformation
1,450	CH_2 scissoring deformation
1,575	Nucleic acid ring stretching vibration, especially of guanine and adenine
1,610	Phenylalanine and tyrosine
~1,660	Amide I
1,735	C=O stretching vibration

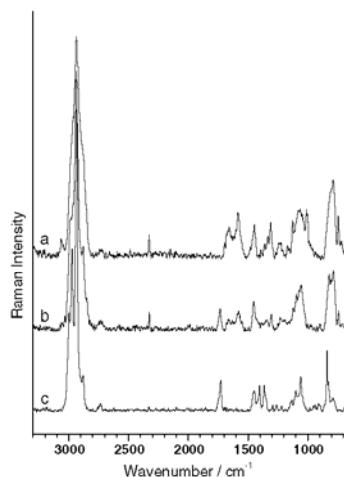


Fig. 4 Raman spectra of *A. cryptum* JF-5 in different growth phase: (a) lag phase, (b) exponential phase, and (c) stationary phase

the signal at $1,735\text{ cm}^{-1}$ assigned to C=O stretching vibration is much broader in the bacterial spectrum than in crystalline PHB. Furthermore, in the CH stretching vibration region, five bands are clearly distinguished in the crystalline spectrum, while in the bacterial spectrum, the bands are broader and form a single large band. However, the spectrum of amorphous PHB (Fig. 3 b) is very similar to the spectrum obtained from a cell in the exponential phase with storage materials, indicating that PHB is the storage material present in bacterial cells. This also suggests that bacteria in exponential growth phase create deposits of polymers in the amorphous state. In case of bacteria in the stationary phase (Fig. 4 c), the microorganism spectra are almost identical with the spectrum of crystalline PHB (Fig. 3 c), suggesting that microorganisms in stationary growth phase accumulate storage materials in the crystalline form.

With increasing amounts of storage material in cells, Raman signals from other cell components decrease in intensity. This behavior likely affects identification since the protein and nucleic acid bands are used to differentiate between microorganisms. Therefore, we also investigated the influence of storage granules on bacterial identification. To select an appropriate time point for sampling, different growth phases of the culture were to be investigated because the age of the cell can influence its chemical composition. Figure 4 shows differences between spectra of *A. cryptum* JF-5 obtained during different growing phases. The main differences between the spectra are due to different amounts of PHB stored in cells at each time

point. Raman spectra of the cells in the lag phase showed no polymer accumulation (Fig. 4 a). Starting from the exponential phase (Fig. 4 b), PHB is stored within the cell, first as amorphous PHB, then, in the stationary phase (Fig. 4 c), as crystalline. Since we were interested to study the influence of PHB on the robustness of the microbial identification by means of Raman spectroscopy, we determined that the appropriate time points for sampling were in the late exponential phase, when accumulation of storage material is still on-going, but the Raman signals of proteins and nucleic acids are not yet completely obscured by PHB. Therefore, the bacteria which are in the late exponential phase will present the highest amount of amorphous PHB. For microorganisms in the stationary phase, the Raman bands of crystalline PHB completely cover the signals from the other cell components, making the discrimination of the organisms impossible.

Raman spectra from various PHB producing Gram-positive or Gram-negative bacteria belonging to the Firmicutes or to different classes of the Proteobacteria were also recorded. We selected *A. cryptum* (Fig. 5 a), *B. megaterium* (Fig. 5 b), *A. lata* (Fig. 5 c), *C. necator* (Fig. 5 d), and *B. thuringiensis* (Fig. 5 e) for this study because of their tendency to accumulate PHB. All the spectra were very similar (Fig. 5), requiring a chemometrical method to discriminate between the different species. Using SVM, a supervised identification method, a clear distinction between spectra belonging to various

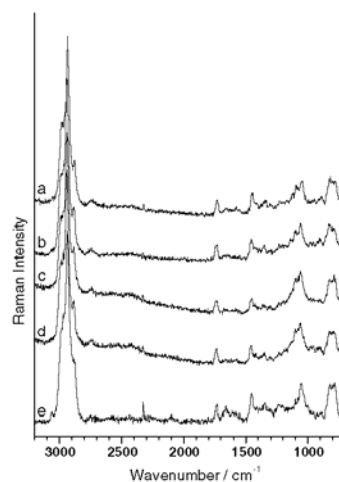


Fig. 5 Raman spectra from various PHB producing bacteria: (a) *Acidiphilium cryptum*, (b) *Bacillus megaterium*, (c) *Azohydromonas lata*, (d) *Cupriavidus necator*, (e) *Bacillus thuringiensis*

Table 2 Identification of PHB producing bacteria via SVM

	<i>A. lata</i>	<i>B. thuringiensis</i>	<i>C. necator</i>	<i>A. cryptum</i>	<i>B. megaterium</i>	Correct %
<i>A. lata</i>	14	–	–	–	5	73.6
<i>B. thuringiensis</i>	–	20	–	–	–	100
<i>C. necator</i>	1	–	22	–	–	95.6
<i>A. cryptum</i>	–	–	–	20	–	100
<i>B. megaterium</i>	4	–	–	–	16	80
Recognition rate						90.1

bacteria was possible, with a recognition rate of 90.1% (Table 2). The training set was formed by 266 spectra, belonging to the above-mentioned species. Spectra from two different strains of *B. thuringiensis* (DSM 530 and ATCC 10782) were incorporated in the training dataset in the *B. thuringiensis* group. For the validation, spectra from bacteria cultivated in different batches than the microorganisms used for the training set were used. In addition, the Raman spectra were recorded at different days, to avoid possible errors in identification induced by measurement artifacts. To challenge the robustness of the identification model, an external dataset of spectra belonging to *B. thuringiensis* DSM 5725 was added to the validation dataset. From 102 spectra, 10 were misclassified: Five *A. lata* spectra were assigned as *B. megaterium*, four *B. megaterium* spectra were assigned as *A. lata*, and one *C. necator* spectrum again as *A. lata*. The spectra belonging to the *B. thuringiensis* DSM 5725 (strain which was not included in the training set) were all correctly assigned to the *B. thuringiensis* group. These results suggest that microbial identification of single bacterial cells by means of Raman spectroscopy can be performed, even if the cells contain high amount of storage materials. However, the bacteria identification is possible as long as the cells contain amorphous PHB and not crystalline. Furthermore, for an ultimate proof of the robustness of bacteria identification by means of Raman spectroscopy, a larger database should be used.

It is well known that the microorganisms which do not present storage materials can be successfully identified by means of Raman spectroscopy [8, 26, 32]. The present study suggests that this spectroscopic technique can be applied for microbes' identification even if those organisms accumulate storage material. However, some limitations related to the physiological status of the bacteria exist. The bacteria used in our experiment were collected in the late exponential phase so that the amount of amorphous PHB accumulated by microorganisms should be at the highest level. Since at these high levels of PHB the identification of bacteria is feasible, we can generalize the outcome and affirm that the identification of microorganisms by means of Raman spectroscopy is achievable if bacteria contain amorphous PHB. In case of bacteria which present

crystalline PHB, the identification using Raman spectroscopy failed.

In practice, for the investigation of an unknown sample, usually there is no information available regarding the physiological status of the bacteria. However, this lack of information does not hinder the bacteria identification process. If bacteria do not accumulate any storage material, the identification is possible by means of Raman spectroscopy, as previous studies demonstrate. If bacteria present storage materials in amorphous form, the identification is achievable, as our study suggest. In case the bacteria accumulate crystalline PHB, another technique should be used for the identification of the microorganisms.

We also investigated if bacterial cells of the same strain can be differentiated even if the cells grow under different conditions and some produce PHA. Raman spectroscopy can be used to discriminate bacterial cells which contain no storage granules and belong to the same strain but are grown in different environmental conditions [15, 49]. However, no information is available for bacteria which accumulate storage materials. For this investigation, *A. cryptum* JF-5 was used because it is facultative anaerobe and therefore can grow under both oxic and anoxic conditions, using oxygen (O_2) or ferric iron as an electron acceptor [50, 51]. In this experiment, *A. cryptum* JF-5 was incubated either with O_2 or with $Fe_2(SO_4)_3$ as an electron acceptor. The cells were harvested in the exponential phase, measured with Raman spectroscopy, and the spectra were analyzed using SVM. Performing a classification with 325 spectra, 307 spectra were correctly identified, which is a recognition rate of 94.5% (Table 3). Of the 18 spectra that were misclassified, eight spectra that belonged to *A. cryptum* JF-5 cells grown anaerobically were assigned as

Table 3 Classification of *A. cryptum* JF-5 in function of the utilized electron acceptor, by means of SVM

	With $Fe_2(SO_4)_3$	With O_2	Correct %
With $Fe_2(SO_4)_3$	137	8	94.5
With O_2	10	170	94.4
Recognition rate			94.5

spectra from cells grown aerobically. Ten spectra recorded from anaerobically grown cells were assigned as spectra from anaerobically grown cells. These data suggest that Raman spectroscopy can classify bacteria, which use different metabolic processes for energy conservation even if the cells accumulate polymers as energy source. Because the cells either use O₂ or ferric iron as electron acceptor, the changes in the Raman spectra can be interpreted to determine the different metabolic pathways involved in *A. cryptum* JF-5 respiration. Therefore, Raman spectroscopy may be a useful tool to differentiate between cells even on the strain level, i.e., the lowest classification level, with different growth histories independent of the presence or absence of storage materials.

Conclusion

The production of storage materials depends on the physiological status of the microorganisms. Our study had to consider the age influence on the biochemical composition of the microbes and the subsequent effect on identification results. Bacteria accumulate storage materials in different forms depending on cell activity status. In stationary phase, crystalline PHA is intracellularly stored, while in exponential phase, the polymer is present in amorphous state. Since identification of various bacteria belonging to different groups was determined only for bacteria which store amorphous PHA, our outcome shows the effect of the microorganisms' age on identification results. However, bacteria in the exponential phase were still successfully identified by means of micro-Raman spectroscopy, with even discrimination between bacteria belonging to the same species but grown under different conditions. To summarize, the present contribution demonstrates that the presence of polyhydroxybutyrate in microbial cells does not hamper Raman spectroscopic identification as long as the microorganisms are in the exponential growth phase.

Acknowledgment We highly acknowledge the financial support from the Deutsche Forschungsgemeinschaft (Graduate School 1257 "Alteration and element mobility at the microbe-mineral interface").

References

- Neufeld JD, Wagner M, Murrell JC (2007) ISME J 1:103
- Amann R, Ludwig W (2000) FEMS Microbiol Rev 24:555
- Amann RI, Ludwig W, Schleifer KH (1995) Microbiol Rev 59:143
- Kirschner C, Maquelin K, Pina P, Ngo Thi NA, Choo-Smith L-P, Sockalingum GD, Sandt C, Ami D, Orsini F, Doglia SM, Allouch P, Mainfaut M, Puppels GJ, Naumann D (2001) J Clin Microbiol 39:17639
- Naumann D, Keller S, Helm D, Schultz Ch, Schrader B (1995) J Mol Struct 347:399
- Lopez-Diez EC, Goodacre R (2004) Anal Chem 76:585
- Maquelin K, Dijkshoorn L, van der Reijen TJK, Puppels GJ (2006) J Microbiol Method 64:126
- Rösch P, Harz M, Peschke K-D, Ronneberger O, Burkhardt H, Popp J (2006) Biopolymers 82:312
- Rösch P, Harz M, Peschke K-D, Ronneberger O, Burkhardt H, Schüle A, Schmauz G, Lankers M, Hofer S, Thiele H, Motzkus H-W, Popp J (2006) Anal Chem 78:2163
- Huang WE, Stoecker K, Griffiths R, Newbold L, Daims H, Whiteley AS, Wagner M (2007) Environ Microbiol 9:1878
- Tarcea N, Harz M, Rösch P, Frosch T, Schmitt M, Thiele H, Hochleitner R, Popp J (2007) Spectrochim Acta A 68:1029
- Maquelin K, Choo-Smith LP, van Vreeswijk T, Endtz HP, Smith B, Bennett R, Bruining HA, Puppels GJ (2000) Anal Chem 72:12
- Krause M, Radt B, Rösch P, Popp J (2007) J Raman Spectrosc 38:369
- Harz M, Kiehnopf M, Stöckel S, Rösch P, Straube E, Deufel T, Popp J (2009) J Biophotonics 2:70
- Harz M, Rösch P, Peschke K-D, Ronneberger O, Burkhardt H, Popp J (2005) Analyst 130:1543
- Urlaub E, Popp J, Kiefer W, Bringmann G, Koppler D, Schneider H, Zimmermann U, Schrader B (1994) Biospectrosc 4:113
- Baranska M, Schulz H, Rösch P, Strehle MA, Popp J (2004) Analyst 129:926
- Krafft C (2004) Anal Bioanal Chem 378:60
- Schulz H, Baranska M, Belz H-H, Rösch P, Strehle MA, Popp J (2004) Vib Spectrosc 35:81
- Min Y-K, Yamamoto T, Kohda E, Ito T, Hamaguchi H (2005) J Raman Spectrosc 36:73
- Schulz H, Baranska M (2007) Vib Spectrosc 43:13
- Schmitt M, Popp J (2006) J Raman Spectrosc 37:20
- Edwards HGM (2004) Analyst 129:870
- Baraldi P, Tinti A (2008) J Raman Spectrosc 39:963
- Pätzold R, Keuntje M, Theophile K, Müller J, Mielcarek E, Ngezahayo A, Ahlfen A-v (2008) J Microbiol Meth 72:241
- Maquelin K, Kirschner C, Choo-Smith L-P, van den Braak N, Ph Endtz H, Naumann D, Puppels GJ (2002) J Microbiol Meth 51:255-271
- Berger AJ, Zhu Q (2003) J Mod Opt 50:2375
- Rösch P, Schmitt M, Kiefer W, Popp J (2003) J Mol Struct 661-662:363
- Rösch P, Harz M, Schmitt M, Peschke K-D, Ronneberger O, Burkhardt H, Motzkus H, Lankers M, Hofer S, Thiele H, Popp J (2005) Appl Environ Microbiol 71:1626
- Hutsebaut D, Vandroemme J, Heyrman J, Dawyndt P, Vandenaebcle P, Moens L, De Vos P (2006) Sys Appl Microbiol 29:650
- Gaus K, Rösch P, Petry R, Peschke K-D, Ronneberger O, Burkhardt H, Buamann K, Popp J (2006) Biopolymers 82:286
- Harz M, Rösch P, Popp J (2009) Cytom A 75:104
- Krause M, Rösch P, Radt B, Popp J (2008) Anal Chem 80:8568
- Bashin M, Reinherz EL, Reche PA (2006) J Comput Biol 13:102
- Noble WS (2006) Nat Biotechnol 24:1565
- Senior PJ, Beech GA, Ritchie GAF, Dawes EA (1972) Biochem J 128:1193
- Lee SY (1996) Biotechnol Bioeng 49:1
- Anderson AJ, Dawes EA (1990) Microbiol Rev 54:450
- Freier T, Kunze C, Nischan C, Kramer S, Sternberg K, Saß M, Hopt UT, Schmitz K-P (2002) Biomaterials 23:2649
- Jo S-J, Maeda M, Ooi T, Taguchi S (2006) J Biosci Bioeng 102:233

The influence of intracellular storage material

41. Page WJ, Knosp O (1989) *Appl Environ Microbiol* 55:1334
42. Yamane T (1993) *Biotechnol Bioeng* 41:165
43. Bormann EJ, Roth M (1999) *Biotechnol Lett* 21:1059
44. Hong K, Sun S, Tian W, Chen GQ, Huang W (1999) *Appl Microbiol Biotechnol* 51:523
45. Degelau A, Scheper T, Bailey JE, Guske C (1995) *Appl Microbiol Biotechnol* 42:653
46. De Gelder J, Willems-Erix D, Schotles MJ, Sanchez JJ, Maquelin K, Vandenaebete P, De Boever P, Puppels GJ, Moens L, De Vos P (2008) *Anal Chem* 80:2155
47. Bormann EJ, Leifner M, Roth M, Beer B, Metzner K (1998) *Appl Microbiol Biotechnol* 50:604
48. Furukawa T, Sato H, Murakami R, Zhang J, Noda I, Ochiai S, Ozaki Y (2006) *Polymer* 47:3132
49. Schmid U, Rösch P, Krause M, Harz M, Popp J, Baumann K (2009) *Chemometr Intell Lab* 96:159
50. Küsel K, Dorsch T, Acker G, Stackebrandt E (1999) *Appl Environ Microbiol* 65:3633
51. Küsel K, Roth U, Drake HL (2002) *Environ Microbiol* 4:414
52. Ryan CG, Clayton E, Griffin WL, Sie SH, Cousens DR (1988) *Nucl Instrum Meth B* 34:396
53. Pearson K (1901) *Philos Mag* 2:559
54. Tax DMJ, Duin RPW (2002) *ICPR* 2:20124
55. Burges CJC (1998) *Data Min Knowl Disc* 2:121

[VC2] Pelagic boundary conditions affect the biological formation of iron-rich particles (iron snow) and their microbial communities

Authorship of publication

M. Reiche: concept development
 sample collection
 measurements of geochemical parameters
 PCR/DGGE analysis
 writing the manuscript

S. Lu: sample collection
 measurements of geochemical parameters
 PCR/DGGE analysis
 writing the manuscript

V. Ciobota: Raman analysis
 discussion of results
 writing of manuscript

T. Neu: discussion of experimental concept and results
 proofreading of manuscript

S. Nietzsche: SEM analysis
 proofreading of manuscript

P. Rösch: discussion of experimental concept and results
 proofreading of manuscript

J. Popp: discussion of experimental concept and results
 proofreading of manuscript

K. Küsel: project management
 discussion of concepts and results
 discussion and proofreading of manuscript

Limnology and Oceanography 56 (2011) 1386-1398

Reprinted with kind permission from the *Association for the Sciences of Limnology and Oceanography, Inc.*

Pelagic boundary conditions affect the biological formation of iron-rich particles (iron snow) and their microbial communities

Marco Reiche,^a Shipeng Lu,^a Valerian Ciobotă,^b Thomas R. Neu,^c Sandor Nietzsche,^d Petra Rösch,^b Jürgen Popp,^{b,e} and Kirsten Küssel^{a,1,*}

^aInstitute of Ecology, Friedrich Schiller University Jena, Jena, Germany

^bInstitute of Physical Chemistry, Friedrich Schiller University Jena, Jena, Germany

^cDepartment of River Ecology, Helmholtz Centre for Environmental Research – UFZ, Magdeburg, Germany

^dCentre of Electron Microscopy, University Hospital Jena, Friedrich Schiller University Jena, Jena, Germany

^eInstitute of Photonic Technology, Jena, Germany

Abstract

We studied the formation of iron-rich particles at steeply opposing gradients of oxygen and Fe(II) within the redoxcline of an acidic lignite mine lake (pH 2.9). Particles formed had a diameter of up to 380 μm , showed high sedimentation velocity ($\sim 2 \text{ m h}^{-1}$), and were dominated by the iron mineral schwertmannite. Although the particles were highly colonized by microbial cells ($\sim 10^{10}$ cells [g dry weight] $^{-1}$), the organic carbon content was below 11%. Bathymetry and the inflow of less acidic, Fe(II)-rich groundwater into the northern basin of the lake results in two distinct mixing regimes in the same lake. The anoxic monimolimnion of the northern basin had higher pH, Fe(II), dissolved organic carbon, and CO_2 values compared with the more central basin. Particles formed in the northern basin differed in color, were smaller, had higher organic carbon contents, but were still dominated by schwertmannite. Microcosm incubations revealed the dominance of microbial Fe(II) oxidation. Comparison of bacterial clone libraries suggested that pH was a major driving force, shaping the microbial communities responsible for the oxidation of Fe(II) in both basins. Acidophilic *Ferrovum* spp. and Chlorobia-related bacteria were present in the central basin, whereas neutrophilic *Sideroxydans* spp. dominated the northern basin. Snow-like particles had a high sinking velocity and acted as a carrier for organic carbon, microorganisms, trace metals, and Fe(III) to the sediment. Because these particles are fundamentally different from organic-rich “snows” from lakes, rivers, and oceans, we propose a new term, “iron snow.”

Oxic-anoxic interfaces are hotspots for the cycling of elements because they provide continuously favorable conditions for both biotic and abiotic redox reactions. In aquatic ecosystems, these interfaces may appear as pelagic boundaries by separating an upper oxic and a lower anoxic water body, yielding permanently or temporally stratified conditions. These boundaries, or redoxclines, may occur in the water column of marine (Jørgensen et al. 1991; Taylor et al. 2001; Pimenov and Neretin 2006) and of freshwater bodies (Bohrer and Schultze 2008; Casamayor et al. 2008). Within such redoxclines, opposing gradients of oxygen and more reduced components, i.e., Fe(II), S^2 , and CH_4 , may establish. While the oxidation of S^2 (Jørgensen et al. 1991; Lüthy et al. 2000) and CH_4 (Rudd et al. 1974; Liu et al. 1996; Bédard and Knowles 1997) at redoxclines has been extensively investigated, less information is available about the oxidation of Fe(II). Some evidence for the cycling of iron at pelagic boundaries exists (Campbell and Torgersen 1980; Bohrer and Schultze 2006; Diez et al. 2007), and the formation of Fe(III)-minerals in acidic aquatic environments has been linked to a microbial oxidation of Fe(II) in the water column (Childs et al. 1998; Peine et al. 2000; Kawano and Tomita 2001). Similar processes might have

occurred in the Late Paleoproterozoic, leading to the formation of Paleozoic ironstones within the redoxclines of ancient marine sediments (Bekker et al. 2010). Since Fe(II) persists under abiotic conditions at pH values below 3.5 despite the presence of oxygen (Singer and Stumm 1970), acidophilic aerobic Fe(II)-oxidizing bacteria (FeOB) likely do not compete with the chemical oxidation of Fe(II) as compared to circumneutral conditions. However, no experiments at pelagic redoxclines have been performed which demonstrate whether this occurs and identify which microorganisms are involved in Fe(II) oxidation.

Opposing gradients of oxygen and Fe(II) can be found at redoxclines in iron-rich lakes that have been established worldwide in pyrite-rich or post-mining landscapes (Blodau 2006; Bohrer and Schultze 2006; Diez et al. 2007). In Germany, > 500 pit lakes originating from lignite mining exist with pH values ranging from below 2.5 to above 7 (Nixdorf and Kapfer 1998; Nixdorf et al. 2001). Pit lakes are characterized by the release of protons, sulfate, and Fe(II) from the oxidative weathering of Fe(II) sulfides in weakly buffered and dump-affected catchments. The subsequent oxidation of Fe(II) in ground- or surface waters leads to dissolved Fe(III) species which then transform into polymeric Fe(III) colloids prior to their precipitation as poorly crystalline Fe(III) oxyhydroxides (Davison 1993; Cornell and Schwertmann 2003; Hansel et al. 2003). Consequently, pit lake sediments are dominated by large quantities of amorphous $\text{Fe}(\text{OH})_3$, goethite, or Fe(III)

* Corresponding author: kirsten.kuessel@uni-jena.de

¹Present address: Aquatic Geomicrobiology Group, Institute of Ecology, Friedrich Schiller University Jena, Jena, Germany

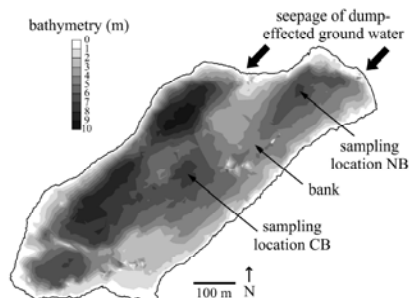


Fig. 1. Sampling sites and bathymetry of Lake 77 (modified after Fleckenstein et al. 2009). Groundwater flows from the north to the south and enters the lake from the dump area in the northern part. A bank rising to about 4 m from the surface separates the northeastern from the southern bottom water layers.

oxyhydroxysulfates, e.g., schwertmannite or jarosite, which are formed according to the pH and geochemistry (Bigham et al. 1992; Bigham and Murad 1997) present in the water column above (Peine et al. 2000; Regenspurg et al. 2004). Since Fe(III) oxyhydroxides can coprecipitate or adsorb organic carbon, heavy metals, and organisms (Eichler and Pfennig 1990; Martinez and McBride 1998; Eusterhues et al. 2008), they could play an important role in these pelagic processes.

In this study, we investigated the potential microbial formation of iron-rich particles at the pelagic redoxline of an acidic lignite mine lake (Lake 77) in east-central Germany. Because the inflow of less acidic, Fe(II)- and sulfate-rich groundwater from the dump area in the northeast (Blodau et al. 2004) has potential implications for the pelagic boundary conditions, particles were sampled from both the central and northeastern basin of the lake and were characterized with mineralogical and molecular methods. We hypothesized that the oxidation of Fe(II) and the formation of iron-rich particles depends on the activity of FeOB.

Methods

Site description and sampling—The acidic lignite mine lake (Lake 77, pH ~ 3) is located in the Lusatian mining area in east-central Germany and was created after lignite mining had ceased in the area in 1960s. The lake has a surface area of ~ 0.24 km², a volume of ~ 1 km³, and a maximum depth of about 9 m. The general pattern of water exchange is characterized by the Fe(II)- and sulfate-rich groundwater inflow from the dump area at the north end of the lake and the outflow of lake water to the aquifer in the south (Fig. 1). Exchange rates range from ~ 1.7 L m⁻² d⁻¹ (outflow) to > 200 L m⁻² d⁻¹ (inflow) (Fleckenstein et al. 2009).

Sampling sites were located in the central basin of the lake (location CB, depth 7 m, 51°31'8.2"N, 13°41'34.7"E) and in the northeastern basin of the lake (location NB,

depth 7 m, 51°31'13.3"N, 13°41'45.8"E) (Fig. 1). On each sampling date (April, July, August, September, and October 2009, and January and April 2010), pH, dissolved oxygen, conductivity, and temperature were measured over depth with a multiparameter water quality checker U-10 (Horiba, Japan). High-resolution water samples in steps of up to 5 cm were obtained using a water sampler (55-cm length) based on the Ruttner design. For gas analysis, 50-mL water samples were added to 150-mL glass flasks, sealed gas tight with rubber stoppers, and treated with 1 mL of 4 mol L⁻¹ HCl. Sediment traps (three Plexiglas tubes sealed with a removable cup at the bottom, 5-cm diameter, 40-cm total length) were installed at a depth of 5.3 m at location CB from which particles were collected every 3 to 4 weeks from April to October 2009. At location NB, particles were enriched by centrifugation of water samples obtained from 5-m depth or collected with sediment traps (April 2010 only). All samples were transported at 4°C and processed within 24 h. Sediment cores were obtained in September 2009 using a gravity corer (5.9-cm inside diameter) and the upper 5 mm were used for microbial diversity analysis. The sediment at location CB was characterized by an upper brownish-orange zone of about 20 cm and a black zone below. In contrast, the brownish-orange zone was < 3 cm deep at location NB. Below this, thin orange and black bands appeared. In general, the sediments contained large amounts of schwertmannite and goethite. Detailed geochemical descriptions of the sediment at location CB have been given elsewhere (Peine et al. 2000; Regenspurg et al. 2004).

Characterization of particles—The sinking velocity of single particles in 10 replicates was estimated at 21°C in a 3-liter glass cylinder filled with lake water. Sedimentation rate was calculated per m² d⁻¹ and was performed after drying (105°C for 24 h) of each subsample of the sediment trap material. Total cell abundance in the particles from location CB was enumerated by the 4,6-diamidino-2-phenylindole (DAPI) method (Porter and Feig 1980) after fixation (4% formaldehyde buffered with 1× phosphate buffered saline [PBS] at pH 7.4, washed three times with 1× PBS) and oxalate extraction (75 mmol L⁻¹ oxalate, 15-min incubation, washed three times with 1× PBS) with a Zeiss Axiolab microscope at ×1000 magnification (Carl Zeiss). The particle density in the water column was quantified on white polycarbonate filters (0.2-μm pore size, 39-mm diameter; Whatman) after filtration of defined volumes of lake water from 0, 3, and 5 m of location CB and 6 m from location NB with a Zeiss Axiolab microscope (Carl Zeiss) at 20× magnification. Mineral phases were determined using Raman spectroscopy and were recorded with a high-resolution LabRam spectrometer (Jobin Yvon Horiba) using 532-nm radiations from a frequency-doubled neodymium:yttrium-aluminum-garnet laser. The laser beam of about 20 μW was focused on the samples by a Leica PLFluor 100× (numerical aperture [NA] 0.75) microscope objective down to a spot diameter of approximately 0.7 μm. The spectral resolution was around 8 cm⁻¹ and the acquisition time for each Raman spectrum varied between 60 and 300 s.

Confocal laser scanning microscopy (CLSM)—To analyze the distribution of microbial cells in the particles, we counterstained bacteria in a fixed (3.4% formaldehyde) subsample of the sediment trap material obtained from location CB in September 2009 with SYTOX Orange (Molecular Probes) nucleic acid stain at a dilution of 1:1000 with deionized water for 5 min. Samples were rinsed once with tap water and transferred into Cover Well imaging chambers with a 0.2-mm spacer (Invitrogen), and immediately examined by CLSM using a true confocal scanner (TCS SP5X, Leica), equipped with an upright microscope and 63× NA 1.2 water immersion lens. Samples were analyzed by CLSM using laser lines at 547 and 633 nm. Emission signals were detected from 540 to 555 nm (inorganic and mineral compounds; detected by reflection signals), 560 to 620 nm (nucleic acid signals of SYTOX Orange), and from 650 to 750 nm (chlorophylls; detected by autofluorescence). Optical sections were scanned in the xy direction up to a depth of 100 μm with a step size of 1 μm . Images were recorded at a resolution of 1024 × 1024 pixels, corresponding to a 246- μm edge length. For visualization, image stacks were presented as overlays as maximum intensity projections. Blind deconvolution was calculated with Huygens version 3.5 (Scientific Volume Imaging).

Scanning electron microscopy (SEM) with energy-dispersive X-ray spectroscopy (EDX)—A subsample of the sediment trap material from either location CB or microcosm incubations was directly dried on adhesive conductive carbon tabs at 60°C to determine the overall morphology of the particles. The cell morphotypes present in the particles were determined after fixation (2.5% glutaraldehyde in PBS at pH 7.4, followed by washing three times with PBS), oxalate extraction (75 mmol L⁻¹ oxalate, 15-min incubation, washed three times with PBS), dehydration for 5 min each in ascending ethanol concentrations (10%, 20%, 30%, 50%, 70%, 80%, 90%, and 100%), and critical-point drying using liquid CO₂. Samples were sputter coated with platinum for high-resolution SEM or carbon coated by vacuum evaporation for EDX and finally examined under the SEM (LEO 1530 Gemini, Carl Zeiss) at magnifications of up to 20,000×. Elemental distribution was investigated using EDX (Quantax 200 with XFlash detector, Bruker) at a SEM (LEO 1450 VP, Carl Zeiss).

Determination of microbial Fe(II) oxidation in microcosms—At location CB, water was sampled from depths of either 3 m (oxic zone) or 6 m (anoxic zone) and at location NB, water was sampled from depths of 4.8 m (redoxcline) or 5.5 m (anoxic zone) in September and October 2009. Fifty milliliters of untreated lake water was transferred to sterile 150-mL incubation flasks (Mueller and Krempel) in triplicates. Headspace was air with an oxygen content of 21%. Samples poor in Fe(II) from 3 m were amended with sterile Fe(II)SO₄ solution to yield 3 and 12 mmol L⁻¹ Fe(II). Microcosms were closed with rubber stoppers, screw-capped, and incubated in the dark at 15°C for 9 d. Potential chemical Fe(II) oxidation was determined in abiotic controls after sterile filtration (0.2 μm).

Analytical techniques—The oxidation of Fe(II) was determined by measuring the amount of Fe(II) after acid extraction. Aliquots (0.5 mL) were removed daily from the microcosms with sterile syringes, transferred to 9.5 mL of 0.5 mol L⁻¹ HCl, and then incubated for 1 h at room temperature. Fe(II) concentrations were measured spectrophotometrically (DR3800, Hach Lange) by the phenanthroline method (Tamura et al. 1974). Rates of Fe(II) oxidation were calculated for the time period over which a linear decrease in the Fe(II) concentration was observed. After addition of ascorbic acid, HCl-extractable Fe(III) was calculated from the increase in Fe(II) concentration. Sulfate was measured turbidimetrically by the barium chloride-gelatin method (Tabatabai 1974). Water sample density was measured with a hydrometer at 6°C. Headspace CO₂ and CH₄ was measured with 5890 series II gas chromatographs equipped with a thermal conductivity detector or flame ionization detector (Hewlett-Packard) (Küsel and Drake 1995). The elemental composition of dried (60°C) and milled particles was directly analyzed with an elemental analyzer (vario Max or vario EL II, Elementar) or by inductively coupled plasma mass spectrometry (ICP-MS; XSeries II, Thermo Fisher Scientific) and inductively coupled plasma optical emission spectrometry (ICP-OES; Spectroflame, Spectro) after aqua regia decomposition. Heavy metal concentrations in lake water were analyzed with ICP-MS or ICP-OES without further treatment. Dissolved organic carbon (DOC) and dissolved nitrogen in water samples from both locations were measured with a total organic carbon analyzer (TOC-V CPN equipped with a total nitrogen module, Shimadzu).

Deoxyribonucleic acid (DNA) extraction and polymerase chain reaction (PCR) amplification of 16S ribosomal ribonucleic acid (rRNA) genes—Genomic DNA was directly extracted from particles captured in the sediment traps of location CB or obtained from the water column at location NB, and from the sediments at both locations using the PowerSoil, DNA Isolation Kit according to the manufacturer's instructions (MO BIO Laboratories). Samples from microcosms were concentrated by centrifugation (5 min at 10,000 × g) after scraping off the rust-colored crust or the extraction of rust-colored flakes before treatment. DNA extracts were PCR amplified with the bacteria domain-specific 16S rRNA gene primers 27F and 1492R-2 (Lane 1991) and purified using the NucleoSpin Extract II PCR purification kit (Macherey-Nagel). Thermocycling was performed with a T-Gradient cycler (Primus 96advanced, peqLab). Reactions were run for 30 cycles of amplification at an annealing temperature of 56°C.

Denaturing gradient gel electrophoresis (DGGE) fingerprinting—Bacterial community DNA extracted from the particles and sediments was fingerprinted using a nested-PCR-DGGE approach. Nested amplification of the bacteria domain-specific 16S rRNA products was executed with the universal bacterial primers GMSF-GC-clamp and 907R (Muyzer et al. 1995) with an annealing temperature of 55°C and 20 cycles of amplification. PCR products were separated on an 8% polyacrylamide gel with a 30% to 70%

denaturant gradient (Muyzer et al. 1993) in $1 \times$ tris-acetate-ethylene diamine tetraacetic acid buffer using the DGGE 1001 system (C.B.S. Scientific). DGGE gels were run for 15 h at 60°C and 100 V. To compare the bacterial community composition between sites, sampling dates, and sampling sources, Jaccard Similarity values were calculated (Schloss and Handelsman 2006). These values consider how many bands are shared between DGGE band patterns relative to the total number of bands. Similarity matrices were turned into dendrograms to visualize the clustering of bacterial communities based on their similarities in band composition, utilizing the Clustering Calculator programs of Brzustowski (2002) and Interactive Tree of Life (Letunic and Bork 2006).

Clone library construction and phylogenetic analyses—Bacteria domain-specific 16S rRNA PCR products obtained in September 2009 from the particles at both locations were ligated into pCR4-TOPO vector (Invitrogen Corporation), cloned according to the manufacturer's recommendations, and sequenced at Macrogen. Cloning and bidirectional sequencing was also done at The Genome Center at Washington University. Sequences were processed with Geneious software (Drummond et al. 2009), aligned against the 16S Greengenes rRNA gene database using NAST (DeSantis et al. 2006a), and analyzed with the ARB software package (Ludwig et al. 2004) in combination with the Greengenes database (DeSantis et al. 2006b). Sequences sharing > 97% similarity were grouped as the same phylotype using FastGroup II (Yu et al. 2006). The percentage of coverage between the clone libraries was calculated with the formula $(1 - [n/N]) \times 100$, where n is the number of unique phylotypes and N is the total number of phylotypes. Double-reciprocal analysis of rarefaction data was then used to estimate the maximum amount of expected phylotypes.

Nucleotide sequence accession numbers—The 16S rRNA gene sequences determined in this study have been deposited in the European Molecular Biology Laboratory database under accession numbers FR667757 to FR667847.

Results

Biogeochemical characteristic of the water column—A dimictic stratification scenario, with typical spring and fall mixes, occurred at CB. Early thermal stratification was established in April with a decrease from 15°C to 9°C between 3- and 5-m depths (data not shown), whereas the other measured parameters remained stable over depth. An anoxic hypolimnion occurred from July to September (Fig. 2A and data not shown) with higher Fe(II) and pH values as compared to April and no change in sulfate concentrations and conductivity. Density of both surface and bottom water was approximately 1.000 g mL⁻¹. The anoxic hypolimnion was separated from the overlying oxic mixolimnion by a pronounced redoxcline of about 60-cm thickness within the thermocline starting at about 4.8 m. The stratification at CB disappeared due to changing

temperature in October and parameters returned to spring values (Fig. 2C). In the winter, the water body was again thermally stratified, but under ice coverage (data not shown).

At NB, values for Fe(II), sulfate, pH, and conductivity increased sharply within the redoxcline and reached the highest values in the hypolimnion, respectively (Fig. 2B,D). Fe(II) and oxygen coincided within the redoxcline by forming a distinct transition zone of about 30 cm (Fig. 2). The density of the bottom water was always higher (1.001 g mL⁻¹) than that of the surface water (1.000 g mL⁻¹). As stratification did not disappear at NB, the water column was continuously divided into an oxic mixolimnion and an anoxic monimolimnion by the sharp redoxcline centered at about 4.3 m (Fig. 2B,D). Even when the surface water was colder than the bottom water, complete vertical mixing was inhibited (Fig. 2D), suggesting a permanent separation of the bottom water bodies at CB and NB, which might be due to a bank (4 m deep) separating the central and the northern basins (Fig. 1).

Lake 77 can therefore be classified as meromictic with a distinct monimolimnion in the northern basin. In contrast to location CB, acid-releasable CO₂ increased from 0.4 mmol L⁻¹ in the mixolimnion within the bottom water layer up to 11.3 mmol L⁻¹ (Table 1). Concentrations for CH₄ were always below the detection limit (< 40 nmol L⁻¹) at both locations. Water from the bottom at NB was slightly opaque and characterized by a yellowish color. Water from the surface and water samples obtained from CB never showed visible coloration.

Dissolved Ni, Co, Cu, Zn, Pb, As, Cd, and U concentrations were below 4 μmol L⁻¹ and appeared similar at CB and NB during stratification in September (data not shown). In contrast, concentrations for Al were lowest in the monimolimnion of location NB (9 μmol L⁻¹) as compared to the hypolimnion at CB (152 μmol L⁻¹) and the connected surface mixolimnion (264 μmol L⁻¹). Concentrations of DOC were high, ranging from about 0.4 mmol L⁻¹ in the mixolimnion to about 2.3 mmol L⁻¹ in the monimolimnion at NB (Table 1).

Characteristics of lake particles—Particles obtained from the oxic mixolimnion were up to 380 μm in size. Single particles in samples collected directly from the anoxic hypolimnion typically ranged from 60 to about 240 μm at CB, and from 20 to 120 μm in the anoxic monimolimnion at NB (Table 2). The sinking velocity of single particles from location CB was 1.5 to 2 m h⁻¹ which equals 3.5 to 4.7 h for horizontal passage through the whole water column or < 1.8 h through the anoxic water layers at the bottom of Lake 77 under undisturbed conditions. Particle densities were lower in the mixolimnion than the hypolimnion at CB and the monimolimnion at NB in September (Table 2). The sedimentation rate of particles obtained with sediment traps from August to October was approximately 3.9 ± 1.1 g (dry wt) m⁻² d⁻¹ at CB, yielding an annual precipitation of about 1400 g (dry wt) m⁻². A single measurement in July 2010 at NB revealed 5.5 g (dry wt) m⁻² d⁻¹ and 2000 g (dry wt) m⁻² over 1 yr.

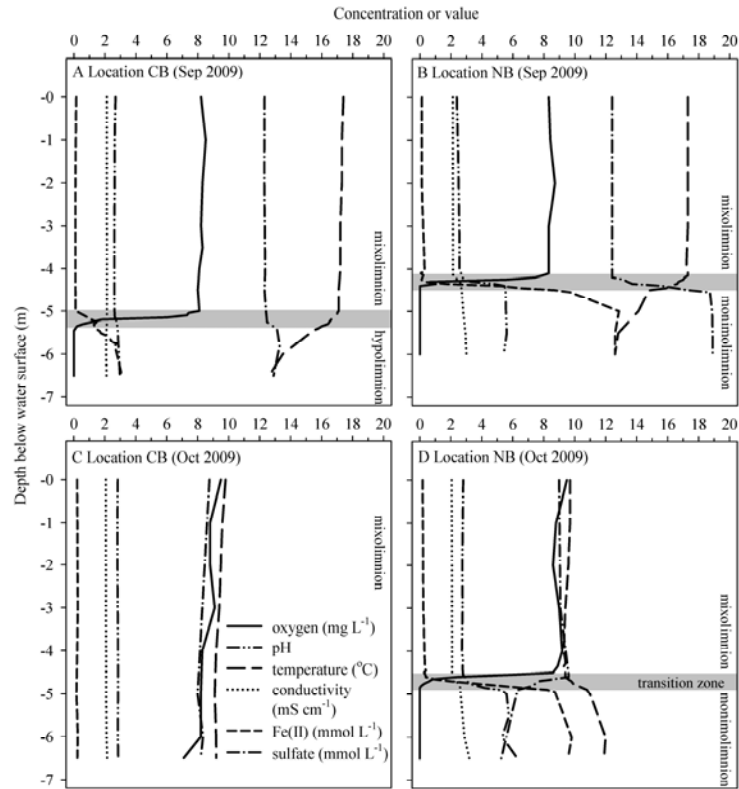


Fig. 2. Water profiles of biogeochemical parameters measured at two sampling locations within the acidic lignite mine Lake 77 in September (A and B) and October (C and D) 2009. CB (A and C) has a dimictic regime with an anoxic hypolimnion in summer and NB (B and D) has a continuous anoxic monimolimnion.

Particles obtained at location CB appeared as rust-colored floating flakes. Flakes were composed of aggregates of hedgehog-like spheres with diameters of 0.7 to 13 μm determined by SEM (Fig. 3A). The hedgehog-like

morphology of the aggregates is characteristic for schwertmannite (ideal formula: $\text{Fe}_8\text{O}_8(\text{OH})_6\text{SO}_4$), a poorly crystalline, yellowish-brown Fe(III) oxyhydroxysulfate mineral (Bigham et al. 1990, 1994; Regenspurg et al. 2004). Mass

Table 1. Water characteristics in different water layers of the acidic lignite mine Lake 77. Samples were obtained at two locations (central basin [CB] and northeastern basin [NB]), which differ in their stratification patterns.

Water layer	Location	Depth (m)	pH*	DOC† (mmol L ⁻¹)	CO ₂ † (mmol L ⁻¹)	Fe* (mmol L ⁻¹)	Al* (mmol L ⁻¹)
Mixolimnion	CB	3	2.6	0.4	0.4	1.8	0.26
Hypolimnion	CB	6	2.9	0.4	0.4	3.8	0.15
Monimolimnion	NB	5	5.6	2.3	11.3	11.7	0.01

* Samples obtained in September 2009.

† Samples obtained in January 2010.

Table 2. Iron-rich particle (iron snow) characteristics in different water layers of the acidic lignite mine Lake 77. Samples were obtained during lake stratification during the summer at two locations (central basin [CB] and northeastern basin [NB]), which differ in their stratification patterns.

Water layer	Location	Depth (m)	Particles (L ⁻¹)	Particle size range (μm)	Sinking velocity (m h ⁻¹)	Sedimentation rate (g [dry wt] m ⁻² d ⁻¹)
Mixolimnion	CB	3	~10 ⁶	60–380	n.d.	n.d.
Hypolimnion	CB	6	~10 ⁸	60–240	1.5–2	3.9
Monimolimnion	NB	5	~10 ⁹	20–120	n.d.	5.5

n.d., not determined.

ratios of elements detected using SEM-EDX and direct scanning using Raman spectroscopy revealed schwertmannite as the dominant mineral (Fig. 4 and data not shown). Minor amounts of the Fe(III) minerals goethite, ferrihydrite, and jarosite, as well as quartz, coal, and gypsum, were also identified by Raman spectroscopy (Fig. 4). Raman spectra did not reveal Fe(II) minerals like pyrite, marcasite, siderite, vivianite, or magnetite. The precipitated particles in the central basin contained 6.9 mmol Fe (g dry wt)⁻¹, which is 39% of the dry weight mass, followed by S (5.0%), C (3.1%), Al (1.8%), Ca (0.4%), and nitrogen (0.2%) (Table 3). The proportions of Ni, Co, Cu, Zn, Pb, As, Cd, and U were all below 0.07% (data not shown).

At NB, particles were more yellowish-orange than those at CB. Spherical structures were about 1 μm in diameter and less structured. Raman spectra revealed high amounts of schwertmannite, gypsum, and other unidentified sulfate-containing minerals. Minor amounts of non-coal carbon and ferrihydrite were also detected. Again, no Fe(II) minerals appeared. These particles contained 35% Fe (equal to 6.3 mmol Fe [g dry wt]⁻¹), followed by C (10.9%), S (3.8%), nitrogen (0.3%), Al (0.2%), and Ca (0.2%) (Table 3). Proportions of Ni, Co, Cu, Zn, Pb, As, Cd, and U were all below 0.04% (data not shown).

Biotic vs. abiotic Fe(II) oxidation—Oxic microcosms incubated with Fe(II)-poor surface water (initial pH 2.9) obtained from the mixolimnion at CB showed a decrease in Fe(II) concentrations over time after addition of Fe(II).

Potential Fe(II) oxidation rates were approximately 0.2 or 0.6 mmol L⁻¹ Fe(II) d⁻¹ when 3 or 12 mmol L⁻¹ Fe(II) were added, respectively (Fig. 5A and data not shown). HCl-extractable Fe(III) concentrations increased similarly with rates of 0.2 and 0.5 mmol L⁻¹ Fe(III) d⁻¹ (data not shown). No chemical Fe(II) oxidation occurred. Oxic microcosms incubated with Fe(II)-rich water (3.1 mmol L⁻¹ Fe(II), initial pH 3.1) obtained from the anoxic hypolimnion at CB yielded an initial potential Fe(II) oxidation rate of 0.7 mmol L⁻¹ Fe(II) d⁻¹ (Fig. 5B). Fe(II) was totally oxidized within 5 d of incubation and the rate of Fe(III) formation was 0.4 mmol L⁻¹ Fe(III) d⁻¹ (data not shown). Again, no chemical Fe(II) oxidation occurred.

Initial potential Fe(II) oxidation in Fe(II)-rich water samples (4.3 mmol L⁻¹ Fe(II), initial pH 3.2) obtained from the redoxcline at NB yielded potential oxidation rates of 0.3 mmol L⁻¹ Fe(II) d⁻¹ (Fig. 5B), and Fe(II) concentrations in sterile filtrated or poisoned samples did not change over time.

Iron particles formed in microcosms—Fe(II) oxidation led to an iron crust attached to the inner glass surface of the microcosms in water samples obtained from CB, whereas iron flakes sedimented in microcosms with water from NB. However, Raman spectroscopy revealed no difference in composition between locations, showing schwertmannite as the dominant Fe(III) oxide. The morphology of the minerals in NB samples was dominated by hedgehog-like spheres as compared to the crumb- and clod-like structures

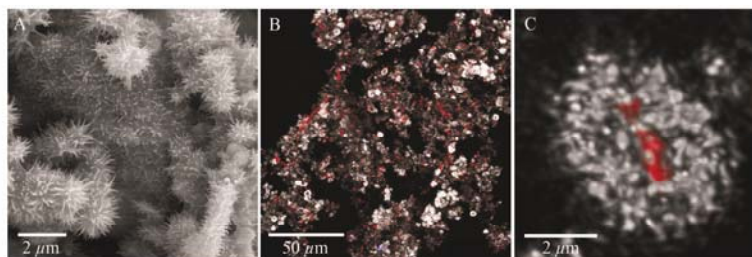


Fig. 3. Micrographs of iron-rich particles (iron snow) captured in sediment traps at CB of the acidic lignite mine Lake 77 in September 2009. (A) Scanning electron micrograph showing hedgehog-like spheres characteristic for schwertmannite, a poorly crystalline, yellowish-brown Fe(III) oxyhydroxysulfate mineral. (B) Confocal laser scanning microscopy (CLSM) of an aggregate colonized by bacteria of different morphology. (C) Close-up of a single bacterium inside reflective material after deconvolution. CLSM color allocation: reflection signal = white, nucleic acid stain = red, phototrophic signals = blue.

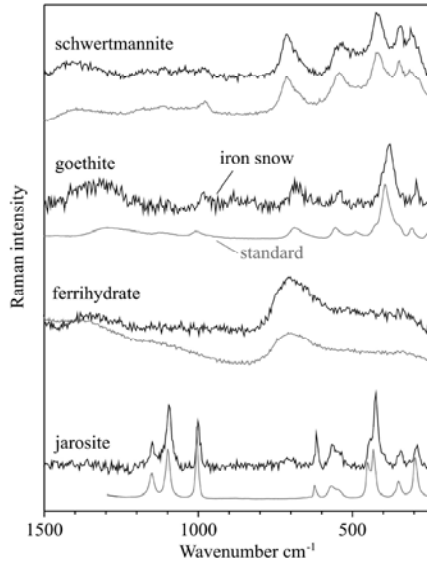


Fig. 4. Raman spectra of the iron particles (iron snow) obtained at CB (black lines) and spectra of authentic standards (gray lines). The main mineral detected was schwertmannite. The particles contained also small amounts of goethite, ferrihydrite, and jarosite.

in CB samples. Recently, Lu et al. (2010) also demonstrated that acidophilic and acid-tolerant Fe(II)-oxidizing bacteria isolated from this lake form schwertmannite.

Biotic composition of lake particles—Stained microbial cells and unstained phototrophs were detected in precipitated particles obtained at location CB using CLSM (Fig. 3B). Microbial cells were homogeneously distributed and cells were often present within the reflective schwertmannite spheres (Fig. 3C). Total DAPI counts yielded up to 10^{10} cells (g dry wt)⁻¹. Cell morphology was generally dominated by filamentous (up to 200- μ m length), cocci (up to 2.3- μ m diameter), rods (up to 5- μ m length), and club rods (up to 2.5- μ m length). Phototrophic signals were rare at a maximum of two algal cells per particle. Two unicellular diatom species with a length of about 22 μ m

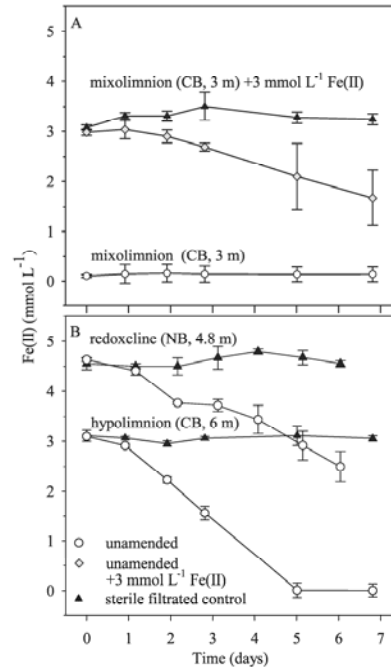


Fig. 5. Fe(II) oxidation in oxic microcosm flasks over time in water samples obtained from different water zones at the central (CB: A and B) and northern basin (NB: B) of the acidic lignite mine Lake 77 in September 2009.

were morphologically similar to *Eunotia* spp. as identified by SEM after oxalate extraction. One of these diatoms and several rod-shaped bacteria, covered or decorated by needle- and coral-like iron minerals, were present in close association with the schwertmannite spheres as detected by SEM. *Eunotia* spp. are widely distributed in both acidic aquatic environments and lignite mining-associated lakes (Nixdorf et al. 2001).

16S rRNA gene-based community analysis—PCR products obtained from particles sampled at CB and NB at

Table 3. Elemental composition of iron-rich particles (iron snow) in the acidic lignite mine Lake 77 obtained from sediment traps at the temporally stratified central location (CB) in September 2009 and obtained from water samples at the permanently stratified northern location (NB) in April 2010.

Water layer	Location	Depth (m)	C (%)	N (%)	Fe (mmol g [dry wt] ⁻¹)	S (mmol g [dry wt] ⁻¹)	Al (mmol g [dry wt] ⁻¹)	Ca (μ mol g [dry wt] ⁻¹)	Mg (μ mol g [dry wt] ⁻¹)	Mn (μ mol g [dry wt] ⁻¹)
Hypolimnion	CB	6	3.1	0.2	6.9	1.6	0.7	105	30	1
Monimolimnion	NB	5	10.9	0.3	6.3	1.2	0.1	61	15	1

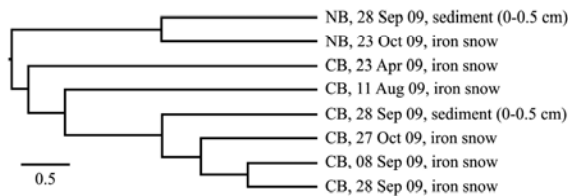


Fig. 6. Similarities of DGGE patterns of bacterial 16S rRNA genes in iron-rich particles (iron snow) and the sediment surface obtained from the northern (NB) and central basin (CB) of Lake 77 based on Jaccard Similarity values.

different times of the year and their respective sediment surfaces produced different DGGE patterns (data not shown). A maximum of 38 different bands was differentiated in each pattern. Clustering of bacterial communities based on their similarities in band composition demonstrated that particles at location CB differed in April and August but appeared to be more similar at the beginning and end of September, and of October (Fig. 6). Consequently, clone library construction was done with the CB particles from the end of September, as it was likely most representative for the period of late stratification. DGGE patterns from particles and sediment surfaces shared great similarity within NB and CB. Patterns were most dissimilar between NB and CB (Fig. 6), suggesting that the different pelagic conditions at each location were responsible for shaping the microbial communities of the particles.

Screening of the clone libraries obtained in September 2009 from CB and NB revealed the presence of 52 and 46 phylotypes out of 90 and 74 clones in the particles, respectively. Both clone libraries shared about 5.5% similarity and had 62% and 66% saturation with respect

to the expected number of phylotypes in locations CB and NB, respectively. Many of the clones obtained at CB belonged to four classes (Fig. 7), and were related to acidophilic FeOB, e.g., nine clones were related to *Ferrovum myxofaciens* (Betaproteobacteria, sequence similarity up to 96%), five clones to *Acidimicrobium ferrooxidans* (Actinobacteria, sequence similarity up to 89%), and two clones to *Chlorobium ferrooxidans* (Chlorobia, sequence similarity up to 98%). Some clones were also related to neutrophilic Fe(III)-reducing bacteria like *Geobacter chapellei* (Deltaproteobacteria, sequence similarity up to 97%) and *Geobacter psychrophilus* (sequence similarity up to 99%).

In contrast, particles from NB were dominated only by Betaproteobacteria (Fig. 7), within which 44% of the sequences were related to the neutrophilic FeOB *Sideroxydans lithotrophicus* (sequence similarity up to 98%). One *Sideroxydans* strain is known to oxidize Fe(II) between pH 4.0 and 6.0 (Lüdecke et al. 2010). Several Fe(III) reducers were also detected with sequences related to *Albidiferax ferrireducens*, *Pelobacter propionicus*, *Geobacter chapellei*, and *Geobacter psychrophilus* strain P35.

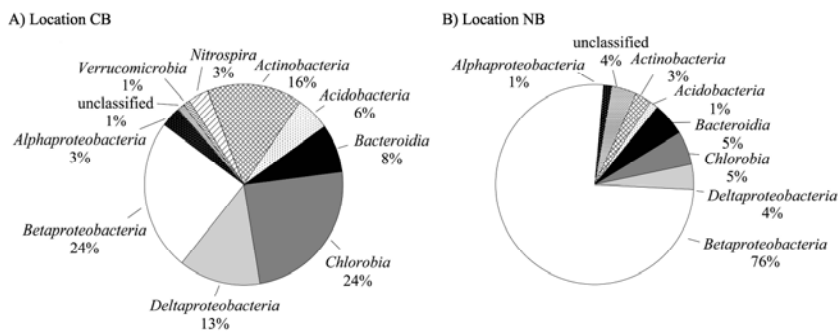


Fig. 7. Frequencies of bacterial phylogenetic lineages detected in 16S rRNA gene-based clone libraries derived from iron-rich precipitated particles (iron snow) below the redoxcline in September 2009 at two sampling locations of acidic lignite mine Lake 77, which differ in stratification patterns and water chemistry. (A) CB has a dimictive regime with an anoxic hypolimnion in summer and (B) NB has a continuous anoxic monimolimnion. Calculations were based on the total number of clones associated with phylotypes of sequenced representatives.

Discussion

The two sampling locations investigated within this iron-rich, acidic lignite mine lake were similar in total water depth but differed in stratification patterns and pelagic boundary conditions. These differences might be caused both by the bank which rises to about 4-m depth and separates the bottom water layers of the northeastern basin from the rest of the lake (Fig. 1) and by local differences in groundwater inflow. At NB, seepage from the northeastern dump area enters the lake. This inflow of less acidic, Fe(II)- and sulfate-rich groundwater (pH 3.8, 3.5 mmol L⁻¹ and 10 mmol L⁻¹ each; J. Beer pers. comm. 2010) to the separated northern basin may lead to an advective accumulation of dissolved substances, resulting in a density stratification and monimolimnion. In contrast, CB showed a seasonal thermal stratification with a typical mixolimnion and hypolimnion during summer. The hypolimnion was likely less affected by outflow from the dump area and chemical gradients appeared to be more diffusion limited. Dissolved Fe(II) might then only be supplied by the ongoing Fe(III) reduction in the anoxic sediment (Küsel et al. 1999; Blöthe et al. 2008).

High amounts of snow-like particles occurred in the anoxic bottom water layers at both locations. Pelagic particles formed in freshwater or marine environments are generally called "lake snow," "river snow," or "marine snow" depending on their respective environment (Grossart and Simon 1993; Neu 2000). These "snows" are important for the turnover and sinking flux of organic and inorganic matter (Simon et al. 2002) and usually contain a large organic fraction dominated by transparent exopolymers, copepod carcasses, phytoplankton, bacteria, protozoa, and fungi (Simon et al. 2002; Rother and Kohler 2005; Tang et al. 2006). Aggregates in oceans and lakes are usually larger than 500 µm (Alldredge and Silver 1988; Grossart and Simon 1993), whereas the median size in rivers is generally < 60 µm (Berger et al. 1996; Rother and Kohler 2005). Due to their slow sinking velocities and long residence times within the water column, these snow-like particles become hotspots for microbial respiration and growth efficiency (Ploug et al. 1999; Grossart and Ploug 2000; Luef et al. 2007). Particles formed in Lake 77 were generally smaller than 380 µm in diameter and were dominated by an Fe(III)-rich fraction of > 35% rather than organic matter. These Fe(III)-dominated, microscopic particles and aggregates sedimented as visible rust-colored snow, yielding an estimated Fe(III) sedimentation rate of about 1.5 and 1.9 g Fe m⁻² d⁻¹ at CB and NB, respectively. Their higher sinking velocity compared to classical lake snow may not allow all of the potentially complex aspects of aggregate formation, microbial colonization, and decomposition to occur. Therefore, we propose a new term, "iron snow," for these types of aggregates.

That the size, color, composition, and mineral morphology of iron snow differed at both locations apparently was caused by the different pelagic boundary conditions and microbial communities present during formation. Particle characteristics may have shown even greater variety were samples analyzed that had been taken with higher temporal

and spatial variation. Raman spectroscopy and SEM-EDX revealed schwertmannite as the dominant iron mineral in all samples. Schwertmannite typically forms in acidic, sulfate-rich waters (Bigham et al. 1990; Schwertmann et al. 1995; Childs et al. 1998) but can form at pH values up to 6.3 (Murad and Rojik 2005). Due to its high specific surface area of a range of 75 to 200 m² g⁻¹ (Bigham et al. 1994; Regenspurg et al. 2004), iron snow provides reactive Fe(III) as electron acceptor for anaerobic microbial respiration not only after, but also during, sedimentation. Indeed, iron snow clone libraries harbored numerous clones related to Fe(III)-reducing bacteria like *Geobacter* spp. (Deltaproteobacteria), although *Geobacter* species are not known to inhabit such acidic environments (Lovley et al. 2004). The similarity of the DGGE patterns obtained from the iron snow and sediment surface at both locations suggest further that the iron snow may serve as carrier for general microbial transport to the sediment. It appeared to also have a carrier function for Al, Ca, Mn, Mg, and heavy metals which likely either coprecipitated during iron snow formation or adsorbed to its surface similarly to what is known for other Fe(II)-precipitates (Spark et al. 1995; Martinez and McBride 1998).

Aquatic particles generally contribute to the sedimentary organic carbon pool (de Vicente et al. 2009). The carbon (C) content of iron snow was 3.1% and 10.9% at CB and NB, respectively, and was mainly attributed to microbes and associated organic matter. The equivalent C sinking loss of iron snow estimated from its C content and sedimentation rate is approximately 121 and 600 mg C m⁻² d⁻¹ at CB and NB, respectively. However, this rough estimate is one to two orders of magnitude lower than C sedimentation rates observed in pH-neutral lakes (Grossart and Simon 1998; Moreira-Turcq et al. 2004), where less extreme geochemical conditions result in a higher planktonic primary production (Gyure et al. 1987; Nixdorf et al. 2003; Kamjunke et al. 2005).

The amount of particles was highest in the anoxic bottom water layer, indicating that they are formed within or next to the redoxcline. Steep gradients of oxygen and Fe(II) formed a transition zone 30 to 60 cm deep within the redoxcline during stratification with suitable conditions for aerobic Fe(II) oxidation. The lack of nitrate in the water column should exclude nitrate-dependent Fe(II) oxidation in the anoxic water depths below the redoxcline. Morphology and mineral composition of the rust-colored aggregates formed during oxic microcosm incubations was similar to iron snow sampled from the lake. Because chemical oxidation was never observed, microorganisms appeared to mediate both Fe(II) oxidation and iron snow formation as was assumed in previous studies (Bigham et al. 1990; Childs et al. 1998; Kawano and Tomita 2001). Bacterial cell surfaces may trigger the precipitation of mineral phases as indicated by the CLSM data (Fig. 3C). The capacity for aerobic Fe(II) oxidation was not restricted to water samples obtained from the oxic-anoxic transition zone, but could be initiated both in Fe(II)-poor surface water and in anoxic bottom water (Fig. 5). The zone of aerobic microbial Fe(II) oxidation is likely to span several centimeters within the redoxcline similar to the Fe(II) oxidation zone observed in

an acidic, iron-rich fen (Lüdecke et al. 2010). After mixing in fall, this zone will be temporarily enlarged to the whole water body in the central basin. The oxic-anoxic interface will then move to the sediment surface, similar to what is observed in more pH-neutral environments, where the zone of microbial Fe(II) oxidation is restricted to a few millimeters or less (Mendelsohn et al. 1995; Roden et al. 2004; Druschel et al. 2008).

DGGE analyses revealed the presence of different microbial communities colonizing the iron snow at CB during the beginning and late stratification. However, the differences between sampling locations was more pronounced. Additionally, the libraries from these locations shared only 5.5% similarity, which might be due to the pH discrepancy. *Sideroxydans*-related clones were highly abundant in the NB clone library but did not appear in the CB clone library. These clones have been isolated from a number of pH-neutral to moderately acidic soils and sediments (Emerson and Moyer 1997; Weiss et al. 2007; Lüdecke et al. 2010). Species of this genus are microaerophiles that use Fe(II) as energy for chemolithotrophic growth with CO₂ as the sole carbon source (Emerson and Moyer 1997). Clones closely related to *Ferrovium myxofaciens* were the most prominent species in the CB clone library. These acidophilic, obligate autotrophs use Fe(II) solely as an energy source (Rowe and Johnson 2008). Within the Actinobacteria, several of our clones were related to the acidophilic, Fe(II)-oxidizing organism *Acidimicrobium ferrooxidans*. Members of this species have been isolated or identified molecularly from warm, acidic, iron-, sulphur-, or mineral-sulfide-rich environments (Clum et al. 2009). The average Secchi depth of about 3 m (data not shown) should provide favorable conditions for phototrophic FeOB as well within and below the redoxcline. At CB, several clones clustered within the phylum Chlorobia, which contains phototrophic sulfur bacteria. A member of this phylum, the green sulfur bacterium *Chlorobium ferrooxidans* strain KoFox, oxidizes Fe(II) under pH-neutral conditions (Heising et al. 1999), even in the presence of low light saturation (Hegler et al. 2008). The NB clone library did not contain clones related to phototrophic bacteria, apparently due to the high particle density and the opaque-yellowish color of the water below the redoxcline which would restrict the light available for phototrophic bacteria near the bottom.

Our data highlight the importance of pelagic boundary conditions on the microbial oxidation of Fe(II) and the formation of iron-rich particles, here introduced as "iron snow," in an iron-rich, acidic lake. The redoxcline favored the activity of aerobic FeOB by providing strong vertical gradients of oxygen and Fe(II) within a centimeter range and the formation of schwertmannite appeared to result from a biological process independent of the pH and the microbial communities involved. Therefore, Fe(II) oxidation in this lake can be attributed primarily to microbial activity. The formation of iron snow links the redoxcline strongly with the sediment, providing a mechanism for rapid removal of not only iron, but also of microbial cells, organic carbon, and trace metals from the water column down to the sediment. This microbially mediated formation of iron snow might

occur not only in lignite mine lakes but also in other lakes with redoxclines of opposing oxygen and Fe(II) gradients.

Acknowledgments

We thank I. Hilke, T. Walter, H. Köpf, J. Beer, and C. Neumann for technical assistance and support, and U. Kuhlicke and S. Linde for sample preparation, confocal laser scanning microscopy, and scanning electron microscope imaging. We thank D. Akob and M. Herrmann for helpful discussions and P. Bouwma for critical reading. This work was supported by the German Research Foundation (Deutsche Forschungsgemeinschaft [DFG]) grant KU 1367/8-1 and by the Jena School for Microbial Communication (JSMC).

References

- ALLDREDGE, A. L., AND M. W. SILVER. 1988. Characteristics, dynamics and significance of marine snow. *Prog. Oceanogr.* **20**: 41–82, doi:10.1016/0079-6611(88)90053-5
- BÉDARD, C., AND R. KNOWLES. 1997. Some properties of methane oxidation in a thermally stratified lake. *Can. J. Fish. Aquat. Sci.* **54**: 1639–1645, doi:10.1139/f97-300
- BEKKER, A., J. F. SLACK, N. PLANAVSKY, B. KRAPEZ, A. HOFMANN, K. O. KONHAUSER, AND O. J. ROUXEL. 2010. Iron formation: The sedimentary product of a complex interplay among mantle, tectonic, oceanic, and biospheric processes. *Econ. Geol.* **105**: 467–508, doi:10.2113/gsecongeo.105.3.467
- BERGER, B., B. HOCH, G. KAVKA, AND G. J. HERNDL. 1996. Bacterial colonization of suspended solids in the River Danube. *Aquat. Microb. Ecol.* **10**: 37–44, doi:10.3354/ame010037
- BIGHAM, J. M., L. CARLSON, AND E. MURAD. 1994. Schwertmannite, a new iron oxyhydroxysulfate from Pyhasalmi, Finland, and other localities. *Mineral. Mag.* **58**: 641–648, doi:10.1180/minmag.1994.058.393.14
- , AND E. MURAD. 1997. Mineralogy of ochre deposits formed by the oxidation of iron sulfide minerals, p. 193–225. *In* K. Auerswald, H. Stanjek, and J. M. Bigham [eds.], *Soils and environment: Soil processes from mineral to landscape scale*. *Advances in GeoEcology*. Catena-Verlag.
- , U. SCHWERTMANN, AND L. CARLSON. 1992. Mineralogy of precipitates formed by the biogeochemical oxidation of Fe(II) in mine drainage, p. 219–232. *In* H. G. W. Skinner and R. W. Fitzpatrick [eds.], *Biomineralization processes of iron and manganese—modern and ancient environments*. *Catena Supplement*, Catena-Verlag.
- , ———, ———, AND E. MURAD. 1990. A poorly crystallized oxyhydroxysulfate of iron formed by bacterial oxidation of Fe(II) in acidic-mine waters. *Geochim. Cosmochim. Acta* **54**: 2743–2758, doi:10.1016/0016-7037(90)90009-A
- BLODAN, C. 2006. A review of acidity generation and consumption in acidic coal mine lakes and their watersheds. *Sci. Total Environ.* **369**: 307–332, doi:10.1016/j.scitotenv.2006.05.004
- , N. BASILIKO, AND T. R. MOORE. 2004. Carbon turnover in peatland mesocosms exposed to different water table levels. *Biogeochemistry* **67**: 331–351, doi:10.1023/B:BIOG.0000015788.30164.e2
- BLÖTHE, M., D. M. AKOB, J. E. KOSTKA, K. GOSCHEL, H. L. DRAKE, AND K. KÜSEL. 2008. pH gradient-induced heterogeneity of Fe(II)-reducing microorganisms in coal mining-associated lake sediments. *Appl. Environ. Microbiol.* **74**: 1019–1029, doi:10.1128/AEM.01194-07
- BOEHRER, B., AND M. SCHULTZE. 2006. On the relevance of meromixis in mine pit lakes, p. 200–213. *In* R. I. Barnhisel [ed.], *7th international conference on acid rock drainage (ICARD)*. American Society of Mining and Reclamation.

- , AND —. 2008. Stratification of lakes. *Rev. Geophys* **46**: 1–27. doi:10.1029/2006RG000210
- BRZUSTOWSKI, J. 2002. Clustering Calculator [Internet]. [Accessed 2009 October 16]. Available from <http://www.biology.ualberta.ca/fbrzusto/cluster.php>
- CAMPBELL, P., AND T. TORGENSEN. 1980. Maintenance of iron meromixis by iron redeposition in a rapidly flushed monimolimnion. *Can. J. Fish. Aquat. Sci.* **37**: 1303–1313. doi:10.1139/f80-166
- CASAMAYOR, E. O., J. GARCIA-CANTIZANO, AND C. PEDROS-ALIO. 2008. Carbon dioxide fixation in the dark by photosynthetic bacteria in sulfide-rich stratified lakes with oxic-anoxic interfaces. *Limnol. Oceanogr.* **53**: 1193–1203. doi:10.4319/lo.2008.53.4.1193
- CHILDS, C. W., K. INOUE, AND C. MIZOTA. 1998. Natural and anthropogenic schwertmannites from Towada-Hachimantai National Park, Honshu, Japan. *Chem. Geol.* **144**: 81–86. doi:10.1016/S0009-2541(97)00121-6
- CLUM, A., M. NOLAN, E. LANG, T. GLAVINA DEL RIO, H. TICE, A. COPELAND, J.-F. CHENG, S. LUCAS, F. CHEN, D. BRUCE, L. GOODWIN, S. PITLUCK, N. IVANOVA, K. MAVROMATIS, N. MIKHAILOVA, A. PATI, A. CHEN, K. PALANIAPPAN, M. GOEKER, S. SPRING, M. LAND, L. HAUSER, Y.-J. CHANG, C. C. JEFFRIES, P. CHAIN, J. BRISTOW, J. A. EISEN, V. MARKOWITZ, P. HUGENHOLTZ, N. C. KYRPIDES, H.-P. KLENK, AND A. LAPIDUS. 2009. Complete genome sequence of *Acidimicrobium ferrooxidans* type strain (ICPT). *Stand. Genomic Sci.* **1**: 38–45. doi:10.4056/signs.1463
- CORNELL, R. M., AND U. SCHWERTMANN. 2003. The iron oxides: Structure, properties, reactions, occurrences and uses, 2nd ed. Wiley-VCH Verlagsgesellschaft.
- DAVISON, W. 1993. Iron and manganese in lakes. *Earth-Sci. Rev.* **34**: 119–163. doi:10.1016/0012-8252(93)90029-7
- DESANTIS, T. Z., P. HUGENHOLTZ, K. KELLER, E. L. BRODIE, N. LARSEN, Y. M. PICENO, R. PHAN, AND G. L. ANDERSEN. 2006a. NAST: A multiple sequence alignment server for comparative analysis of 16S rRNA genes. *Nucleic Acids Res.* **34**: 394–399. doi:10.1093/nar/gkl244
- , N. LARSEN, M. ROJAS, E. L. BRODIE, K. KELLER, T. HUBER, D. DALEVI, P. HU, AND G. L. ANDERSEN. 2006b. Greengenes, a chimera-checked 16S rRNA gene database and workbench compatible with ARB. *Appl. Environ. Microbiol.* **72**: 5069–5072. doi:10.1128/AEM.03006-05
- DE VICENTE, I., E. ORTEGA-RETUERTA, O. ROMERA, R. MORALES-BAQUERO, AND I. REICHE. 2009. Contribution of transparent exopolymer particles to carbon sinking flux in an oligotrophic reservoir. *Biogeochemistry* **96**: 13–23. doi:10.1007/s10533-009-9342-8
- DIEZ, S., G. O. NOONAN, J. K. MACFARLANE, AND P. M. GSCHWEND. 2007. Ferrous iron oxidation rates in the pycnocline of a permanently stratified lake. *Chemosphere* **66**: 1561–1570. doi:10.1016/j.chemosphere.2006.08.017
- DRUMMOND, A. J., B. ASHTON, M. CHEUNG, J. HELED, M. KEARSE, R. MOIR, S. STONES-HAVAS, T. THERIER, AND A. WILSON. 2009. Genieous v4.8 [Internet]. Auckland (New Zealand): Biomatters, Ltd., [accessed 2009 September 12]. Available from <http://www.genieous.com/>
- DRUSCHEL, G. K., D. EMERSON, R. SUTKA, P. SUCHECKI, AND G. W. LUTHER. 2008. Low-oxygen and chemical kinetic constraints on the geochemical niche of neutrophilic iron(II) oxidizing microorganisms. *Geochim. Cosmochim. Acta* **72**: 3358–3370. doi:10.1016/j.gca.2008.04.035
- EICHLER, B., AND N. PFENNIG. 1990. Seasonal development of anoxygenic phototrophic bacteria in a holomictic drumlin lake (Schleinssee, F.R.G.). *Arch. Hydrobiol.* **119**: 369–392.
- EMERSON, D., AND C. MOYER. 1997. Isolation and characterization of novel iron-oxidizing bacteria that grow at circumneutral pH. *Appl. Environ. Microbiol.* **63**: 4784–4792.
- EUSTERHUES, K., F. E. WAGNER, W. HAUSLER, M. HANZLIK, H. KNICKER, K. U. TOTSCHKE, I. KOGEL-KNABNER, AND U. SCHWERTMANN. 2008. Characterization of ferrihydrite-soil organic matter coprecipitates by X-ray diffraction and Mossbauer spectroscopy. *Environ. Sci. Technol.* **42**: 7891–7897. doi:10.1021/es800881w
- FLECKENSTEIN, J. H., C. NEUMANN, N. VOLZE, AND J. BEER. 2009. Spatio-temporal patterns of lake-groundwater exchange in an acid mine lake. *Grundwasser* **14**: 207–217. doi:10.1007/s00767-009-0113-1
- GROSSART, H. P., AND H. PLOUG. 2000. Bacterial production and growth efficiencies: Direct measurements on riverine aggregates. *Limnol. Oceanogr.* **45**: 436–445. doi:10.4319/lo.2000.45.2.0436
- , AND M. SIMON. 1993. Limnetic macroscopic organic aggregates (lake snow)—occurrence, characteristics, and microbial dynamics. *Limnol. Oceanogr.* **38**: 532–546. doi:10.4319/lo.1993.38.3.0532
- , AND —. 1998. Significance of limnetic organic aggregates (lake snow) for the sinking flux of particulate organic matter in a large lake. *Aquat. Microb. Ecol.* **15**: 115–125. doi:10.3354/ame015115
- GYURE, R. A., A. KONOPKA, A. BROOKS, AND W. DOEMEL. 1987. Algal and bacterial activities in acidic (pH 3) strip mine lakes. *Appl. Environ. Microbiol.* **53**: 2069–2076.
- HANSEL, C. M., S. G. BENNER, J. NEISS, A. DOHNALKOVA, R. K. KUKKADAPU, AND S. FENDORF. 2003. Secondary mineralization pathways induced by dissimilatory iron reduction of ferrihydrite under advective flow. *Geochim. Cosmochim. Acta* **67**: 2977–2992. doi:10.1016/S0016-7037(03)00276-X
- HEGLER, F., N. R. POSTH, J. JIANG, AND A. KAPPLER. 2008. Physiology of phototrophic iron(II)-oxidizing bacteria: Implications for modern and ancient environments. *FEMS Microbiol. Ecol.* **66**: 250–260. doi:10.1111/j.1574-6941.2008.00592.x
- HEISING, S., L. RICHTER, W. LUDWIG, AND B. SCHINK. 1999. *Chlorobium ferrooxidans* sp. nov., a phototrophic green sulfur bacterium that oxidizes ferrous iron in coculture with a “*Geospirillum*” sp. strain. *Arch. Microbiol.* **172**: 116–124. doi:10.1007/s002030050748
- JØRGENSEN, B. B., H. FOSSING, C. O. WIRSEN, AND H. W. JANNASCH. 1991. Sulfide oxidation in the anoxic Black-Sea chemocline. *Deep-Sea Res.* **38**: S1083–S1103.
- KAMUNKE, N., J. TITTEL, H. KRUMBECK, C. BEULKER, AND J. POERSCHMANN. 2005. High heterotrophic bacterial production in acidic, iron-rich mining lakes. *Microb. Ecol.* **49**: 425–433. doi:10.1007/s00248-004-0270-9
- KAWANO, M., AND K. TOMITA. 2001. Geochemical modeling of bacterially induced mineralization of schwertmannite and jarosite in sulfuric acid spring water. *Am. Miner.* **86**: 1156–1165.
- KÜSEL, K., T. DORSCH, G. ACKER, AND E. STACKEBRANDT. 1999. Microbial reduction of Fe(III) in acidic sediments: Isolation of *Acidiphilium cryptum* JF-5 capable of coupling the reduction of Fe(III) to the oxidation of glucose. *Appl. Environ. Microbiol.* **65**: 3633–3640.
- , AND H. L. DRAKE. 1995. Effects of environmental parameters on the formation and turnover of acetate by forest soils. *Appl. Environ. Microbiol.* **61**: 3667–3675.
- LANE, D. J. 1991. 16S/23S rRNA sequencing, p. 115–175. *In* E. Stackebrandt and M. Goodfellow [eds.], *Nucleic acid techniques in bacterial systematics*. Wiley.

- LETUNIC, I., AND P. BORK. 2006. Interactive Tree Of Life (iTOL): an online tool for phylogenetic tree display and annotation. *Bioinformatics* **23**: 127–128, doi:10.1093/bioinformatics/btl529
- LIU, R. M., A. HOFMANN, F. O. GULACAR, P. Y. FAVARGER, AND J. DOMINIK. 1996. Methane concentration profiles in a lake with a permanently anoxic hypolimnion (Lake Lugano, Switzerland-Italy). *Chem. Geol.* **133**: 201–209, doi:10.1016/S0009-2541(96)00090-3
- LOVLEY, D. R., D. E. HOLMES, AND K. P. NEVIN. 2004. Dissimilatory Fe(III) and Mn(IV) reduction. *Adv. Microb. Physiol.* **49**: 219–286, doi:10.1016/S0065-2911(04)49005-5
- LU, S., S. GISCHKAT, M. REICHE, D. M. AKOB, K. B. HALLBERG, AND K. KÜSEL. 2010. Ecophysiology of Fe-cycling bacteria in acidic sediments. *Appl. Environ. Microbiol.* **76**: 8174–8183, doi:10.1128/AEM.01931-10
- LÜDECKE, C., M. REICHE, K. EUSTERHUES, AND K. KÜSEL. 2010. Microorganisms involved in iron cycling at the oxic-anoxic interface in an acidic fen. *Environ. Microbiol.* **12**: 2814–2825.
- LUDWIG, W., O. STRUNK, R. WESTRAM, L. RICHTER, H. MEIER, YADHUKUMAR, A. BUCHNER, T. LAI, S. STEPI, G. JOBB, W. FORSTER, I. BREITSCHE, S. GERBER, A. W. GINHART, O. GROSS, S. GRUMANN, S. HERMANN, R. JOST, A. KONIG, T. LISS, R. LUSSMANN, M. MAY, B. NONHOFF, B. REICHEL, R. STREHLow, A. STAMATAKIS, N. STUCKMANN, A. VILBIG, M. LENKE, T. LUDWIG, A. BODE, AND K. H. SCHLEIFER. 2004. ARB: A software environment for sequence data. *Nucleic Acids Res.* **32**: 1363–1371, doi:10.1093/nar/gkh293
- LUEF, B., F. ASPETSBERGER, T. HEIN, F. HUBER, AND P. PEDUZZI. 2007. Impact of hydrology on free-living and particle-associated microorganisms in a river floodplain system (Danube, Austria). *Freshw. Biol.* **52**: 1043–1057, doi:10.1111/j.1365-2427.2007.01752.x
- LÜTHY, L., M. FRITZ, AND R. BACHOFEN. 2000. In situ determination of sulfide turnover rates in a meromictic alpine lake. *Appl. Environ. Microbiol.* **66**: 712–717, doi:10.1128/AEM.66.2.712-717.2000
- MARTINEZ, C. E., AND M. B. MCBRIDE. 1998. Solubility of Cd²⁺, Cu²⁺, Pb²⁺, and Zn²⁺ in aged coprecipitates with amorphous iron hydroxides. *Environ. Sci. Technol.* **32**: 743–748, doi:10.1021/es970262+
- MENDELSSOHN, I. A., B. A. KLEISS, AND J. S. WAKELEY. 1995. Factors controlling the formation of oxidized root channels—a review. *Wetlands* **15**: 37–46, doi:10.1007/BF03160678
- MOREIRA-TURCO, P., J. M. JOUANNEAU, B. TURCO, P. SEYLER, O. WEBER, AND J. L. GUYOT. 2004. Carbon sedimentation at Lago Grande de Curuai, a floodplain lake in the low Amazon region: Insights into sedimentation rates. *Paleogeogr. Paleoclimatol. Paleocool.* **214**: 27–40.
- MURAD, E., AND P. ROJK. 2005. Iron mineralogy of mine-drainage precipitates as environmental indicators: Review of current concepts and a case study from the Sokolov Basin, Czech Republic. *Clay Miner.* **40**: 427–440, doi:10.1180/0009855054040181
- MUYZER, G., E. C. DEWAAL, AND A. G. UITTERLINDEN. 1993. Profiling of complex microbial-populations by denaturing gradient gel-electrophoresis analysis of polymerase chain reaction-amplified genes-coding for 16S ribosomal-RNA. *Appl. Environ. Microbiol.* **59**: 695–700.
- , A. TESKE, C. O. WIRSEN, AND H. W. JANNASCH. 1995. Phylogenetic-relationships of *Thiomicrospira* species and their identification in deep-sea hydrothermal vent samples by denaturing gradient gel-electrophoresis of 16S rDNA fragments. *Arch. Microbiol.* **164**: 165–172, doi:10.1007/BF02529967
- NEU, T. R. 2000. In situ cell and glycoconjugate distribution in river snow studied by confocal laser scanning microscopy. *Aquat. Microb. Ecol.* **21**: 85–95, doi:10.3354/ame021085
- NIXDORF, B., A. FYSON, AND H. KRUMBECK. 2001. Review: Plant life in extremely acidic waters. *Environ. Exp. Botany* **46**: 203–211, doi:10.1016/S0098-8472(01)00104-6
- , AND M. KAPFER. 1998. Stimulation of phototrophic pelagic and benthic metabolism close to sediments in acidic mining lakes. *Water Air Soil Pollut.* **108**: 317–330, doi:10.1023/A:1005165615804
- , H. KRUMBECK, J. JANDER, AND C. BEULKER. 2003. Comparison of bacterial and phytoplankton productivity in extremely acidic mining lakes and eutrophic hard water lakes. *Acta Oecol. Int. J. Ecol.* **24**: S281–S288.
- PEINE, A., A. TRITSCHLER, K. KÜSEL, AND S. PEIFFER. 2000. Electron flow in an iron-rich acidic sediment—evidence for an acidity-driven iron cycle. *Limnol. Oceanogr.* **45**: 1077–1087, doi:10.4319/lo.2000.45.5.1077
- PIMENOV, N. V., AND L. N. NERETIN. 2006. Composition and activities of microbial communities involved in carbon, sulfur, nitrogen and manganese cycling in the oxic/anoxic interface of the Black Sea, p. 501–521. *In* L. N. Neretin [ed.], Past and present water column anoxia. NATO science series, IV. Earth and environmental sciences. Springer.
- PLOUG, H., H. P. GROSSART, F. AZAM, AND B. B. JORGENSEN. 1999. Photosynthesis, respiration, and carbon turnover in sinking marine snow from surface waters of Southern California Bight: Implications for the carbon cycle in the ocean. *Mar. Ecol. Prog. Ser.* **179**: 1–11, doi:10.3354/meps179001
- PORTER, K. G., AND Y. S. FEIG. 1980. The use of Dapi for identifying and counting aquatic microflora. *Limnol. Oceanogr.* **25**: 943–948, doi:10.4319/lo.1980.25.5.0943
- REGENSPURG, S., A. BRAND, AND S. PEIFFER. 2004. Formation and stability of schwertmannite in acidic mining lakes. *Geochim. Cosmochim. Acta* **68**: 1185–1197, doi:10.1016/j.gca.2003.07.015
- RODEN, E. E., D. SOBOLLEV, B. GLAZER, AND G. W. LUTHER. 2004. Potential for microscale bacterial Fe redox cycling at the aerobic-anaerobic interface. *Geomicrobiol. J.* **21**: 379–391, doi:10.1080/01490450490485872
- ROTHER, A., AND J. KOHLER. 2005. Formation, transport and retention of aggregates in a river-lake system (Spree, Germany). *Int. Rev. Hydrobiol.* **90**: 241–253, doi:10.1002/iroh.200410777
- ROWE, O. F., AND D. B. JOHNSON. 2008. Comparison of ferric iron generation by different species of acidophilic bacteria immobilized in packed-bed reactors. *Syst. Appl. Microbiol.* **31**: 68–77, doi:10.1016/j.syapm.2007.09.001
- RUDD, J. W. M., R. D. HAMILTON, AND N. E. CAMPBELL. 1974. Measurement of microbial oxidation of methane in lake water. *Limnol. Oceanogr.* **19**: 519–524, doi:10.4319/lo.1974.19.3.0519
- SCHLOSS, P. D., AND J. HANDELSMAN. 2006. Introducing SONS, a tool for operational taxonomic unit-based comparisons of microbial community memberships and structures. *Appl. Environ. Microbiol.* **72**: 6773–6779, doi:10.1128/AEM.00474-06
- SCHWERTMANN, U., J. M. BIGHAM, AND E. MURAD. 1995. The first occurrence of schwertmannite in a natural stream environment. *Eur. J. Mineral.* **7**: 547–552.
- SIMON, M., H. P. GROSSART, B. SCHWEITZER, AND H. PLOUG. 2002. Microbial ecology of organic aggregates in aquatic ecosystems. *Aquat. Microb. Ecol.* **28**: 175–211, doi:10.3354/ame028175

- SINGER, P. C., AND W. STUMM. 1970. Acidic mine drainage: The rate-determining step. *Science* **167**: 1121–1123, doi:10.1126/science.167.3921.1121
- SPARK, K. M., B. B. JOHNSON, AND J. D. WELLS. 1995. Characterizing heavy-metal adsorption on oxides and oxyhydroxides. *Eur. J. Soil Sci.* **46**: 621–631, doi:10.1111/j.1365-2389.1995.tb01358.x
- TABATABAI, M. A. 1974. Rapid method for determination of sulfate in water samples. *Environ. Lett.* **7**: 237–243, doi:10.1080/00139307409437403
- TAMURA, H., K. GOTO, T. YOTSUYAN, AND M. NAGAYAMA. 1974. Spectrophotometric determination of Iron(II) with 1,10-phenanthroline in presence of large amounts of Iron(III). *Talanta* **21**: 314–318, doi:10.1016/0039-9140(74)80012-3
- TANG, K. W., K. M. L. HUTALLE, AND H. P. GROSSART. 2006. Microbial abundance, composition and enzymatic activity during decomposition of copepod carcasses. *Aquat. Microb. Ecol.* **45**: 219–227, doi:10.3354/ame045219
- TAYLOR, G. T., M. IABICHELLA, T. Y. HO, M. I. SCRANTON, R. C. THUNELL, F. MULLER-KARGER, AND R. VARELA. 2001. Chemoautotrophy in the redox transition zone of the Cariaco Basin: A significant midwater source of organic carbon production. *Limnol. Oceanogr.* **46**: 148–163, doi:10.4319/lo.2001.46.1.0148
- WEISS, J. V., J. A. RENTZ, T. PLALA, S. C. NEUBAUER, M. MERRILL-FLOYD, T. LILBURN, C. BRADBURN, J. P. MEGONIGAL, AND D. EMERSON. 2007. Characterization of neutrophilic Fe(II)-oxidizing bacteria isolated from the rhizosphere of wetland plants and description of *Ferritrophicum radicolica* gen. nov. sp. nov., and *Sideroxydans paludicola* sp. nov. *Geomicrobiol. J.* **24**: 559–570, doi:10.1080/01490450701670152
- YU, Y. N., M. BREITBART, P. McNAIRNIE, AND F. ROHWER. 2006. FastGroupII: A web-based bioinformatics platform for analyses of large 16S rDNA libraries. *BMC Bioinformatics* **7**: 1–9, doi:10.1186/1471-2105-7-57

Associate editor: Markus H. Huettel

Received: 19 September 2010

Accepted: 28 February 2011

Amended: 15 April 2011

[VC3] Identification of minerals and organic materials of the Middle Eocene ironstones, the Bahariya Depression, Western Desert, Egypt by means of micro-Raman spectroscopy

Authorship of publication

<u>V. Ciobota:</u>	concept development Raman measurements writing of manuscript
W. Salama:	sample collection discussion of results writing of manuscript
N. Tarcea:	discussion of experimental concept and results proofreading of manuscript
P. Rösch:	discussion of experimental concept and results proofreading of manuscript
M. El Aref:	discussion of experimental concept and results proofreading of manuscript
R. Gaupp:	discussion of experimental concept and results proofreading of manuscript
J. Popp:	project management discussion of concepts and results discussion and proofreading of manuscript

Journal of Raman Spectroscopy 43 (2012) 405-410

Reprinted with kind permission from *John Wiley & Sons, Ltd.*

Identification of minerals and organic materials in Middle Eocene ironstones from the Bahariya Depression in the Western Desert of Egypt by means of micro-Raman spectroscopy

Valerian Ciobotă,^a Walid Salama,^b Nicolae Tarcea,^a Petra Rösch,^a Mourtada El Aref,^b Reinhard Gaupp^c and Jürgen Popp^{a,d,*}



The Middle Eocene ironstones of the Bahariya Depression consist of four iron ore types: manganiferous mud-ironstone, fossiliferous ironstone, stromatolitic ironstone and nummulitic-oidal-onooidal ironstone. The upper surfaces of these sequences were subjected to subaerial weathering and a lateritic iron ore type was formed. The chemical composition of these ironstone types was investigated by means of micro-Raman spectroscopy. Various closely related iron-containing and manganese-containing minerals were detected by means of the above-mentioned approach. The high spatial resolution and sensitivity of this method allowed us to identify minerals that could not be detected by other techniques. Well-preserved organic materials were observed in one type of ironstones. Therefore, using Raman spectroscopy, we were able to provide evidence that the formation of some of the investigated rocks was biologically mediated. The application of Raman spectroscopy is considered a powerful technique for the identification of both organic and inorganic substances in the studied iron ore deposits. Copyright © 2011 John Wiley & Sons, Ltd.

Supporting information may be found in the online version of this article.

Keywords: micro-Raman spectroscopy; mud-ironstone; stromatolitic ironstone; fossiliferous ironstone; nummulitic-oidal-onooidal ironstone

Introduction

Ironstones are sedimentary rocks with >15 wt% iron, corresponding to 21.4 wt% Fe₂O₃.^[1,2] The ironstones may or may not contain >5 vol.% ooids, pisoids, peloids and oncooids. Ooids are spherical or ellipsoidal coated grains ~2 mm in diameter displaying regular concentric laminae surrounding a central core. Grains similar to ooids but >2 mm are known as pisoids. Oncooids are similar to pisoids, but have a biogenic origin and irregular concentric laminae. Peloids are grains of fine-grained material with diameters in the range of ooids to pisoids, but without recognizable internal structure. These coated grains were formed in either continental or marine depositional environments.^[1,2] The distribution of the ooidal ironstones was generally abundant during the Early and Middle Eocene period because of the major changes in the paleogeographic position of the shoreline that occurred during the Eocene Epoch.^[3,4]

The main ooidal-onooidal ironstone deposits of Egypt are well represented in the Western Desert of Egypt. They are located in the northeastern part of the Bahariya Depression in three mine areas, i.e. Ghorabi, El Harra and El Gedida. The Middle Eocene ironstones of the Bahariya Depression are subdivided into two sequences: lower and upper. These ironstone sequences consist of four shallow marine iron ore types. The marine ironstone types include black manganiferous mud-ironstone and yellowish-brown stromatolitic ironstone types, which were formed from colloidal suspension in quiet waters in lagoonal-tidal flat environments, and storm-related black fossiliferous ironstone and shallow subtidal-intertidal yellowish-brown nummulitic-oidal-onooidal

ironstone types, which were formed during agitated water conditions. The upper surfaces of these sequences were subjected to subaerial weathering, along which lateritic iron ores were formed.^[1,2,5] A more detailed description of the investigated samples can be found in the supporting information.

For a fundamental understanding of the origin and evolution of planets, detailed information regarding the crust surface is required. Mineralogical analysis of the surface can be performed successfully using Raman spectroscopy; the identification of inorganic and organic minerals and biological compounds being possible because of it.^[6–8] Not only solid state materials but also liquids and gases, which could be present as inclusions in crystalline minerals and glasses, can be investigated by means of Raman spectroscopy. The spatial resolution of the technique can be improved by combining the spectrometer with a microscope allowing for a lateral resolution below 1 μm. In addition, the morphology of various minerals at the rock

* Correspondence to: Jürgen Popp, Institute of Physical Chemistry, Friedrich Schiller University Jena, Germany. E-mail: juergen.popp@uni-jena.de

^a Institute of Physical Chemistry, Friedrich Schiller University Jena, Germany

^b Geology Department, Faculty of Science, Cairo University, Egypt

^c Institute of Earth Sciences, Friedrich Schiller University Jena, Germany

^d Institute of Photonic Technology, Jena, Germany

surface can be investigated using Raman spectroscopy. All the above-mentioned properties of the Raman technique make this method a powerful tool for *in situ* planetary studies.

A number of studies have been dedicated to the application of Raman spectroscopy in archaeology and the arts.^[6–12] Investigation of pigments used in paintings,^[6,7,11] of varnishes and binding media utilized for art conservation^[9,10] or discrimination between genuine and fake artifacts and gems^[12] are common applications of Raman spectroscopy in this field. Raman spectroscopy alone, or in combination with other techniques, has also been successfully applied to mineral and organic material characterization and identification.^[13–27] Determination of the chemical composition of various meteorites^[28–30] and rocks derived from the Earth's surface,^[14–16,31] discrimination between closely related minerals^[17,18] or detection of biosignatures from geological specimens^[32,33] are possible by means of Raman spectroscopy.

The aim of this study was to gain more information about the formation of ironstones. Here, we were especially interested in investigating if biotic components were involved in the formation of ooids and oncooids.

Experimental

For Raman measurements, two types of samples were used: (1) rough and (2) polished. No other sample preparation was performed. Point measurements were carried out on both types of samples. In addition, Raman maps of the polished samples were recorded. On the basis of the frequency of detection of various minerals when point measurements were performed, we concluded that some minerals were more abundant than others.

Raman setup

The Raman measurements of the rocks were performed with a commercial micro-Raman setup (HR LabRam inverse system, Jobin Yvon Horiba). The Raman scattering was excited by a frequency-doubled Nd: YAG laser at a wavelength of 532 nm with a laser power between 20 and 200 μW incident on the sample. The laser beam was focused on the sample by means of a Leica PLFluotar × 100/0.75 microscope objective down to a spot diameter of approximately 0.7 μm. The dispersive spectrometer has an entrance slit of 100 μm, a focal length of 800 mm and is equipped with a grating of 300 lines/mm. The Raman scattered light was detected by a Peltier-cooled charge coupled device (CCD) detector. The integration time for one Raman spectrum ranged from 60 to 240 s. The low values for the laser power and the relatively short acquisition times were chosen to avoid any possible changes in the samples.

Results and Discussion

The five different ironstone types can be grouped into three ironstone groups based on optical microscopic evaluation, revealing their mineralogical composition:

1. The black manganiferous mud and fossiliferous ironstone types
2. The yellowish-brown microbially-mediated ironstone types (stromatolitic and nummulitic–ooidal–oncooidal ironstone types).
3. The dark brown lateritic iron ore.

The investigated stromatolitic and nummulitic–ooidal–oncooidal ironstone samples of the present study indicate that the main iron mineral detected by means of Raman spectroscopy in these two types is goethite (Fig. 1). Goethite is an iron oxyhydroxide

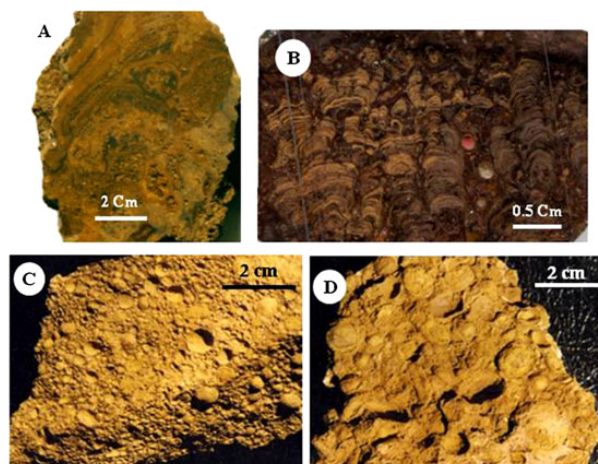


Figure 1. (A) A hand sample shows the even to wavy stromatolitic laminations of the stratiform stromatolites; (B) A hand sample shows stromatolite columns; (C) A hand sample of the nummulitic–ooidal–oncooidal ironstone type shows ferriferous ooids and few oncooids; and (D) A hand sample of the ferriferous oncooids.

(α -FeOOH), which presents a *Pbnm* space group symmetry. The Raman bands assigned to α -FeOOH are located at 291, 390, 471, 543, 681 and 990 cm^{-1} (Fig. 2(f)).¹⁹ In addition to goethite, hematite was also detected in the investigated rock samples as the next dominant iron mineral. In contrast to the stromatolitic and nummulitic-oidal-ocoidal ironstone samples, hematite was the main iron mineral in the manganeseiferous mud and fossiliferous ironstone samples. Hematite, α -Fe₂O₃, has a structural type of corundum, the space group is *R3c* with two formula unit per unit cell. Raman signals at 288, 406, 496, 607 and 1314 cm^{-1} (Fig. 2(g)) are characteristic of this mineral.¹³⁴ Because goethite and hematite exhibit larger Raman cross-sections than the manganese-containing minerals and are present in high concentration within the samples, the most intense bands of these two iron oxides are often detected together with signals from the other manganese minerals. For example, in Fig. 2 the spectra assigned to romanechite ((Ba,H₂O)₂(Mn⁴⁺,Mn³⁺)₃O₁₀), todorokite (Na,Ca,K)₂(Mn⁴⁺,Mn³⁺)₅O₁₂·3–4.5(H₂O)), manjiroite ((Na,K)(Mn⁴⁺,Mn²⁺)₁₀O₁₆·n(H₂O)), hollandite (Ba(Mn²⁺,Mn³⁺)₈O₁₆) and pyrolusite (MnO₂) show low wavenumber bands because of the presence of iron oxides/oxyhydroxides. However, the main Raman bands of various manganese oxides are located in the wavenumber region 500–650 cm^{-1} , thus away from the wavenumber area where goethite and hematite exhibit the strongest Raman signals (200–400 cm^{-1}). Therefore, the identification of Mn-containing minerals is not hindered by the presence of various iron oxides and/or oxyhydroxides.

Figure 2(a) shows the Raman spectrum of pyrolusite, with bands at 332, 534, 660 and 748 cm^{-1} . The Raman signals at 290,

407 and 1314 cm^{-1} are characteristic for hematite, which can be found in large amounts in the sample. The very weak Raman signals of pyrolusite at lower wavenumbers reported by other authors were probably completely overlapped by the intense Raman signals of the iron oxide.²⁰ The hollandite spectrum presented in Fig. 2(b) is dominated by the peak at 582 cm^{-1} with a shoulder at 624 cm^{-1} . The manjiroite and todorokite Raman spectra are presented in Figs 2(c) and (d), respectively. The main band of the two minerals is located at 643 and 645 cm^{-1} , respectively. The major difference between the two spectra is the appearance of a shoulder at 595 cm^{-1} in the spectrum of todorokite. The Raman bands appearing at lower wavenumbers can be assigned as well to iron oxides/oxyhydroxides. Figure 2(e) depicts the Raman spectrum of romanechite which is dominated by two partially overlapping bands at 583 and 644 cm^{-1} . The assignment of the Raman bands of the Mn-containing minerals are in concordance with previously reported investigations.²⁰

The samples under study contain a large variety of manganese oxides. In the investigated samples, Mn forms oxides alone (pyrolusite) or in combination with barium (romanechite and hollandite) or sodium (manjiroite and todorokite). Although the provenience of the rock samples is from an arid zone (Western Dessert, Egypt), minerals which incorporate water inside the cell structure were also detected (todorokite and manjiroite). Interestingly, in all the Mn-containing minerals, Mn in the 4+ oxidation state was present. This suggests that the formation of the rocks took place in an acidic environment.

Pyrolusite, hollandite and romanechite were the most abundant Mn-containing minerals detected in all three types of the investigated samples. The other manganese minerals were detected only in the mud and fossiliferous ironstone samples.

Besides Mn in various forms, the rock samples also contained calcium-containing minerals. Figure 3 shows Raman spectra obtained from different calcium-containing minerals. In combination with phosphate, calcium was detected in the investigated materials as apatite in the lateritic and microbially-mediated ironstones. The Raman spectrum is dominated by the stretching vibration of the P–O bond at 960 cm^{-1} (Fig. 3(a)). Other Raman bands assigned to apatite can be found at 585 and 1076 cm^{-1} . As with the Mn-containing minerals, the low wavenumber Raman bands are attributed to the presence of iron oxides. Two different calcium carbonates were detected in the samples. Calcite (CaCO₃) (Fig. 3(b)) and dolomite (CaMg(CO₃)₂) (Fig. 3(e)) show intense Raman bands at 1086 and 1098 cm^{-1} , respectively, which can be assigned to the symmetric stretching vibrations of the C–O bonds in CO₃ tetrahedra.¹³⁵ Aside from the Raman band at 1086 cm^{-1} , two other bands are assigned to calcite: the bands at 282 and 712 cm^{-1} . Because very small amounts of dolomite are present in the microbially-mediated ironstone samples, only the most intense Raman band of this mineral appears in the Raman spectra of the investigated rocks. The remaining Raman bands in the spectrum shown in Fig. 3(e) belong to goethite (Fig. 2(f)). Figure 3(c) displays the Raman spectrum of anhydrite. The Raman bands which are attributed to this calcium sulfate mineral are found at 414, 497, 605, 624, 672, 1013, 1108, 1126 and 1158 cm^{-1} . The most intense Raman signal at 1013 cm^{-1} can be assigned to the S–O symmetric stretching vibration. In the case of gypsum (CaSO₄·2H₂O) (Fig. 3(d)), the S–O band is shifted to lower wavenumbers at 1009 cm^{-1} . The Raman signals at 416, 624, 672 and 1135 cm^{-1} are also assigned to this mineral. The remaining Raman bands shown in Fig. 3(d) belong to goethite. The last spectrum plotted in Fig. 3(f) is attributed to rapidcreekite,

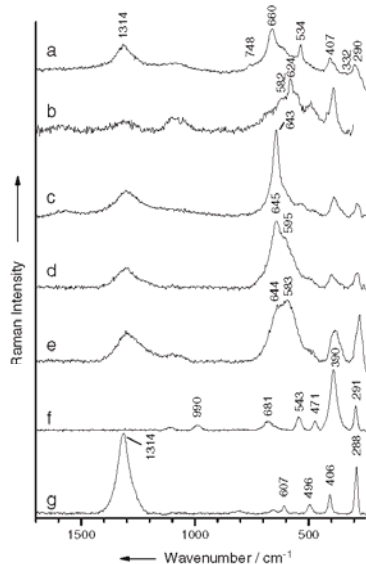


Figure 2. Raman spectra of various manganese and iron minerals recorded from various parts of the investigated samples: a – pyrolusite; b – hollandite; c – manjiroite; d – todorokite; e – romanechite; f – goethite; g – hematite.

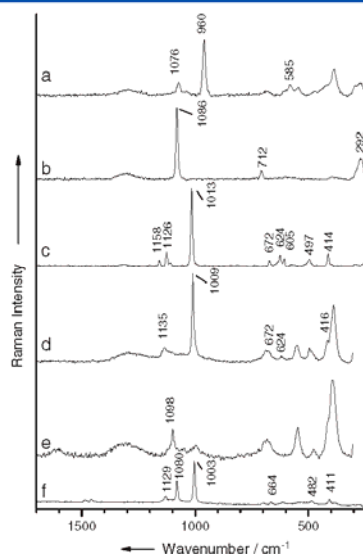


Figure 3. Raman spectra of different minerals containing calcium: a – apatite; b – calcite; c – anhydrite; d – gypsum; e – dolomite; f – rapidcreekite.

$\text{Ca}_2\text{SO}_4\text{CO}_3\cdot 4\text{H}_2\text{O}$. The C–O symmetric stretching vibration band is located at 1003 cm^{-1} , whereas the S–O symmetric stretching vibration band shows up at 1080 cm^{-1} . The Raman bands at 382, 411, 486, 611, 664 and 1129 cm^{-1} are typical for rapidcreekite.^[39]

Figure 4 shows the Raman spectra of other minerals detected in the investigated rock samples. The Raman bands at 265, 288, 457, 480, 517, 658, 751 and 816 cm^{-1} are assigned to microcline (KAlSi_3O_8) (Fig. 4(a)). Microcline and orthoclase are polymorphs, microcline having a triclinic structure while orthoclase a monoclinic one. The main difference between the Raman spectra of the two minerals represents the triplet bands at 656, 751 and 816 cm^{-1} , which are much more intense in the case of microcline compared to orthoclase^[37] (Fig. 4 (b)). Another difference between the two spectra is the number of Raman bands exhibited by the two minerals. Makreski *et al.* showed that the spectra of the more ordered feldspars are richer in bands than the spectra of feldspars with a lower structural symmetry.^[38] Another mineral detected in the samples was quartz (SiO_2) (Fig. 4(c)) with its main Raman band, the Si–O stretching vibration, leading to the very intense Raman signal at 464 cm^{-1} . Additionally, bands at 357, 390, 698 and 798 cm^{-1} are also attributed to quartz. Figure 4(d) presents the Raman spectrum of barite (BaSO_4) with its characteristic Raman signals at 383, 453, 613, 644 and 988 cm^{-1} .^[36]

A further indication of an acidic pH of the environment during mineral formation (*vide supra*) can be seen in the detection of jarosite ($\text{KFe}(\text{SO}_4)_2(\text{OH})_6$) and anglesite (PbSO_4). Jarosite and anglesite can only be formed in an acidic pH in arid climates via oxidation of iron and lead sulfides, respectively. Raman signals at 434, 626, 1005, 1105 and 1154 cm^{-1} (Fig. 4(e)) are assigned to these minerals.^[39,40]

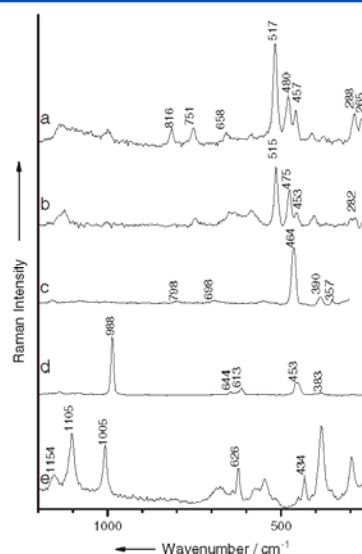


Figure 4. Various minerals detected by means of Raman spectroscopy: a – microcline; b – orthoclase; c – quartz; d – barite; e – jarosite.

Besides inorganic minerals, Raman signals for organic matter can also be found in the ironstone spectra. Figure 5(a) displays the Raman spectrum of a carotenoid with its three characteristic Raman bands at 1000, 1150 and 1515 cm^{-1} . The position and the sharpness of the Raman bands suggest that the organic compounds were very well preserved in the rocks.^[41] The size of the spots where carotenoids were detected has a diameter of a few micrometers. A large variety of organisms can produce different types of pigments (chromophores); therefore, the carotenoids can represent a biomarker for bacteria, fungi and/or algae. The presence of carotenoids in the samples demonstrates that the formation of the second group of ironstone samples was biologically mediated.

Much more difficult to interpret are the Raman spectra (b) and (c) of Fig. 5. Spectrum (b) can be assigned to a proteinaceous matter^[6] while spectrum (c) presents the main bands of a lipid compound.^[42] A possible explanation of the origin of those materials can be that they are from marine organisms such as mollusks, echinoderms and nummulites, and also microbial organisms.

Cellulose was also detected in the oncoids (Fig. 5(d)). The cellulose particles have usual rod shapes and are a few tens of micrometers in length. In the supporting information, a Raman image of such a particle is presented. However, no lignin was detected in the samples. Therefore, the absence of lignin might suggest that the cellulose originated from algae, fungi or bacteria and not from plants.^[43]

Raman measurements performed on freshly broken samples also show bands from organic matter and thus prove that organic matter is really a component of the ironstones and not just an artifact.

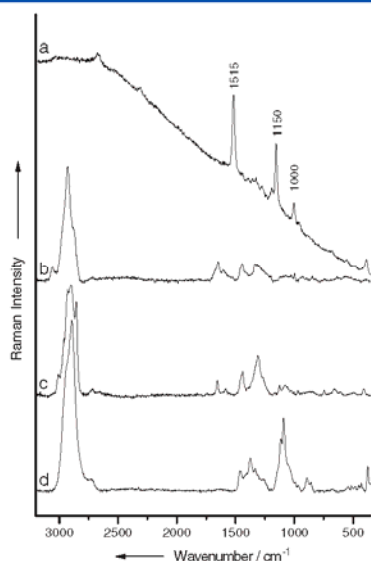


Figure 5. Organic materials detected by means of micro-Raman spectroscopy: a – carotenoid; b – proteinaceous compound; c – lipid compound; d – cellulose.

The main iron-containing minerals detected in the mud and fossiliferous ironstones were hematite and goethite, whereas the main manganese minerals were todorokite, birnessite, manjiroite, aurorite, pyrolusite, hollandite and romanechite. The detrital (transported) minerals such as quartz, orthoclase, microcline, rutile and late-cementing minerals such as barite, calcite and anhydrite were also identified in the samples.

The mineralogical composition of the stromatolitic laminae and the cortical laminae of the ferriferous oncoids and ooids consisted of ferric iron oxyhydroxides (goethite) mixed with ferric iron hydroxysulfate (jarosite), whereas the ferric iron oxide (hematite) was mainly detected as cement surrounding the ooids and oncoids. Other mineral groups were also identified, including phosphates (apatite), carbonates (calcite and dolomite), sulfates (gypsum, anhydrite and barite), manganese minerals (pyrolusite, hollandite and romanechite) and silicates (quartz). In addition, various preserved organic materials inside the stromatolitic laminae and the cortical laminae of the ferriferous oncoids and ooids were detected by means of Raman spectroscopy.

The lateritic ironstones were mainly made up of ferric iron oxides and oxyhydroxides (hematite and goethite), ferric iron hydroxysulfate (jarosite) and manganese minerals (pyrolusite, hollandite and romanechite). Other mineral groups such as authigenic phosphates (apatite), late cement carbonate (calcite) and sulfates (gypsum, anhydrite, rapidcreekite and barite), and detrital silicates (quartz) were also identified.

Goethite, hematite, quartz and calcite are common minerals in all ironstone types. They were also identified with the optical microscope and the conventional X-ray diffraction technique. On the other hand, the black color of the manganese minerals,

yellowish-brown color of goethite and jarosite and the colorless minerals such as gypsum, anhydrite, rapidcreekite, barite, anglesite, nitratine, dolomite and apatite did not allow their identification under the optical microscope. Moreover, the small crystal sizes and/or inhomogeneous distribution (cavity and fracture-filling phases) of such minerals did not allow the collection of enough materials for the X-ray diffraction (XRD) analyses.

Information about the diagenetic modifications in the studied materials was obtained by combining Raman spectroscopy with optical and scanning electron microscopy (SEM). The original iron oxyhydroxide precipitates were amorphous or nanocrystalline that were transformed by recrystallization into goethite and then by dehydration to hematite.^[44] The organic matter degradation can release substantial amounts of phosphorus into pore waters. The supersaturation of the pore waters with phosphorus resulted in the development of diagenetic apatite crystals.^[45] Moreover, diagenetic clay minerals, such as kaolinite and illite develop at the expense of detrital feldspar crystals, such as orthoclase and microcline. The clay minerals were identified by XRD, SEM and energy-dispersive X-ray spectroscopy (EDX).^[2]

Conclusions

The present study illustrates the application of micro-Raman spectroscopy for the solution of a geological problem concerning the origin of the Egyptian Middle Eocene ironstones. Information about the complex environmental conditions prevailing during and after the ironstone formation can be gained by analyzing all the organic and inorganic mineral phases of these ironstones.

The application of micro-Raman spectroscopy provides important and precise information concerning the identification of iron oxides and oxyhydroxide minerals (goethite and hematite), manganese minerals (todorokite, birnessite, pyrolusite, hollandite, romanechite, aurorite and manjiroite), sulfates (jarosite, gypsum, anhydrite, rapidcreekite, barite and anglesite), nitrates (nitratine), carbonates (calcite and dolomite), silicates (quartz, orthoclase, microcline), heavy minerals (rutile) and phosphate (apatite) minerals. Attempts to identify such mineral species with optical microscopy and the conventional X-ray diffraction technique were difficult or impossible.

However, we were not able to identify clay minerals by means of Raman spectroscopy.

The detection of romanechite, anglesite and jarosite is a good indication of low pH acidic conditions during the formation of these minerals. The presence of sulfate, nitrate and carbonate minerals (calcite, gypsum, anhydrite, rapidcreekite, nitratine and halite), which occurs as cavity filling, indicate recent to subrecent mineralogical and chemical alterations typical for the young weathering crusts in the arid zone of NE Africa's desert. Furthermore, the detection of organic materials and apatite within the ferriferous ooids and oncoids provides a clear evidence of the biological mediation involved in the process of mineral formation.

Supporting information

Supporting information may be found in the online version of this article.

Acknowledgements

We highly acknowledge the financial support from the Deutsche Forschungsgemeinschaft (Graduate School 1257 'Alteration and

element mobility at the microbe–mineral interface). In addition, this work was supported by the German Academic Exchange Service (DAAD), and the Thüringische Ministerium für Bildung, Wissenschaft und Kultur (TMBWK) under the project code "MikroPlex" PE113–1, through two years Sandwich program (Channel system) grant of Walid Salama.

References

- [1] M. M. El Aref, A. A. Mesaed, M. A. Khalil, W. S. Salama, *Egypt. J. Geol.* **2006a**, *50*, 29.
- [2] W. S. Salama, Geological and Mineralogical Studies on the Microbially-mediated Ironstone Facies, El Baahriya Depression, Western Desert, Egypt. Ph. D. Thesis, Faculty of Science, Cairo University, **2010**.
- [3] N. J. Shackleton, *Palaeogeogr., Palaeoclimatol., Palaeoecol.* **1986**, *57*, 91.
- [4] D. R. Prothero, W. A. Berggren, P. R. Björk, *Geol. Soc. Am. News Inform.* **1990**, *12*, 74.
- [5] M. M. El Aref, A. A. Mesaed, M. A. Khalil, W. S. Salama, *Egypt. J. Geol.* **2006b**, *50*, 59.
- [6] H. G. M. Edwards, *Analyst* **2004**, *129*, 870.
- [7] A. Hernanz, J. M. Gavira-Vallejo, J. F. Ruiz-López, H. G. M. Edwards, *J. Raman Spectrosc.* **2008**, *39*, 972.
- [8] M. Castriota, V. Cosco, T. Barone, G. D. Santo, P. Carafa, E. Cazzanelli, *J. Raman Spectrosc.* **2008**, *39*, 295.
- [9] M. Christensen, M. Frosch, P. Jensen, U. Schnell, Y. Shashoua, O. F. Nielsen, *J. Raman Spectrosc.* **2006**, *37*, 1171.
- [10] P. Vandenabeele, B. Wehling, L. Moens, H. Edwards, M. De Reu, G. Van Hooydonk, *Anal. Chim. Acta* **2000**, *407*, 261.
- [11] F. Ospitali, D. C. Smith, M. Lorblanchet, *J. Raman Spectrosc.* **2006**, *37*, 1063.
- [12] H. G. M. Edwards, D. W. Farwell, *Spectrochim. Acta, Part A* **1995**, *51*, 2073.
- [13] P. Vargas Jentzsch, B. Kampe, P. Rösch, J. Popp, *J. Phys. Chem. A* **2011**, *115*, 5540.
- [14] S. Cinta Pinzaru, B. P. Onac, *Vib. Spectrosc.* **2009**, *49*, 97.
- [15] J. Jehlicka, H. G. M. Edwards, *Org. Geochem.* **2008**, *39*, 371.
- [16] S. K. Sharma, P. G. Lucey, M. Ghosh, H. W. Hubble, K. A. Horton, *Spectrochim. Acta, Part A* **2003**, *59*, 2391.
- [17] R. L. Frost, R.-A. Wills, M. L. Weier, W. Martens, S. Mills, *Spectrochim. Acta, Part A* **2006**, *63*, 1.
- [18] M.-C. Bernard, A. H.-L. Goff, B. V. Thi, S. C. de Torresi, *J. Electrochem. Soc.* **1993**, *140*, 3065.
- [19] D. L. A. Faria, S. V. Silva, M. T. Oliveira, *J. Raman Spectrosc.* **1997**, *28*, 873.
- [20] C. M. Julien, M. Massot, C. Poinssignon, *Spectrochim. Acta, Part A* **2004**, *60*, 689.
- [21] I. Martinez-Arkarazo, M. Angulo, O. Zuloaga, A. Usobiaga, J. M. Madariaga, *Spectrochim. Acta, Part A* **2007**, *68*, 1058.
- [22] E. A. Stefaniak, A. Worobiec, S. Potgieter-Vermaak, A. Alsecz, S. Török, R. Van Grieken, *Spectrochim. Acta, Part B* **2006**, *61*, 824.
- [23] T. Dörfer, W. Schumacher, N. Tarcea, M. Schmitt, J. Popp, *J. Raman Spectrosc.* **2010**, *41*, 684.
- [24] R. Petry, R. Mastalerz, S. Zahn, T. G. Mayerhöfer, G. Völksch, L. Viereck-Götte, B. Kreher-Hartmann, L. Holz, M. Lankers, J. Popp, *Chemphyschem* **2006**, *7*, 414.
- [25] V. Ciobotă, E.-M. Burkhardt, W. Schumacher, P. Rösch, K. Küsel, J. Popp, *Anal. Bioanal. Chem.* **2010**, *397*, 2929.
- [26] F. Rull, J. Martínez-Frías, J. A. Rodríguez-Losada, *J. Raman Spectrosc.* **2007**, *38*, 239.
- [27] W. Schumacher, M. Kühnert, P. Rösch, J. Popp, *J. Raman Spectrosc.* **2011**, *42*, 383.
- [28] N. Tarcea, M. Harz, P. Rösch, T. Frosch, M. Schmitt, H. Thiele, R. Hochleitner, J. Popp, *Spectrochim. Acta, Part A* **2007**, *68*, 1029.
- [29] T. Frosch, N. Tarcea, M. Schmitt, H. Thiele, F. Langenhorst, J. Popp, *Anal. Chem.* **2007**, *79*, 1101.
- [30] R. Hochleitner, N. Tarcea, G. Simon, W. Kiefer, J. Popp, *J. Raman Spectrosc.* **2004**, *35*, 515.
- [31] V. Klein, J. Popp, N. Tarcea, M. Schmitt, W. Kiefer, S. Hofer, T. Stuffer, M. Hilchenbach, D. Doyle, M. Dieckmann, *J. Raman Spectrosc.* **2004**, *35*, 433.
- [32] S. E. Jorge Villar, H. G. M. Edwards, L. G. Benning, *Icarus* **2006**, *184*, 158.
- [33] J. Jehlicka, H. G. M. Edwards, P. Vitek, *Planet. Space Sci.* **2009a**, *57*, 606.
- [34] G. N. Kustova, E. B. Burgina, V. A. Sadykov, S. G. Poryvaev, *Phys. Chem. Miner.* **1992**, *18*, 379.
- [35] Z. Tomić, P. Makreski, B. Gajić, *J. Raman Spectrosc.* **2010**, *41*, 582.
- [36] J. Jehlicka, P. Vitek, H. G. M. Edwards, M. Heagraves, T. Capoun, *Spectrochim. Acta, Part A* **2009b**, *73*, 410.
- [37] J. Yang, G. Godard, D. C. Smith, *Eur. J. Mineral.* **1998**, *10*, 969.
- [38] P. Makreski, G. Jovanovski, B. Kaitner, *J. Molec. Struct.* **2009**, *924–926*, 413.
- [39] H. G. M. Edwards, P. Vandenabeele, S. E. Jorge-Villar, E. A. Carter, F. R. Perez, M. D. Hargreaves, *Spectrochim. Acta, Part A* **2007**, *68*, 1133.
- [40] P. Makreski, G. Jovanovski, S. Dimitrovska, *Vib. Spectrosc.* **2005**, *39*, 229.
- [41] C. P. Marshall, A. Olcott Marshall, *Phil. Trans. R. Soc. A* **2010**, *368*, 3137.
- [42] M. Harz, M. Kiehnopf, S. Stöckel, P. Rösch, T. Deufel, J. Popp, *Analyst* **2008**, *133*, 1416.
- [43] M. Strömme, A. Mhryanyan, R. Ek, *Mater. Lett.* **2002**, *57*, 569.
- [44] H. Harder, in Geological Society Special Publications, vol. 46 (Eds.: T. P. Young, W. E. G. Taylor), Geological Society of London, London, **1989**, pp. 9.
- [45] N. Tribouillard, T. J. Algeo, T. Lyons, A. Riboulleau, *Chem. Geol.* **2006**, *232*, 12.

[VC4] Quantification of the Inorganic Phase of the Pelagic Aggregates of an Iron Contaminated Lake by means of Raman Spectroscopy

Authorship of publication

V. Ciobota:

concept development
Raman measurements
writing of manuscript

S. Lu:

sample collection
DGGE analysis
discussion of results
writing of manuscript

N. Tarcea:

discussion of experimental concept and results
proofreading of manuscript

P. Rösch:

discussion of experimental concept and results
proofreading of manuscript

K. Küsel:

discussion of experimental concept and results
proofreading of manuscript

J. Popp:

project management
discussion of concepts and results
discussion and proofreading of manuscript

Submitted

1 Quantification of the inorganic phase of the pelagic
2 aggregates of an iron contaminated lake by means of
3 Raman spectroscopy

4
5 Valerian Ciobotă^a, Shipeng Lu^b, Nicolae Tarcea^a,
6 Petra Rösch^a, Kirsten Küsel^b and Jürgen Popp^{a,c,*}

7
8 ^aInstitute of Physical Chemistry and Abbe School of Photonics, Friedrich Schiller
9 University, Jena, Germany

10 ^bInstitute of Ecology, Friedrich Schiller University, Jena, Germany

11 ^cInstitute of Photonic Technology, Jena, Germany

12
13 ^{*} Corresponding author. Tel.: +49-3641/9-48320; Fax: +49-3641/9-48302; E-mail
14 address: juergen.popp@uni-jena.de.

15 **Abstract**

16 A quantitative investigation of the inorganic phase of pelagic, iron-rich aggregates (iron
17 snow, IS) formed in an iron polluted aquatic environment was performed by means of
18 Raman spectroscopy. IS samples were collected from two basins of an acidic lignite mine
19 lake and from two different water depths. Although the water chemistry differed at all
20 four sites with respect to oxygen, pH, and, Fe(II) concentrations, the Raman analyses
21 showed that the main mineral formed was schwertmannite (ideal formula:
22 $\text{Fe}_8\text{O}_8(\text{OH})_6\text{SO}_4$) with concentrations of more than 88% in all IS samples. To determine
23 potential differences in the microbial communities of the IS samples we used denaturing
24 gradient gel electrophoresis. Microbial communities differed between two basins, but
25 showed similarities between redoxcline and deeper water layers of IS samples from the
26 same basin. Surprisingly, these microbiological differences did not lead to strikingly
27 qualitative similarities in the mineral composition, although the initial step in mineral
28 formation, the oxidation of Fe(II) to Fe(III), is a pure microbial process at low pH. Thus,
29 a quantitative method was necessary to elucidate differences in the consecutive
30 mineralization process which is apparently more controlled by water geochemical
31 conditions.

32

33 **Keywords:** acidic lignite mine lake, iron snow, mineral quantification, Raman
34 spectroscopy, schwertmannite

35 **1. Introduction**

36 Raman spectroscopy uses the inelastic scattered radiation by the investigated samples
37 to gain information about their vibrational and rotational energy levels. The energy levels
38 of the molecules are highly specific, therefore it is possible using Raman spectroscopy to
39 distinguish between molecules with very similar chemical composition or between
40 substances with the same chemical compositions but different crystal structures. In
41 contrast to other methods (XRD or magnetic techniques), Raman spectroscopy can be
42 successfully applied for the identification of minerals with crystals in the nanometer
43 range [1, 2]. In the mineralogy field, Raman spectroscopic approaches were used for the
44 identification of various soil components [3-5], characterization of different rocks [6-10],
45 discrimination between closely related minerals [11-17] or identification of minerals used
46 as dyes in paintings [18-21], for example. In addition, Raman imaging techniques were
47 applied to distribution studies of various minerals [22], or for quantification of the
48 amount of various minerals in different samples [4, 23].

49 Iron-containing minerals were widely investigated by means of Raman spectroscopy.
50 Various authors showed that using this spectroscopic technique discrimination between
51 polymorphic iron oxides, hydroxides or similar iron sulfides, for example, was achievable
52 [1, 2, 7, 24, 25]. Iron-rich minerals were extensively studied for their pollution or
53 remediation potential in acid mine drainage and other polluted sites [26-29]. However,
54 the mineral composition of pelagic aggregates formed in aquatic ecosystems has been
55 rarely studied. The particulate matter formed in lakes and oceans consists of both organic
56 and inorganic materials derived from a variety of sources like authigenic production by
57 biota, colonization by microorganisms, precipitation of inorganic minerals, fluvial and
58 aeolian inputs, suspension of sedimentary material, etc. [30]. Most pelagic aggregates,
59 named lake snow or marine snow depending on the environment where they appear, are
60 dominated by dead organic matter and living biomass consisting of bacteria, protozoa,
61 and, fungi [31]. A number of studies were devoted to the organic phase of different
62 pelagic particles formed in various aquatic environments [32-34]. In aquatic ecosystems
63 characterized by many terrestrial-aquatic coupling processes, the mineral fraction is very
64 important for many biological and chemical processes taking place in the water [32, 35].
65 However, the quantification of the inorganic phase of the pelagic particles has not been
66 investigated in detail.

67 Recently, the term iron snow (IS) was defined for specific pelagic aggregates which
68 are formed in lakes with opposing oxygen and Fe(II) gradients to highlight their
69 predominant iron fraction [36]. Under low pH conditions, the oxidation of Fe(II) to
70 Fe(III), which is the first step in the iron mineral formation, is dominated by autotrophic
71 bacteria. In contrast to lake snow, which reach an aggregate size of more than 500 μm , IS
72 aggregates are smaller and precipitate faster due to their higher amount of iron-containing
73 minerals. Thus, microbial colonization of IS aggregates has to occur rapid due their
74 limited residence time in the water [36]. The high surface area of the iron minerals
75 present in the IS will alleviate adsorption of dissolved organic compounds serving as
76 potential electron donor for the activity of heterotrophic microorganisms colonizing the
77 aggregates. Similarly, anaerobic iron-reducing microorganisms would profit, because a
78 high surface area allows better access to iron as alternative electron acceptor when the
79 aggregates reach the anoxic water layer [37]. Since the amount and type of iron-
80 containing minerals will drastically influence the activity of iron-reducing bacteria [38],

81 not only a descriptive but also quantitative information regarding the inorganic phase of
82 the aggregates is required to achieve a better understanding of the biological iron-cycling
83 processes. By determining the relations between the mineralogy of the pelagic aggregates
84 and the bacterial communities, information of capital importance for a future
85 bioremediation attempt are obtained.

86 To our knowledge, the only analysis of the mineral phase of the pelagic particulate
87 matter was performed on the inorganic colloids from a slightly alkaline ultra-oligotrophic
88 lake [39, 40]. The authors used a combination of three techniques (energy dispersive X-
89 ray spectroscopy, selected area electron diffraction and transmission electron
90 microscopy) to gain semi-quantitative information about the mineral phase of the pelagic
91 aggregates. Different types of aluminosilicates were detected and characterized, however
92 problems appear in the identification of different oxides and hydroxides [40]. In addition,
93 a limited number of measurements were performed and the size of the particles was not
94 considered. Since Raman spectroscopy is a powerful technique capable to distinguish
95 between various oxides and hydroxides [1], we propose Raman imaging as an approach
96 for the quantification of various minerals which form the particulate matter of an aquatic
97 environment. Beside the advantage that a single method (implicit a single device) is used
98 for the quantification of the minerals which form the pelagic aggregates, no sample
99 preparation is required for the investigation of the minerals. Raman measurements can be
100 performed even under anoxic conditions if the sample is introduced in a glass cell
101 containing an inert gas, and measured thorough the glass window. Thus the
102 transformations which could take place when metastable components come in contact
103 with air can be avoided. Furthermore, the Raman mapping results are not influenced by
104 the size of the particles. By selecting the distance between two adjacent measurement
105 points equal to the laser spot and the thickness of the sample layer equal to the
106 penetration depth of the laser, all particles located in the scanned area are measured
107 during the Raman mapping. The big particles are measured at different points, and the
108 number of measurements is proportional to the surface area of the particle. However, a
109 relatively long running time is required using this spectroscopic approach for a single
110 Raman scan.

111 In this report, a semi-quantitative study has been established and carried out to
112 quantify the inorganic phase of pelagic aggregates formed in an acidic iron-rich mine
113 lake using Raman spectroscopy. In addition, the microbial communities of the aggregates
114 were compared using a DNA-based fingerprinting method called denaturing gradient gel
115 electrophoresis (DGGE) to evaluate if potential differences in the mineral composition
116 are reflected by differences of the microbial communities potentially involved in iron
117 cycling.

118

119 **2. Material and methods**

120 **2.1 Site description and sampling**

121 The acidic lignite mine lake (Lake 77) is located in the Lusatian mine area in east
122 central Germany. A bank on the bottom of the lake rising to about 4 m depth separates
123 the bottom water of the northern basin from the rest of the lake (Fig. 1). The central basin
124 shows a dimictic stratification scenario with typical spring and fall mixes, while the
125 stratification remains stable in the northern basin with an oxic surface water layer and a
126 deeper anoxic water layer separated by a sharp redoxcline. The inflow of less acidic,

127 Fe(II)- and sulfate- rich groundwater reaches the northern basin [36]. Sediment traps (3
128 plexiglas tubes with removable cups at the bottom of each tube, 5 cm diameter, 40 cm
129 total length) were installed for two weeks at both central and northern basins for
130 collecting IS formed within redoxcline and in deeper (bottom) anoxic water layer,
131 respectively. The sample name CR stands for central basin redoxcline, CB for central
132 basin bottom; NR for northern basin redoxcline and NB for northern basin bottom. Fresh
133 samples were collected on July 2010 and transferred to the laboratory in an ice box
134 before using for Raman microscopy investigation and molecular microbial community
135 analysis.

136 **2.2 Lake water chemistry**

137 Dissolved oxygen, pH, conductivity and temperature were measured over depth with
138 the multi-parameter water quality checker U-10 (Horiba, Japan). Water samples were
139 collected with a water sampler based on Ruttner design and transported at 4 °C and
140 processed within 24 h. Fe(II) and Fe(III) contents of water sample were measured after
141 acidification with 1 M HCl [41]. Sulfate concentration was measured using the barium-
142 chloride method [42].

143 **2.3 Sample preparation for Raman investigations**

144 A very thin layer of each IS was spread on the fused silica glass slide and dried at
145 room temperature. Raman measurements were carried out on the dried samples.

146 **2.4 Raman setup**

147 The Raman measurements of IS were performed with a commercial micro-Raman
148 setup (HR LabRam inverse system, Jobin Yvon Horiba). A frequency doubled Nd:YAG
149 laser at a wavelength of 532 nm was used to excite the Raman scattering. To avoid
150 changes in the mineral structure or composition due to heat generated by the laser, a
151 power of 20 μ W was chosen for Raman imaging measurements. The laser beam was
152 focused on the sample by means of a Zeiss LD EC Epiplan-Neofluar 100x/0.75
153 microscope objective down to a spot diameter of approximately 1 μ m. The dispersive
154 spectrometer had an entrance slit of 100 μ m, a focal length of 800 mm and was equipped
155 with a grating of 300 lines/mm. The Raman scattered light was detected by a Peltier
156 cooled CCD detector. Each Raman spectrum was collected with 40 s total integration
157 time. For the Raman mapping experiments, an automatically tunable x-y stage
158 (Merzhäuser) was used. The distance between two adjacent points in the x and y direction
159 was 1 μ m. On average, 28 scans for each location were performed, which correspond to a
160 total number of circa 20000 spectra. The size of a scan varied between 30X30 μ m and
161 60X35 μ m.

162 **2.5 Data analysis of the Raman outcome**

163 The spectra were first background corrected to minimize the effect of the
164 fluorescence background. The presence or absence of a mineral in the sample was
165 decided based on the intensity of the characteristic Raman band or the intensity ratio of
166 two bands (in case of ferrihydrite). The threshold value of the Raman marker band used
167 for the detection of the mineral was manually set for each scan. If the intensity of a
168 Raman band was higher or lower than the selected threshold value, then the mineral was
169 considered present or absent in the probe, respectively. The decision to manually select
170 the threshold values for all the Raman bands used for the identification of the minerals
171 was taken due to the high variance of the fluorescence background observed in various

172 samples. The amount (in percentage) of a mineral present at a location was calculated as
173 the ratio between the number of spectra which presented the Raman marker band of the
174 mineral divided by the total number of spectra recorded on the samples from the analyzed
175 site.

176 **2.6 Deoxyribonucleic acid (DNA) extraction and denaturing gradient gel** 177 **electrophoresis (DGGE) fingerprinting analysis**

178 Total genomic DNA was directly extracted from fresh IS samples captured in the
179 sediment traps using the PowerSoil DNA Isolation Kit (MO BIO laboratories, USA)
180 according to the manufacturer's instructions. Bacterial community was fingerprinted
181 using a nested-polymerase chain reaction (PCR)-DGGE approach. First, bacterial 16S
182 ribosomal ribonucleic acid (rRNA) genes were amplified using universal primer set 27F
183 (Lane, 1991) and 1492R (Loy et al. 2003). The nested amplification was then executed
184 with the primer EUB-341F-GC with GC-clamp (5'-CGC CCG CCG CGC CCC GCG
185 CCC GTC CCG CCG CCC CCG CCC GCC TAC GGG AGG CAG CAG-3') and
186 reverse primer 907R (5'-CCG TCA ATT CMT TTR AGT TT-3') (Muyzer et al. 1993)
187 with an annealing temperature of 65 °C for 20 cycles of amplification, followed by 10
188 cycles with annealing temperature of 55 °C. The Taq enzyme for PCR was from Jena
189 Bioscience (Jena Bioscience, Germany) and other reagents were from Sigma (Sigma-
190 Aldrich, Germany). The PCR Thermocycling was performed with a T-Gradient cycler
191 (Primus 96advanced, peqLab). PCR products were separated on a polyacrylamide gel
192 with denature reagent concentration ranging from 20% to 70% at the consistent
193 temperature of 60 °C for 15 hours. The polyacrylamide gel was stained with SYBR Gold
194 before documentation.

195

196 **3. Results and discussion**

197 **3.1 Water geochemistry**

198 The microbial oxidation of Fe(II) to Fe(III) is the initial step in iron oxide formation
199 at low pH, however it is still unclear to which extent the subsequent mineralization is
200 controlled by microorganisms. Mineral formation and mineral stability is also influenced
201 by geochemical conditions of the surrounding water phase [27, 43]. Thus, we studied the
202 water chemistry to obtain a better understanding of the biogeochemical processes. The
203 oxie overlying water layer showed similar characteristics in both basins with pH values
204 of about 3, similar sulfate and Fe(III) concentrations of about 8 mM and 2 mM,
205 respectively, but lacking Fe(II). In the redoxcline of the central and northern basin,
206 oxygen concentrations declined to 2.9 and 1.7 mg/L whereas Fe(II) concentrations
207 increased to 1.1 and 1.7 mM, respectively (Table 1). Highest pH value, sulfate and Fe(II)
208 concentrations were observed in the bottom water of the northern basin (Table 1) which
209 is affected by the inflow of less acidic iron-rich groundwater [36]. Due to the
210 considerable variations in pH between deeper water layers in central basin and northern
211 basins different mineral phases of iron oxyhydroxides were expected to be formed.
212 Fe(III) sedimentation rates approximate 1.5 and 1.9 g Fe m⁻² d⁻¹ at central and northern
213 basin [36]. Biologically mediated transformation reactions are not likely to occur due to
214 the low residence time of the particles in the lake.

215

216

217 **3.2 Qualitative analysis of the mineral phase**

218 Preliminary measurements of the IS samples performed under anoxic conditions (the
219 samples were measured in a glass cell in the absence of oxygen) and oxic conditions (the
220 samples were dried on the substrate and measured in atmospheric conditions) showed no
221 difference in the mineral phases of the samples. In addition, no changes in the color of the
222 IS was noticed during the drying process, therefore transformation of metastable iron
223 sulfides (black minerals) to schwertmannite (yellow mineral) can be excluded. Because
224 the spectra measured in atmospheric conditions had a higher signal to noise ratio than the
225 spectra measured through a glass window, we decided for the further investigations to
226 perform Raman measurements only under oxic conditions. Therefore, all the data
227 presented in this contribution were measured under atmospheric conditions.

228 For the assignment of the Raman spectra we used an in-house constructed library.
229 The iron minerals were synthesized according to the methods reported by Cornell and
230 Schwertmann [44]. The Raman spectra of the synthesized minerals were similar with
231 those reported in the literature [1, 44].

232 In a previous study we showed that these lake snow aggregates contain high amounts
233 of inorganic materials [36]. The mineral phase of the investigated pelagic aggregates was
234 dominated by the iron-containing minerals. Fig. 2 showed the Raman spectra of various
235 minerals detected in the investigated IS samples and the corresponding Raman marker
236 bands which were used for the identification of the minerals in the Raman imaging
237 experiments (the grey boxes). By far, the most abundant mineral detected in the samples
238 was schwertmannite, an Fe(III) oxyhydroxysulfate (Fig. 2(a), Table 2). Schwertmannite
239 is a mineral which is usually formed in acidic fresh waters rich in dissolved iron and
240 sulfate [44]. The interaction between Fe(III) and $(\text{SO}_4)^{2-}$ in schwertmannite is via
241 hydrogen bonds. In an acidic liquid solution, the Fe cations form a complex with the
242 sulfates through hydrogen bonds. These similarities of the interaction between Fe(III) and
243 $(\text{SO}_4)^{2-}$ is likely the reason why schwertmannite is a common mineral of the acid mine
244 drainage precipitates [45]. Therefore, the dominance of schwertmannite in the IS from an
245 acidic lignite mine lake with a pH around 3 was not surprising. Schwertmannite is also
246 the dominant mineral of the upper sediment collected in the central basin [46, 47].
247 Schwertmannite is a stable mineral at a pH in the range of 3 to 5, however in anoxic
248 conditions at higher pH values and in the presence of Fe(II) cations, the stability of the
249 schwertmannite decrease drastically [48]. Interestingly, high amounts of schwertmannite
250 were detected also in the samples from the anoxic monimolimnion of the north site,
251 although there the pH value of the water was around 6. The Raman spectrum of
252 schwertmannite consists of five relatively intense bands, among them the most prominent
253 band at 712 cm^{-1} served as marker band for the analysis of the distribution of
254 schwertmannite mineral in the samples. In the region around 700 cm^{-1} not only
255 schwertmannite gives a Raman signal but also ferrihydrite ($\text{Fe}_2\text{O}_3 \cdot 0.5\text{H}_2\text{O}$) (Fig. 2(b)).
256 The Raman band of ferrihydrite at circa 700 cm^{-1} is very broad and has a low intensity
257 compared to the 712 cm^{-1} band of schwertmannite, although it is the strongest Raman
258 band of ferrihydrite. The Raman spectrum of schwertmannite presents also a strong
259 Raman signal at circa 420 cm^{-1} , while ferrihydrite has no Raman band in that region.
260 Therefore, the ratio of the intensities of the bands at 712 cm^{-1} and 420 cm^{-1} (I_{712}/I_{420}) is
261 higher for ferrihydrite than for schwertmannite. On the basis of the intensity ratio of the

262 above mentioned bands, we were able to identify and distinguish ferrihydrite and
263 schwertmannite in the Raman maps.

264 Another Fe(III)-mineral identified in the samples from the transition zone of the north
265 site was hematite (α -Fe₂O₃) (Fig. 2(c)). The Raman spectrum of hematite can be
266 distinguished easily from the spectra of other minerals by the strong Raman signal at
267 approximate 1314 cm⁻¹, which was thus used as a marker band for the presence of
268 hematite in the samples. Fig. 2(d) shows the Raman spectrum of goethite, an iron
269 oxyhydroxide (α -FeOOH). The characteristic Raman band of this mineral used in this
270 study is located at 391 cm⁻¹. The goethite mineral was detected only in the anoxic
271 samples from the north site where the pH of the water is around 6. The formation of
272 goethite at this site can be connected to the mineral transformation from schwertmannite
273 at higher pH [44].

274 Not only iron-containing minerals were detected by means of Raman spectroscopy in
275 the IS samples. Quartz (SiO₂) was detected in three locations (Table 2). The typical
276 Raman band for this mineral is located at 464 cm⁻¹. Titanium dioxide (rutile and anatase),
277 gypsum (CaSO₄·2H₂O), barite (BaSO₄) and graphite (C) were also detected. The
278 presence of graphite in relatively high amounts in all the samples was expected since the
279 samples were obtained from a lignite mine lake.

280 Interestingly, no iron mineral in the 2⁺ oxidation state was detected in the samples,
281 although the Raman technique has been successfully used in the past for the identification
282 of various Fe(II)-minerals like siderite (FeCO₃), magnetite (Fe₃O₄), pyrite (FeS₂), or
283 vivianite (Fe₃(PO₄)₂·8H₂O) in earlier studies [1, 23, 49]. Hypothetically speaking, if iron
284 sulfides (pyrrhotite (Fe_(1-x)S), mackinawite (Fe, Ni)S_{0.9} or greigite (Fe₃S₄), for example)
285 were part of the IS, elemental sulfur and iron oxyhydroxide (goethite, ferrihydrite and/or
286 lepidocrocite (γ -FeOOH)) should be present in the samples after the air drying process, as
287 end products of the aerobic oxidation [50-52]. No elemental sulfur was detected in IS,
288 hence the presence of ferrous sulfides in the pelagic aggregates is highly unlikely.
289 Therefore it could be concluded that Fe(II) ions might be found in water as soluble iron
290 and/or forming complexes with the organic matter.

291 In our previous measurements, small amount of jarosite (KFe₃(OH)₆(SO₄)₂) was
292 detected in the IS from central basin [36]. However, no jarosite was found in this study.
293 This could be due to the sampling variation or different sampling time, or the jarosite was
294 formed only under some known specific conditions from schwertmannite [53], and/or
295 might be present in the IS in very small amounts, below the Raman detection limit.

296 The pelagic aggregates are of great importance for the transformation and cycling of
297 the elements in the aquatic ecosystem [32]. Being rich in inorganic and organic nutrients,
298 the aggregates are important sites for adsorption and desorption of soluble compounds
299 and for biological processes which take place in the water [31]. To understand the
300 dynamic processes which take place in this aquatic environment, a quantitative analysis
301 of the aggregates is required.

302 3.3 Quantitative analysis of the inorganic phase

303 To quantify the amounts of minerals presented in the IS, Raman imaging was used.
304 Fig. 3 displays the analysis of the Raman map of a sample collected from the anoxic layer
305 of the northern basin. Fig. 3(A) shows the brightfield image of an IS sample where the
306 box mark the region which was scanned by means of Raman spectroscopy. Three
307 minerals were detected in this investigated sampling field: schwertmannite, graphite and

262 above mentioned bands, we were able to identify and distinguish ferrihydrite and
263 schwertmannite in the Raman maps.

264 Another Fe(III)-mineral identified in the samples from the transition zone of the north
265 site was hematite (α -Fe₂O₃) (Fig. 2(c)). The Raman spectrum of hematite can be
266 distinguished easily from the spectra of other minerals by the strong Raman signal at
267 approximate 1314 cm⁻¹, which was thus used as a marker band for the presence of
268 hematite in the samples. Fig. 2(d) shows the Raman spectrum of goethite, an iron
269 oxyhydroxide (α -FeOOH). The characteristic Raman band of this mineral used in this
270 study is located at 391 cm⁻¹. The goethite mineral was detected only in the anoxic
271 samples from the north site where the pH of the water is around 6. The formation of
272 goethite at this site can be connected to the mineral transformation from schwertmannite
273 at higher pH [44].

274 Not only iron-containing minerals were detected by means of Raman spectroscopy in
275 the IS samples. Quartz (SiO₂) was detected in three locations (Table 2). The typical
276 Raman band for this mineral is located at 464 cm⁻¹. Titanium dioxide (rutile and anatase),
277 gypsum (CaSO₄·2H₂O), barite (BaSO₄) and graphite (C) were also detected. The
278 presence of graphite in relatively high amounts in all the samples was expected since the
279 samples were obtained from a lignite mine lake.

280 Interestingly, no iron mineral in the 2⁺ oxidation state was detected in the samples,
281 although the Raman technique has been successfully used in the past for the identification
282 of various Fe(II)-minerals like siderite (FeCO₃), magnetite (Fe₃O₄), pyrite (FeS₂), or
283 vivianite (Fe₃(PO₄)₂·8H₂O) in earlier studies [1, 23, 49]. Hypothetically speaking, if iron
284 sulfides (pyrrhotite (Fe_(1-x)S), mackinawite (Fe, Ni)S_{0.9} or greigite (Fe₃S₄), for example)
285 were part of the IS, elemental sulfur and iron oxyhydroxide (goethite, ferrihydrite and/or
286 lepidocrocite (γ -FeOOH)) should be present in the samples after the air drying process, as
287 end products of the aerobic oxidation [50-52]. No elemental sulfur was detected in IS,
288 hence the presence of ferrous sulfides in the pelagic aggregates is highly unlikely.
289 Therefore it could be concluded that Fe(II) ions might be found in water as soluble iron
290 and/or forming complexes with the organic matter.

291 In our previous measurements, small amount of jarosite (KFe₃(OH)₆(SO₄)₂) was
292 detected in the IS from central basin [36]. However, no jarosite was found in this study.
293 This could be due to the sampling variation or different sampling time, or the jarosite was
294 formed only under some known specific conditions from schwertmannite [53], and/or
295 might be present in the IS in very small amounts, below the Raman detection limit.

296 The pelagic aggregates are of great importance for the transformation and cycling of
297 the elements in the aquatic ecosystem [32]. Being rich in inorganic and organic nutrients,
298 the aggregates are important sites for adsorption and desorption of soluble compounds
299 and for biological processes which take place in the water [31]. To understand the
300 dynamic processes which take place in this aquatic environment, a quantitative analysis
301 of the aggregates is required.

302 3.3 Quantitative analysis of the inorganic phase

303 To quantify the amounts of minerals presented in the IS, Raman imaging was used.
304 Fig. 3 displays the analysis of the Raman map of a sample collected from the anoxic layer
305 of the northern basin. Fig. 3(A) shows the brightfield image of an IS sample where the
306 box mark the region which was scanned by means of Raman spectroscopy. Three
307 minerals were detected in this investigated sampling field: schwertmannite, graphite and

308 quartz. The distribution of schwertmannite is presented in Fig. 3(B), where the light grey
309 pixels represent the spots where the mineral is present while the black pixels show the
310 regions where schwertmannite is absent. Similarly, the distribution of graphite and quartz
311 are presented in Fig. 3(C) and Fig. 3(D), respectively. The false color images presented in
312 Fig. 3 clearly show that the main mineral in the investigated sample is schwertmannite
313 while graphite and quartz are presented only in minor amounts. Since the sample was
314 spread on the fused silica slide in a thin and relatively uniform layer, the amount of
315 various minerals within the sample was directly proportional to the surface region of the
316 sample where the respective minerals were detected. The surface region of a mineral in a
317 Raman map is proportional with the number of measured spots (pixels) where that
318 mineral is identified. Therefore, by counting the number of spots where each mineral was
319 detected, quantitative information could be obtained regarding to the minerals present in
320 the sample. Subsequently, an overview over the quantities of different minerals present in
321 the collected samples was able to be gained, by performing multiple scans on the IS
322 samples.

323 The possibility of ferrihydrite and schwertmannite to be present in the same aggregate
324 was also considered. As we already mentioned, to distinguish between schwertmannite
325 and ferrihydrite the intensity ratio of the 712 and 420 cm^{-1} bands was used. If (I_{712}/I_{420}) of
326 a Raman spectrum was smaller than $2 \cdot (I_{712}/I_{420})$ of the reference spectrum of
327 schwertmannite, the Raman spectrum was assigned as a schwertmannite spectrum. If
328 (I_{712}/I_{420}) of a Raman spectrum was higher than $0.5 \cdot (I_{712}/I_{420})$ of the reference spectrum of
329 ferrihydrite, the Raman spectrum was assigned as a ferrihydrite spectrum. In case the
330 (I_{712}/I_{420}) value of a Raman spectrum was between the above mentioned thresholds, the
331 Raman spectrum was considered to contain information from both schwertmannite and
332 ferrihydrite.

333 We considered our approach semi-quantitative because the variation in Raman
334 scattering efficiency of different minerals was not taken into account. In addition, errors
335 appear in the quantification process due to the fact that a pure mineral spectrum is
336 considered to have the same weight as a mixed spectrum. The error is associated with the
337 fact that the amount of a specific mineral which give a pure Raman spectrum is higher
338 than the amount of a mineral which has a contribution in a mixed spectrum. However, in
339 our experiment the number of mixed spectra is very low, therefore in this case the
340 outcome is expected to be only slightly affected by errors.

341 A summary of the minerals detected in the IS are shown in Table 2. Fe(III)-minerals
342 dominate the inorganic phase of the aggregates. In all four IS samples, the main
343 components of the pelagic aggregates were schwertmannite and graphite. As the IS
344 originates from a lignite coal mine, the presence of graphite in all the samples was
345 expected. Ferrihydrite was detected in CB, NR and NB samples in extreme low
346 concentration (<1%). Goethite was found only in the sample NB (1%), where the bulk
347 water pH was 5.9. Previous studies have shown that the transformation rate of
348 schwertmannite to goethite increase markedly at circumneutral pH values in the presence
349 of soluble Fe(II) and absence of oxygen [48]. The transformation rate is highly enhanced
350 by the sorption of Fe(II) on the surface of schwertmannite. Therefore, the low amount of
351 goethite detected in the NB sample could be explained by a low number of sorption sites
352 on the surface of schwertmannite. This imply that either other cations and organic matter
353 blocked the dissolution sites of the schwertmannite in the IS samples or that the cations

354 and organic matter prevent the polymerization of thermodynamically stable, crystalline
355 ferric minerals [54]. Actually, the large majority of the Raman spectra collected from NB
356 exhibit two small broad bands assigned to the C-C stretching vibrations of the aromatic
357 compounds [55]. Apparently organic matter covered a large surface of the
358 schwertmannite and in this way hindered the sorption of Fe(II) on the IS. The outcome is
359 in concordance with the results reported by Collins and coworkers, who showed that
360 silicate and natural organic matter retard the Fe(II)-catalyzed minerals transformation
361 [56].

362 Hematite was identified only in the NR sample (3%). The presence of hematite in
363 those samples is surprisingly since at a pH of 3 and a temperature of circa 10 °C, goethite
364 and not hematite should be the most stable form of Fe(III)-containing minerals [43]. In
365 addition, a small amount of titanium dioxide was also detected in the northern basin.

366 The quantification results offered us a nice picture over the iron minerals from IS.
367 Similar mineral compositions were observed between IS samples from the same basin,
368 whereas obvious differences were also noticed between basins, mentioning the content of
369 schwertmannite and graphite. The higher mineral diversity from the northern basin was
370 probably caused by the seepage water inflow from the northeastern mine tailing dump
371 area. As to the organic part, the microbial communities were also investigated. For this
372 purpose we used DGGE.

373 **3.4 Bacterial communities**

374 The microbial community composition is always affected by the geochemical
375 conditions of its habitat, especially by the oxygen content and the pH. Microbial Fe(II)
376 oxidation can be mediated in a broad pH range (0 to 8) and can occur under oxic,
377 microoxic and anoxic conditions. Since chemical Fe (II) oxidation is completely inhibited
378 at pH values below 4.2 [57], acidophilic or at least acid tolerant iron oxidizing bacteria
379 are responsible for the initial step in iron oxyhydroxides mineral formation [58, 59]. PCR
380 products obtained from IS particles sampled from the central basin (CR and CB)
381 produced similar DGGE patterns indicating similar microbial communities, although
382 some differences were observed at the upper part of the gel-lane (Fig. 4). Fingerprints of
383 IS particle samples of the northern basin (NR and NB) were identical to each other,
384 suggesting high similarities between these two samples. Thus, the stronger pH and Fe(II)
385 concentration gradients observed in the redoxcline of the northern basin did not affect
386 apparently the IS microbial community composition which suggested the majority
387 microorganisms being metabolically active over the broad pH. In contrast, communities
388 of IS particles sampled in the central and in the northern basin were dissimilar based on
389 differences of the signal-intensive bands on a respective DGGE gel lane which should be
390 indicative of abundant microorganisms in each sample. Earlier studies suggest that
391 acidophilic *Ferrovum* spp. and *Chlorobia*-related bacteria are present in the central basin,
392 whereas neutrophilic *Sideroxydans* spp. dominate the northern basin (Reiche et al. 2011).
393 The distinctive microbial communities detected in northern and central IS samples could
394 have affected iron oxyhydroxides formation, the subsequent mineral colonization by
395 several groups of microorganisms preferring a solid surface, and the microbial reduction
396 of Fe(III) back to Fe(II) which can occur under anoxic conditions.

397 **3.5 Mineral-microbe interaction**

398 The microorganisms are the main force which drives the formation of iron minerals
399 under acidic conditions [60]. The majority of the iron minerals of the IS had high surface

400 area and poor crystalline. These properties make them attractive for microbial and abiotic
401 processes [46, 60]. Schwertmannite has been observed in numerous acidic mine drainage
402 systems all over the world. The high stability of schwertmannite at pH values higher than
403 5, in the presence of Fe(II) might be due to the presence of natural organic matter (e.g.
404 humic substances, exopolysaccharide excretion by biofilm bacteria) in this aquatic
405 environment.

406 Hematite was detected only in the redoxcline of the northern basin but not in the
407 deeper anoxic water. This absence of hematite in the anoxic water layer could be due to
408 enhanced activity of Fe(III)-reducing bacteria, the reduction taking place before reaching
409 the bottom of the lake, since hematite was shown to be bio-reducible at circum-neutral
410 pH [61].

411 Ferrihydrite is widespread in many natural environments and it is used by a number
412 of Fe(III)-reducing bacteria as electron acceptor or it is produced by other Fe(II)-
413 oxidizing microorganisms at circum-neutral pH conditions [60]. Previous studies have
414 shown that ferrihydrite appears mostly at a pH above 5 [27]. The detection of
415 ferrihydrite in more acidic IS samples suggest that and it can be also formed by
416 acidophilic or at least acid tolerant microorganisms.

417 The aggregation of organic matter, inorganic matter, and, microorganisms to form
418 sinking snow particles plays a major part in aquatic ecosystems [62]. The high hydrolytic
419 enzyme activities of bacteria convert the aggregate organic matter into non-sinking
420 dissolved organic matter (DOM), forming plumes in the ocean. However, formation of
421 DOM plumes might not occur with IS due to its higher inorganic fraction leading to a
422 higher sinking velocity [36]. Nonetheless, the intensely colonized aggregates create hot
423 spots of microbial life having substantial roles in the cycling of iron in the acidic lignite
424 mine lake. With the means of Raman spectroscopy which is able to reveal slight
425 quantitative differences in the inorganic phase, we were able to obtain a deeper
426 understanding on sophisticated microbe-mineral interactions in this aquatic habitat.

427 **4. Conclusions**

428 Raman spectroscopy was applied successfully for the quantification of the mineral
429 phase of pelagic aggregates formed in an acidic iron- and sulfate-rich aquatic
430 environment. Discrimination between minerals composed by nanocrystals (e.g.,
431 schwertmannite and ferrihydrite) or between closely related minerals (e.g., goethite and
432 hematite) was doable using Raman spectroscopy. Schwertmannite was the main mineral
433 in all aggregates regardless of the pH in the niche environment and differences in the
434 bacterial communities inhabiting this aggregate. Although substantial differences in the
435 microbial communities of the investigated sites were detected, only small variations of
436 the mineral phase of the Iron Snow were revealed by Raman imaging. The outcome
437 suggests that the formation of the mineral phase of the IS was mainly dictated by the
438 geochemical conditions of the aquatic environment, despite the fact that microbial
439 communities were actively involved in the initiation of iron mineral formation.
440 Therefore, the implications of these findings should be considered before any attempt of
441 bioremediation performed on similar polluted ecosystems.

442 **Acknowledgements**

443 We highly acknowledge the financial supports from the German Research Foundation
444 (Graduate School 1257 “Alteration and element mobility at the microbe-mineral
445 interface”) as well as from the TMBWK (MikroPlex) PE113-1. Shipeng Lu was
446 supported by the Graduate School of Excellence Jena School for Microbial
447 Communication (JSMC) funded by the German Research Foundation (Deutsche
448 Forschungsgemeinschaft [DFG]). The authors thank Marco Reiche, Marco Jung and
449 Martina Hermann for technical assistances.

450 **References**

- 451 [1] M. Hanesch, *Geophys. J. Int.* 177 (2009) 941-948.
452 [2] J. Monnier, L. Bellot-Gurlet, D. Baron, D. Neff, I. Guillot, P. Dillmann, *J. Raman*
453 *Spectrosc.* 42 (2011) 773-781.
454 [3] R.L. Frost, T. Kloprogge, M.L. Weier, W.N. Martens, Z. Ding, H.G.H. Edwards,
455 *Spectrochim. Ac. A* 59 (2003) 2241-2246.
456 [4] Z.C. Ling, A. Wang, B.L. Jolliff, *Icarus* 211 (2011) 101-113.
457 [5] Z. Tomić, P. Makreski, B. Gajić, *J. Raman Spectrosc.* 41 (2010) 582-586.
458 [6] J. Fritz, A. Greshake, D. Stoffler, *Antarctic Meteor. Res.* 18 (2005) 96-116.
459 [7] V. Ciobotă, W. Salama, N. Tarcea, P. Rösch, M.E. Aref, R. Gaupp, J. Popp, *J.*
460 *Raman Spectrosc.* 43 (2012) 405-410.
461 [8] T. Frosch, N. Tarcea, M. Schmitt, H. Thiele, F. Langenhorst, J. Popp, *Anal.*
462 *Chem.* 79 (2007) 1101-1108.
463 [9] F. Rull, J. Martinez-Frias, A. Sansano, J. Medina, H.G.M. Edwards, *J. Raman*
464 *Spectrosc.* 35 (2004) 497-503.
465 [10] L.C. Prinsloo, P. Colomban, J.D. Brink, I. Meiklejohn, *J. Raman Spectrosc.* 42
466 (2010) 626-632.
467 [11] P. Vargas Jentzsch, R.M. Bolanz, V. Ciobotă, B. Kampe, P. Rösch, J. Majzlan, J.
468 *Popp, Vib. Spectrosc.* 61 (2012) 206-213.
469 [12] P. Vargas Jentzsch, V. Ciobotă, B. Kampe, P. Rösch, J. Popp, *J. Raman*
470 *Spectrosc.* 43 (2012) 514-519.
471 [13] P. Vargas Jentzsch, B. Kampe, P. Rösch, J. Popp, *J. Phys. Chem. A* 115 (2011)
472 5540-5546.
473 [14] S. Cintă Pinzaru, B.P. Onac, *Vib. Spectrosc.* 49 (2009) 97-100.
474 [15] W. Schumacher, M. Kühnert, P. Rösch, J. Popp, *J. Raman Spectrosc.* 42 (2011)
475 383-392.
476 [16] C.H. Chio, S.K. Sharma, L.-C. Ming, D.W. Muenow, *Spectrochim. Ac. A* 75
477 (2010) 162-171.
478 [17] P. Vargas Jentzsch, R.M. Bolanz, V. Ciobotă, B. Kampe, P. Rösch, J. Majzlan, J.
479 *Popp, Vib. Spectrosc.* 61 (2012) 206-213.
480 [18] A. Hernanz, I. Bratu, O. Marutoiu, C. Marutoiu, J. Gavira-Vallejo, H. Edwards,
481 *Anal. Bioanal. Chem.* 392 (2008) 263-268.
482 [19] L.D. Kock, D. De Waal, *Spectrochim. Ac. A* 71 (2008) 1348-1354.
483 [20] L.C. Prinsloo, W. Barnard, I. Meiklejohn, K. Hall, *J. Raman Spectrosc.* 39 (2008)
484 646-654.
485 [21] P. Vandenabeele, K. Lambert, S. Matthys, W. Schudel, A. Bergmans, L. Moens,
486 *Anal. Bioanal. Chem.* 383 (2005) 707-712.
487 [22] C.E. Amri, M.-C. Maurel, G. Sagon, M.-H. Baron, *Spectrochim. Ac. A* 61 (2005)
488 2049-2056.
489 [23] T. Dörfer, W. Schumacher, N. Tarcea, M. Schmitt, J. Popp, *J. Raman Spectrosc.*
490 41 (2010) 684-689.
491 [24] S.N. White, *Chem. Geol.* 259 (2009) 240-252.
492 [25] D. Neff, L. Bellot-Gurlet, P. Dillmann, S. Reguer, L. Legrand, *J. Raman*
493 *Spectrosc.* 37 (2006) 1228-1237.
494 [26] J. Tofan-Lazar, H.A. Al-Abadleh, *J. Phys. Chem. A* 116 (2012) 1596-1604.
495 [27] E. Murad, P. Rojik, *Clay Miner.* 40 (2005) 427-440.

- 496 [28] T.M. Valente, C. Leal Gomes, *Sci. Total Environ.* 407 (2009) 1135-1152.
 497 [29] P. Mäkie, G. Westin, P. Persson, L. Österlund, *J. Phys. Chem. A* 115 (2011)
 498 8948-8959.
 499 [30] S.W. Fowler, G.A. Knauer, *Prog. Oceanogr.* 16 (1986) 147-194.
 500 [31] H.-P. Grossart, T. Berman, M. Simon, K. Pohlmann, *Aquat. Microb. Ecol.* 14
 501 (1998) 59-67.
 502 [32] H.-P. Grossart, M. Simon, *Limnol. Oceanogr.* 38 (1993) 532-546.
 503 [33] T.R. Neu, *Aquat. Microb. Ecol.* 21 (2000) 85-95.
 504 [34] B. Schweitzer, I. Huber, R. Amann, W. Ludwig, M. Simon, *Appl. Environ.*
 505 *Microb.* 67 (2001) 632-645.
 506 [35] B.D. Honeyman, L.S. Balistrieri, J.W. Murray, *Deep Sea Res.* 35 (1988) 227-246.
 507 [36] M. Reiche, S. Lu, V. Ciobotă, T.R. Neu, S. Nietzsche, P. Rösch, J. Popp, K.
 508 Küsel, *Limnol. Oceanogr.* 56 (2011) 1386-1398.
 509 [37] E.E. Roden, *Environ. Sci. Technol.* 37 (2003) 1319-1324.
 510 [38] J.M. Zachara, J.K. Fredrickson, S.W. Li, D.W. Kennedy, S.C. Smith, P.L.
 511 Gassman, *Am. Mineral.* 83 (1998) 1426-1443.
 512 [39] T. Schäfer, V. Chanudet, F. Claret, M. Filella, *Environ. Sci. Technol.* 41 (2007)
 513 7864-7869.
 514 [40] V. Chanudet, M. Filella, *Environ. Sci. Technol.* 40 (2006) 5045-5051.
 515 [41] M. Blöthe, D.M. Akob, J.E. Kostka, K. Goschel, H.L. Drake, K. Küsel, *Appl.*
 516 *Environ. Microbiol.* 74 (2008) 1019-1029.
 517 [42] M. Tabatabai, *Environ. Lett.* 7 (1974) 237-243.
 518 [43] R.G. Robins, *J. Inorg. Nucl. Chem.* 29 (1967) 431-435.
 519 [44] R.M. Cornell, U. Schwertmann, *The iron oxides: structure, properties, reactions,*
 520 *occurrences and uses*, 2nd Edition ed., Wiley-VCH Weinheim, 2003.
 521 [45] J. Majzlan, S.C.B. Myneni, *Environ. Sci. Technol.* 39 (2004) 188-194.
 522 [46] A. Peine, A. Tritschler, K. Küsel, S. Peiffer, *Limnol. Oceanogr.* 45 (2000) 1077-
 523 1087.
 524 [47] K. Küsel, *Water Air Soil Pollut.* 3 (2003) 67-90.
 525 [48] E.D. Burton, R.T. Bush, L.A. Sullivan, D.R.G. Mitchell, *Geochim. Cosmochim.*
 526 *Ac.* 72 (2008) 4551-4564.
 527 [49] K.A. Rodgers, H.W. Kobe, C.W. Childs, *Mineral. Petrol.* 47 (1993) 193-208.
 528 [50] N. Belzile, Y.-W. Chen, M.-F. Cai, Y. Li, *J. Geochem. Explor.* 84 (2004) 65-76.
 529 [51] J.A. Bourdoiseau, M. Jeannin, R. Sabot, C. Rémazeilles, P. Refait, *Corros. Sci.* 50
 530 (2008) 3247-3255.
 531 [52] J.-A. Bourdoiseau, M. Jeannin, C. Rémazeilles, R. Sabot, P. Refait, *J. Raman*
 532 *Spectrosc.* 42 (2011) 496-504.
 533 [53] S. Regenspurg, A. Brand, S. Peiffer, *Geochim. Cosmochim. Ac.* 68 (2004) 1185-
 534 1197.
 535 [54] A.M. Jones, R.N. Collins, J. Rose, T.D. Waite, *Geochim. Cosmochim. Ac.* 73
 536 (2009) 4409-4422.
 537 [55] B. Wopenka, J.D. Pasteris, *Am. Mineral.* 78 (1993) 533-557.
 538 [56] R.N. Collins, A.M. Jones, T.D. Waite, *Geochim. Cosmochim. Ac.* 74 (2010) 482-
 539 496.
 540 [57] G. Meruane, T. Vargas, *Hydrometallurgy* 71 (2003) 149-158.

-
- 541 [58] D. Emerson, E.J. Fleming, J.M. McBeth, *Annu. Rev. Microbiol.* 64 (2010) 561-
542 583.
543 [59] S. Hedrich, M. Schlömann, D.B. Johnson, *Microbiol.* 157 (2011) 1551-1564.
544 [60] A. Kappler, K.L. Straub, *Rev. Mineral. Geochem.* 59 (2005) 85-108.
545 [61] S. Bose, M.F. Hochella Jr, Y.A. Gorby, D.W. Kennedy, D.E. McCready, A.S.
546 Madden, B.H. Lower, *Geochim. Cosmochim. Ac.* 73 (2009) 962-976.
547 [62] F. Azam, F. Malfatti, *Nat. Rev. Micro.* 5 (2007) 782-791.

548 **Tables**

549

550 **Table 1:** Geochemical parameters were measured in water samples obtained from the
 551 redoxcline and the deeper, anoxic bottom water layer of the central and the northern basin
 552 of lignite mine Lake 77, from where the Iron Snow samples were obtained. CR stands
 553 for central redoxcline, while CB for central bottom, NR for northern redoxcline, NB for
 554 northern bottom.
 555

	depth	pH	oxygen content	sulfate	Fe(II)	Fe(III) ^a	conductivity	temperature
	[m]		[mg/l]	[mm]	[mm]	[mm]	[ms/cm]	[°C]
CR	3.9	3.3	2.9	8.3	1.1	2.3	2.0	16.0
CB	6.0	3.5	0	10.3	6.9	0.3	2.1	10.0
NR	3.8	3.3	1.7	8.2	1.7	1.9	2.0	15.5
NB	6.0	5.9	0	15.4	20.0	0.0	3.0	11.3

556

557

^a Fe(III) concentrations were measured from the water phases without IS particles included.

558

^b All data were obtained from the day the sediment traps were placed into the lake.

559

560

561

562

563

564

Table 2: The abundance of various minerals detected in Iron Snow samples at survey
 565 sites given by Raman spectroscopy.
 566

	schwertmannite	goethite	ferrihydrate	hematite	graphite	quartz	gypsum	barite	rutile/ anatase
CR	97%	n.d. ^a	n.d.	n.d.	2%	n.d.	n.d.	n.d.	<1%
CB	96%	n.d.	<1%	n.d.	3%	<1%	n.d.	n.d.	n.d.
NR	90%	n.d.	<1%	3%	5%	<1%	n.d.	n.d.	<1%
NB	88%	1%	<1%	n.d.	5%	<1%	1%	2%	<1%

567

568

^a n.d., not detected.

569 **Figure Legends**

570

571 **Fig. 1:** Schematically representation of acidic lignite mine Lake 77 with stratification
572 scenario during summer season when the Iron Snow (IS) samples were collected.

573

574 **Fig. 2:** Raman spectra of a – schwertmannite, b – ferrihydrite, c – hematite, d – goethite,
575 and e – quartz. The grey boxes show the regions of the Raman marker bands used for the
576 quantification of various minerals in the sample.

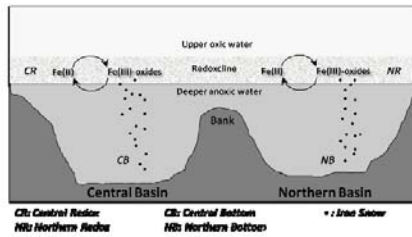
577

578 **Fig. 3:** A - The brightfield image of a sample from northern basin bottom layer. The
579 rectangle shows the region where Raman maps were performed. The spatial distribution
580 of schwertmannite (B), graphite (C) and quartz (D) in the sample is illustrated by the
581 false color images. The light grey pixels present the positions where the investigated
582 mineral was detected, while black pixels show the regions where the mineral was not
583 found. The pixel length represents the distance between two adjacent measurement points
584 and is equal to 1 μm .

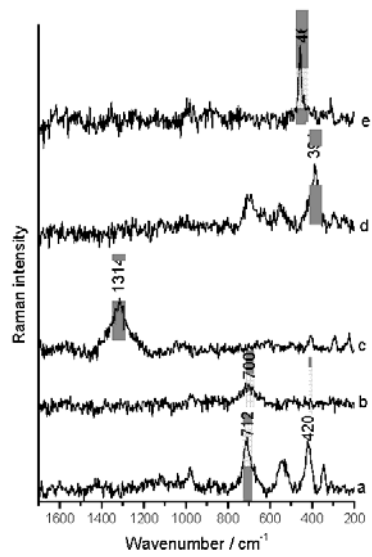
585

586 **Fig. 4:** Denaturing gradient gel electrophoresis (DGGE) patterns showing diverse
587 bacterial communities of Iron Snow samples from central redoxcline (CR); central
588 bottom (CB); northern redoxcline (NR); northern bottom (NB) of acidic lignite mine
589 Lake 77.

590 **Fig. 1**
591

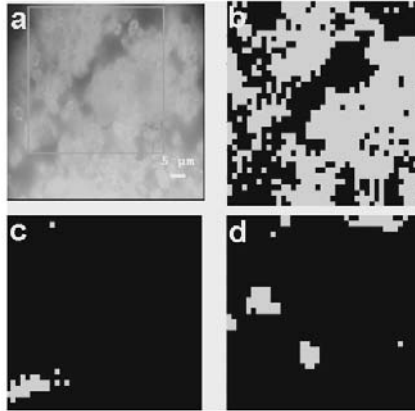


592
593
594
595 **Fig. 2**
596

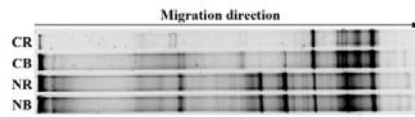


597

598 **Fig. 3**
599



600
601
602
603
604 **Fig. 4**
605



606
607

3. Conference Contributions

Posters:

International Conference on Raman Spectroscopy (ICORS) – 08.2008 London:

Identification and chemical characterization of anaerobic bacteria by means of Raman spectroscopy

V. Ciobota, P. Rösch, E.-M. Burkhardt, K. Küsel, J. Popp

Photonic for life (P4L) – 11.2008 Bruxelles:

Characterization of microorganisms by means of Raman spectroscopy

V. Ciobota, P. Rösch, E.-M. Burkhardt, K. Küsel, J. Popp

International Conference on Advanced Vibrational Spectroscopy (ICAVS) – 07.2009 Melbourne:

Heavy metals influence on the chemical composition of *Acidiphilium cryptum* JF-5

V. Ciobota, P. Rösch, E.-M. Burkhardt, K. Küsel, J. Popp

FTIR spectroscopy in microbiological and medical diagnostics – 10.2009 Berlin:

Characterization of *Acidiphilium cryptum* JF-5 by means of Raman spectroscopy

V. Ciobota, P. Rösch, E.-M. Burkhardt, K. Küsel, J. Popp

International Conference on Raman Spectroscopy (ICORS) – 08.2010 Boston:

The influence of intracellular storage material on bacterial identification by means of Raman spectroscopy

V. Ciobota, E.-M. Burkhardt, W. Schumacher, P. Rösch, K. Küsel, J. Popp

GeoRaman X, 06.2012 Nancy:

Investigation of the Middle Eocene ironstones from Bahariya Depression, Western Desert, Egypt by means of micro-Raman spectroscopy

V. Ciobota, W. Salama, N. Tarcea, P. Rösch, M. El Aref, R. Gaupp, J. Popp

GeoRaman X, 06.2012 Nancy:

Mineralogy of Iron Snow aggregates from an acidic lignite mine lake

V. Ciobota, S. Lu, N. Tarcea, P. Rösch, K. Küsel, J. Popp

Oral Presentations:

7th Symposium on remediation in Jena “Jenaer Sanierungskolloquium” - 22.09.2008,
Jena, Germany

Characterization of microorganisms by means of Raman spectroscopy

V. Ciobota

8th Symposium on remediation in Jena “Jenaer Sanierungskolloquium” - 29.09.2009,
Jena, Germany

The potential of Raman spectroscopy in the field of precipitation and bioremediation

V. Ciobota

9th Symposium on remediation in Jena “Jenaer Sanierungskolloquium” - 4.10.2010,
Jena, Germany

Heavy metals influence on the chemical composition of *Acidiphilium cryptum* JF-

5

V. Ciobota

4. Publication List

Peer-reviewed publications:

1. Analytical and Bioanalytical Chemistry 397 (2010) 2929-2937
The influence of intracellular storage material on bacterial identification by means of Raman spectroscopy
V. Ciobota, E.-M. Burkhardt, W. Schumacher, P. Rösch, K. Küsel, J. Popp
2. Journal of Raman Spectroscopy 43 (2012) 405-410
Identification of minerals and organic materials of the Middle Eocene ironstones, the Bahariya Depression, Western Desert, Egypt by means of micro-Raman spectroscopy
V. Ciobota, W. Salama, N. Tarcea, P. Rösch, M. El Aref, R. Gaupp, J. Popp
3. Journal of Raman Spectroscopy 43 (2012) 514-519
Origin of salt mixtures and mixed salts in atmospheric particulate matter
P. Vargas Jentsch‡; V. Ciobota‡; B. Kampe; P. Rösch; J. Popp
‡P. Vargas Jentsch and V. Ciobota contributed equally to the present work
4. Limnology and Oceanography 56 (2011) 1386-1398
Pelagic boundary conditions affect the biological formation of iron-rich particles (iron snow) and their microbial communities
M. Reiche, S. Lu, V. Ciobota, T. Neu, S. Nietzsche, P. Rösch, J. Popp, K. Küsel
5. Vibrational Spectroscopy 61 (2012) 206-213
Raman spectroscopic study of calcium mixed salts of atmospheric importance
P. Vargas Jentsch, R. M. Bolanz, V. Ciobota, B. Kampe, P. Rösch, J. Majzlan, J. Popp
6. Journal of Molecular Structure 1022 (2012) 147-152
Raman and infrared spectroscopic study of synthetic ungemachite, $K_3Na_8Fe(SO_4)_6(NO_3)_2 \cdot 6H_2O$
P. Vargas Jentsch, V. Ciobota, R. M. Bolanz, B. Kampe, P. Rösch, J. Majzlan, J. Popp

Submitted papers:

7. Quantification of the inorganic phase of the pelagic aggregates of an iron contaminated lake by means of Raman spectroscopy

V. Ciobota, S. Lu, N. Tarcea, P. Rösch, K. Küsel, J. Popp

8. Raman investigations of Upper Cretaceous phosphorite and black shale from Safaga District, Red Sea, Egypt

V. Ciobota, W. Salama, P. Vargas Jentzsch, R. Saed, N. Tarcea, P. Rösch, A. El Kammar, J. Popp

9. The effect of antimonate, arsenate and phosphate on the transformation of ferrihydrite to goethite, hematite, ferrioxhyte, and tripuyhite

R. M. Bolanz , U. Bläss, S. Ackermann, V. Ciobota, P. Rösch, N. Tarcea, J. Popp, J. Majzlan

10. STXM and NanoSIMS investigations on EPS fractions before and after adsorption to goethite

X. Liu, K. Eusterhues, J. Thieme, V. Ciobota, C. Höschen, C. Müller, K. Küsel, I. Kögel-Knabner, P. Rösch, J. Popp, K. U. Totsche

11. Origin and significance of inorganic salts in atmospheric particulate matter: Raman spectroscopy as an analytical tool

P. Vargas Jentzsch, B. Kampe, V. Ciobota, P. Rösch, J. Popp

12. Reactions of alkaline minerals in the atmosphere

P. Vargas Jentzsch, V. Ciobota, P. Rösch, J. Popp

Book chapters:

M. Harz, S. Stöckel, V. Ciobota, D. Cialla, P. Rösch, J. Popp,

Applications of Raman spectroscopy to virology and microbial analysis.

in: Emerging Raman Applications and Techniques in Biomedical and Pharmaceutical Fields, P. Matousek, M. Morris (Eds.), Springer, Heidelberg, 2010, pp. 439-466.

S. Stöckel, A. Walter, A. Boßecker, S. Meisel, V. Ciobota, W. Schumacher, P. Rösch,
J. Popp,
Identification and characterization of microorganisms by vibrational spectroscopy.
in: Handbook of Biophotonics, J. Popp, V. V. Tuchin, A. Chiou, S. Heinemann (Eds.),
Wiley-VCH Weinheim, Vol. 2(Photonics for Health Care), 2011, pp.105-142.

Acknowledgments

First and foremost I offer my sincerest gratitude to my mentor, Prof. Jürgen Popp, who has supported me through my thesis with his patience and knowledge. I am grateful to him for providing me the opportunity to work in his group.

I am greatly indebted to my supervisor Dr. Petra Rösch. Her guidance helped me in all the time of my research. Without her support the thesis will not have reached its final phase. I express my thankfulness to Dr. Nicolae Tarcea for his time and his knowledge in the mineralogical field.

I thank immensely my second mentor Prof. Kirsten Küsel for guiding me with her valuable suggestion in the field of microbiology.

I like to thank my collaborators from Institute of Ecology, Shipeng Lu, Dr. Eva-Maria Burkhardt, Dr. Marko Reiche, Dr. Juanjuan Wang, Tsing Bohu, Stephan Gischkat, Maren Sickinger, Maria Fabish and Anke Hädrich for their support in terms of providing me with all of the bacterial and mineral samples covered in this thesis.

I take opportunity to thank Prof. Reinhard Gaupp for his advice and insight throughout my work on geological samples and his group, Dr. Walid Salama for the nice collaboration and the valuable inputs which helped to gain expertise over sedimentary rocks. I also thank Wafaa Zidan, Dr. Andreea Maier for their interest in collaborations.

I express my gratefulness to Prof. Juraj Majzlan for allowing me to utilize the XRD facility available in his institute and I thank Ralph Bolanz for helping me carry out XRD measurements on the synthesized minerals.

I will like to take this opportunity to express my deep gratitude to Prof. Kai-Uwe Totsche, Prof. Georg Büchel and Prof. Gerd Gleixner. I am thankful for their support and excellent collaboration. I also thank Xinran Liu, Matthias Händel, Sathish Mayanna and Julia Baumert.

My special thanks go to Paul Vargas Jentzsch for his enthusiasm, ideas and criticism showed during our common experiments, and of course for the synthesis of so many minerals.

I also like to thank all the technical staff from Institute for Physical Chemistry especially Mrs. Ludwig for measuring IR spectra for me, Mr. Fähndrich, Mrs. Jacob and Mrs. Süß for their technical support.

In my daily work I was lucky to have a friendly and cheerful group of fellow students. I like to thank Stephan Stöckel for helping me with the beautiful but complicated German language.

I thank German Research Foundation (DFG) for the doctoral scholarship which gave me the opportunity to work in this interesting field.

Finally, I would like to thank my family for their unconditioned support throughout all my studies.

Curriculum Vitae

- 2007 – 2012 Doctoral student at Institute of Physical Chemistry
Friedrich-Schiller University, Jena, Germany
- 2007 - 2010 DFG scholarship in the Graduate College 1257 “Alteration and
element mobility at the microbe-mineral interface”
- 2005 – 2007 Master in *Oxide materials physics* at Physics Faculty
Babes-Bolyai University, Cluj-Napoca, Romania
- 2006 SOCRATES-ERASMUS scholarship at Julius Maximilian
University, Würzburg, Germany
- 2000 - 2005 Bachelor at Physics Faculty
Babes-Bolyai University, Cluj-Napoca, Romania

Jena, 3 December 2012

Selbstständigkeitserklärung

Ich erkläre, dass ich die vorliegende Arbeit selbstständig und unter Verwendung der angegebenen Hilfsmittel, persönlichen Mitteilungen und Quellen angefertigt habe.

Jena, 3. December 2012

Valerian Ciobotă